UNIVERSITAT POLITÈCNICA DE VALÈNCIA

DEPARTAMENTO DE INGENIERÍA HIDRÁULICA Y MEDIO AMBIENTE

PROGRAMA DE DOCTORADO DE INGENIERÍA DEL AGUA Y MEDIOAMBIENTAL

TESIS DOCTORAL

Metodología de Aplicaciones de Técnicas Computacionales y Experimentales para la Optimización de la Hidrodinámica de Reactores Electroquímicos

AUTOR

JUAN ESCUDERO GONZÁLEZ

DIRECTOR

Dr. PETRA AMPARO LÓPEZ JIMÉNEZ

Junio del 2014 - Valencia, España

Agradecimientos

El presente trabajo ha sido logrado por la orientación y apoyo incondicional de Amparo. Por su motivación y energía puesta en este proyecto. Un agradecimiento especial por su entrega.

Al Departamento de Ingeniería Hidráulica y Medio Ambiente de la Universidad Politécnica de Valencia. A los amigos de doctorado con los que he compartido momentos importantes, por sus consejos y ayuda durante el proceso de este proyecto.

A los compañeros de la empresa Resenergie S.L. por su apoyo incondicional en el desarrollo del doctorado ofreciéndome todos su ayuda.

Al Departamento de Electroquímica de la Universidad de Alicante por su colaboración y prestación de instalaciones para las aportaciones precisas a este proyecto.

A la familia y amigos, a mis padres Enrique y Rosa María, a mis abuelos y en especial a Ali por su apoyo constante durante este camino.

Resumen

La presente tesis propone una metodología basada en la modelación de la mecánica de fluidos computacional para optimizar la hidrodinámica del flujo del electrolito en los reactores electroquímicos con validaciones experimentales.

Se presenta una investigación para que, a través de la proposición y análisis de unos parámetros indicadores, se pueda mejorar los diseños actuales de las celdas que constituyen los reactores en este estudio y proponer un óptimo realizable.

En consecuencia, el objetivo de la presente tesis es analizar y revelar los estados de flujo del electrolito dentro del reactor mediante el uso de un código numérico que resuelva la mecánica del flujo del electrolito en las geometrías propuestas. Ello permite, por un lado, determinar unos parámetros cuantificables que analizan la bondad de los diseños en aras de tener visualizaciones de los flujos; y, por otro lado, disponer de aspectos cuantificables que permitan la optimización de los diseños. El diseño y los parámetros propuestos se validan experimentalmente en dos geometrías diferentes construidas para tal fin.

Este objetivo de carácter general se divide en una serie de objetivos más específicos que se detallan a continuación:

- Realizar un estudio de la viabilidad económica basado en el caso de España para este tipo de baterías.
- Realizar un estudio detallado acerca de las investigaciones realizadas hasta la fecha relativa a la optimización mediante técnicas CFD (por sus siglas en inglés: Computational Fluid Dynamics) del interior de un reactor electroquímico redox, ya sea mediante metodologías funcionales o mediante otro tipo de técnicas de diseño.
- Evaluar la bondad de los distintos modelos desarrollados mediante las técnicas CFD frente a modelos experimentales, observando la adecuación de los modelos computacionales frente a los modelos físicos.
- Proponer parámetros propios en este campo para la cuantificación de la eficiencia del reactor en base a la velocidad a la que circula el fluido en el interior de la celda.

- Definir el ajuste más adecuado de los distintos operadores de diseño para cada una de las propuestas de optimización realizadas.
- Obtener una geometría óptima en función de los parámetros de diseño para la construcción de una celda a escala real.

A partir de la metodología propuesta se ha seguido un proceso de optimización en relación con la influencia del flujo del electrolito en el interior de la celda para desarrollar una geometría final optimizada.

A partir de los análisis desarrollados, se ha demostrado la importancia que tiene la tecnología de almacenamiento de energía que se propone en el sistema energético español y se ha realizado un análisis económico de una batería concreta que avala su viabilidad. Se ha estimado, en este caso, un tiempo de amortización de 8 años y medio.

Asimismo, se ha realizado un modelo validado para un prototipo experimental con mediciones en laboratorio y contrastaciones numéricas que avalan el uso de la fluidodinámica computacional que se propone. A través del software comercial STAR-CCM+ de CD-Adapco©, se ha validado un modelo inicial a escala de laboratorio en el Departamento de Electroquímica de la Universidad de Alicante (España). Esta validación ha dado unos errores menores del 2,22 % al comparar el modelo físico con el numérico. Se han definido ciertos parámetros de funcionamiento en este primer prototipo como, por ejemplo, el porcentaje de volumen de fluido circulando en la dirección principal del flujo, siendo este del 83 %.

En la presente tesis se propone una metodología conjunta basada en la experiencia adquirida en fases previas para proponer parámetros de diseño. Dicha metodología atiende a la definición de los siguientes conceptos: coeficiente de simetría, coeficiente de uniformidad, coeficiente del rango de velocidades y volumen de fluido en la dirección principal.

El coeficiente de simetría indica la diferencia de caudal que circula por ambas partes de la celda en la dirección longitudinal; el coeficiente de uniformidad evalúa la velocidad media de cada canal; el coeficiente del rango de velocidades analiza la velocidad en un punto específico de la membrana para determinar la variabilidad del frente de velocidad; y, por último, se define el volumen de fluido en la dirección principal que cuantifica la laminaridad y dirección del fluido en el interior de la celda. Esta metodología se usa para optimizar la batería basada en modificaciones sobre disposiciones ya existentes, de manera que se llega a una geometría final en la que el número de los canales más cercanos a la membrana es de 84, con una distancia de 1 mm entre canal y canal. Esta geometría construida a escala real y ensayada en el Laboratorio Justo Nieto de Mecánica de Fluidos de la

Universidad Politécnica de Valencia esta validada con mediciones experimentales de presiones y velocidades lo que permite ratificar el modelo numérico propuesto.

La batería diseñada tiene prácticamente una simetría perfecta y una distribución uniforme cuando el fluido alcanza la membrana. El 100 % del fluido que transcurre por la zona de membrana circula en la misma dirección, lo que provoca que se minimicen las zonas de recirculación o zonas muertas. La metodología descrita cuantifica la bondad de un diseño claramente mejorado frente a los ya existentes, al mismo tiempo que valida la metodología propuesta para el diseño de este tipo de elementos basados en la mecánica del flujo del electrolito en el interior de la misma.

La presente tesis se avala con una comunicación a congreso y cuatro artículos presentados a revistas indexadas en la base de datos "Journal Scitation Reports" que se detallan a continuación.

- Escudero González, J.; Alberola, A.; López Jiménez, P.A. 2012. Computational Fluid Dynamics Applied to a Prototype Flow Battery. III International Flow Battery Forum (IFBF 2012). Munich, June de 2012. Minutes Book. Pages 14-16. ISBN 978-0-9571055-2-2.
- Escudero Gonzalez, J.; Alberola, A.; López-Jiménez, P.A. 2013. Redox Cell Hydrodynamics Modelling. Simulation and Experimental Validation. Engineering Applications of Computational Fluid Mechanics. Volume 7. N 2. Pages 168-181. June 2013. (Factor de Impacto en 2012: 1.144; Q2).
- Escudero-González, J.; López-Jiménez, P.A. 2014. Methodology to Optimize Fluid-Dynamic Design in a Redox Cell. 2014. Journal of Power Sources. Volume 251, 1 April 2014, Pages 243–253. (Factor de Impacto en 2012: 4.675; Q1)
- Escudero-González, E.; López-Jiménez, P.A. 2014. Iron redox battery as electrical energy storage system in the Spanish energetic framework. International Journal of Electrical Power & Energy Systems. Volume 61, October 2014, Pages 421–428. (Factor de Impacto en 2012: 3.432; Q1)
- Escudero-González, J.; López-Jiménez, P.A. Pendiente de publicación. Redox Cell Hydrodynamics Modelling. Towards a Real Improved Geometry based on CFD Analysis. Artículo aceptado para su publicación, en proceso de edición en la revista Engineering Applications of Computational Fluid Mechanics. (Factor de Impacto en 2012: 1.144; Q2).

Abstract

This thesis proposes the use of a methodology that estimates the importance of the electrolyte flow hydrodynamic optimization in electrochemical reactors with experimental validations. This methodology is based on the computational fluid mechanics modelling.

Through the set up and analysis of some indicator parameters, the research described here will allow the implementation of improvements to optimize in a feasible way the current designs of the reactors' cells.

Therefore, the aim of this thesis is to analyse and reveal the different flow paths of the electrolyte inside the chemical reactor through the use of a numerical code that solves the electrolyte fluid mechanics in the proposed geometries. This approach allows, on the one side, to determine some quantifiable parameters which analyse the kindness of the designs in order to obtain flow visualizations and, on the other side, to obtain quantifiable parameters that allow possible optimization designs. The proposed design and parameters are experimentally validated in two different geometries made for that purpose.

This general objective could be subdivided in a series of more specific objectives, which are detailed as follows:

- Study the economic viability based in the Spanish market of this kind of batteries.
- Analyse in depth researches carried out up to now on CFD techniques (Computational Fluid Dynamics) optimisation of the flow channels inside the electrochemical reactor, either through functional methodologies or through other design techniques.
- Evaluate the goodness of the different developed CFD models compared to experimental models, with special attention to the feasibility of the computational model results compared with the physical ones.
- Propose our own parameters in order to quantify the reactor efficiency, based on flow velocity inside the cell.
- Define the best adjustment of the diverse design operators for each of the optimization proposals.

- Obtain an optimal geometry based on the design parameters for the full scale construction cell.

From the proposed methodology, an optimization protocol has been followed regarding the final influence of the electrolyte flow inside the cell.

The developed analysis proves the capital importance in the Spanish energetic sector of the energy storage devices proposed in this thesis. An economic analysis of a particular cell shows that such a battery is economically viable, estimating a return of investment in between 8 to 9 years.

As well, a validated model of an experimental prototype has been developed with lab measurements and numeric simulations that lead to believe that the use of computational fluid dynamics is valid.

Through the use of the commercial software STAR-CCM+ from CD-Adapco©, we have validated an initial scaled down prototype in use at the Electrochemistry Department of the Universidad de Alicante (Spain). This validation gives a mean error of 2.22 % and has estimated some working parameters, such as the fluid volume that circulates along the main flow direction, being this one of an 83 %.

In this thesis, a joint methodology is proposed, based on the obtained experience in the previous phases according to the following concepts: symmetry coefficient, uniformity coefficient, variability range coefficient and rate of fluid circulating in the main direction.

The symmetry coefficient indicates the circulating flow rate difference through each of the two sides of the cell in the longitudinal direction. The uniformity coefficient evaluates the average velocity in the channel. The variability range coefficient analyses the velocity of the fluid in a specific point of the membrane in order to determine the velocity variability. Finally, the defined volume flow in the main direction estimates the laminarity and direction of the flow inside the cell. This methodology is used to optimize the battery by modifying pre-existent dispositions, obtaining a final geometry in which the number of channels before the membrane is 84, with an interchannel separation of 1 mm, validated with experimental pressure and velocity measurements in a prototype at the Justo Nieto mechanical fluids laboratory in the Polytechnic University of Valencia which allows to confirm the purpose numerical model.

The developed battery shows an improved design regarding previous designs. The battery has a perfect symmetry and a uniform distribution when the fluid reaches the membrane with a nearly null volume of circulation in the membrane zone. This battery validates the proposed methodology for the design of this type of elements based on the flow mechanics of the electrolyte inside it.

This thesis includes a conference communication and four articles published in peer reviewed journals indexed in the "Journal Scitation Reports" as detailed below.

- Escudero González, J.; Alberola, A.; López Jiménez, P.A. 2012. Computational Fluid Dynamics Applied to a Prototype Flow Battery. III International Flow Battery Forum (IFBF 2012). Munich, June de 2012. Minutes Book. Pages 14-16. ISBN 978-0-9571055-2-2.
- Escudero Gonzalez, J.; Alberola, A.; López-Jiménez, P.A. 2013. Redox Cell Hydrodynamics Modelling. Simulation and Experimental Validation. Engineering Applications of Computational Fluid Mechanics. Volume 7. N 2. Pages 168-181. June 2013. (Journal Impact Factor in 2012: 1.144; Q2).
- Escudero-González, J.; López-Jiménez, P.A. 2014. Methodology to Optimize Fluid-Dynamic Design in a Redox Cell. 2014. Journal of Power Sources. Volume 251, 1 April 2014, Pages 243–253. (Journal Impact Factor in 2012: 4.675; Q1)
- Escudero-González, E.; López-Jiménez, P.A. 2014. Iron redox battery as electrical energy storage system in the Spanish energetic framework. International Journal of Electrical Power & Energy Systems. Volume 61, October 2014, Pages 421–428. (Journal Impact Factor in 2012: 3.432; Q1)
- Escudero-González, J.; López-Jiménez, P.A. It is awaiting publication. Redox Cell Hydrodynamics Modelling. Towards a Real Improved Geometry based on CFD Analysis. Article in press, accepted for publication in Engineering Applications of Computational Fluid Mechanics. (Journal Impact Factor in 2012: 1.144; Q2).

Resum

La present tesi proposa una metodologia basada en la modelació de la mecànica de fluids computacional per a optimitzar la hidrodinàmica del flux d'electròlit en els reactors electroquímics amb validacions experimentals.

Es presenta una investigació de manera que a través de la proposició i anàlisi d'uns paràmetres indicadors, es puga millorar els dissenys actuals de les cel·les que constitueixen els reactors en aquest estudi i proposar un òptim realitzable.

El objectiu de la present tesi és, per tant, analitzar i revelar els estats de flux de l'electròlit dins del reactor electroquímic utilitzant un codi numèric que resolgui en profunditat, en les geometries proposades la mecànica del flux d'electròlit. Açò permet, per una banda, determinar uns paràmetres quantificables que analitzen la bondat dels dissenys a fi de tindre visualitzacions dels fluxos; i d´una banda, disposar d'aspectes quantificables que permeten l'optimització dels dissenys de l´altra. El disseny i el paràmetres propostos es validen experimentalment en dues geometries diferents desenvolupades per tal fi.

Este objectiu de caràcter general s'ha concretat en una sèrie d'objectius més específics, que són detallats a continuació:

- Realitzar un estudi de la viabilitat econòmica basat en el cas d'Espanya d'este tipus de bateries.
- Realitzar estudi detallat sobre les investigacions realitzades fins a la data relativa a l'optimització per mitjà de tècniques CFD (per les seues sigles a l'anglès: Computaional Fluid Dynamics) de l'interior d'un reactor electroquímic redox, ja siga per mitjà de metodologies funcionals o per mitjà d'un altre tipus de tècniques de disseny.
- Avaluar la bondat dels distints models desenrotllats per mitjà de les tècniques CFD enfront de models experimentals, observant l'adequació dels models computacionals enfront dels models físics.
- Proposar paràmetres propis en este camp per a la quantificació de l'eficiència del reactor basant-se en la velocitat a què circula el fluid en l'interior de la cel·la.

- Definir l'ajust més adequat dels distints operadors de disseny per a cada una de les propostes d'optimització realitzades.
- Obtindrem d'una geometria òptima en funció dels paràmetres de disseny per a la construcció d'una cel·la a escala real.

A partir de la metodologia proposada, s'ha seguit un procés per a la determinació d'un òptim quant al paper que juga el flux del fluid d'intercanvi en l'interior de la cel·la per a desenvolupar una geometria final optimitzada.

A partir dels anàlisis ací desenrotllats, s'ha conclòs la importància que en el sistema energètic espanyol té la tecnologia d'emmagatzemament d'energia que ací es proposa i s'ha realitzat una anàlisi econòmica d'una bateria concreta que avala la viabilitat de les bateries proposades, estimant si és el cas particular un temps d'amortització de 8 anys i mig.

Així mateix s'ha realitzat un model validat para prototip experimental amb mesuraments en laboratori i contrastacions numèriques que avalen l'ús de la fluid-dinàmica computacional que es proposa. A través del programari comercial STAR-CCM+ de CD-Adapco©, s'ha validat un model inicial a escala de laboratori departament d'Electroquímica de la Universitat d'Alacant (Espanya) , en que començar a assajar els paràmetres. Esta validació ha donat uns errors menors del 2,22 % al comparar el model físics amb el numèric. S'han estimat en este primer prototip certs paràmetres de funcionament, com per exemple, el percentatge de volum de fluid circulant en la direcció principal del flux, d'aquesta el 83 %.

La present tesis proposa una metodologia conjunta a la llum de l'experiència adquirida en les fases prèvies basada en la definició dels conceptes següents: coeficient de simetria, coeficient d'uniformitat, coeficient del rang de velocitats i volum de fluid en la direcció principal.

El coeficient de simetria indica la diferència de cabal que circula per ambdós parts de la cel·la en la direcció longitudinal, el coeficient d'uniformitat avalua la velocitat mitjana de cada canal. El coeficient del rang de velocitats analitza la velocitat en un punt específic de la membrana per a determinar la variabilitat del front de velocitat i finalment, el volum de fluid en la direcció principal, el qual quantifica quantificar la laminaritat i direcció del fluid en l'interior de la cel·la. Esta metodologia , s'usa per a optimitzar la bateria basat en modificacions sobre disposicions ja existents de manera que s'arriba a una geometria final en què: el nombre de canals mes apropat de la membrana és de 84, amb una distància de 1 mm entre canals. Esta geometria construïda a escala real i assajada en el Laboratori Justo Nieto de Mecànica de Fluids de la Universitat Politècnica de València està validada amb mesuraments experimentals de pressions i velocitats que permet ratificar el model numèric proposat.

La bateria així dissenyada té pràcticament una simetria perfecta i una distribució uniforme quan el flux aconsegueix la membrana. El 100 % del fluid que transcorre per la zona de membrana circula en la mateixa direcció, la qual cosa provoca que es minimitzen les zones de recirculació o zones mortes. La metodologia així descrita, quantifica la bondat d'un disseny clarament millorat enfront dels ja existents, al mateix temps que valida la metodologia proposada per al disseny d'este tipus d'elements basats en la mecànica del flux de l'electròlit en l'interior de la mateixa.

La bateria així dissenyada té pràcticament una simetria perfecta i una distribució uniforme quan el flux aconsegueix la membrana amb un volum de recirculació en la zona de membrana pràcticament nul. La metodologia així desenrotllada, quantifica la bondat d'un disseny clarament millorat enfront dels ja existents, al mateix temps que valida la metodologia proposada per al disseny d'este tipus d'elements basats en la mecànica del flux de l'electròlit en l'interior de la mateixa.

La present tesis és avalada amb una comunicació a Congrés i quatre articles presentats a revistes indexades en la base de dades "Journal Scitation Reports", com es detallats a continuació.

- Escudero González, J.; Alberola, A.; López Jiménez, P.A. 2012. Computational Fluid Dynamics Applied to a Prototype Flow Battery. III International Flow Battery Forum (IFBF 2012). Munich, June de 2012. Minutes Book. Pages 14-16. ISBN 978-0-9571055-2-2.
- Escudero Gonzalez, J.; Alberola, A.; López-Jiménez, P.A. 2013. Redox Cell Hydrodynamics Modelling. Simulation and Experimental Validation. Engineering Applications of Computational Fluid Mechanics. Volume 7. N 2. pp 168-181. June 2013. (Factor de Impacte al 2012: 1.144; Q2).
- Escudero-González, J.; López-Jiménez, P.A. 2014. Methodology to Optimize Fluid-Dynamic Design in a Redox Cell. 2014. Journal of Power Sources. Volume 251, 1 April 2014, Pages 243–253. (Factor de Impacte al 2012: 4.675; Q1)
- Escudero-González, E.; López-Jiménez, P.A. 2014. Iron redox battery as electrical energy storage system in the Spanish energetic framework. International Journal of Electrical Power & Energy Systems. Volume 61, October 2014, Pages 421–428. (Factor de Impacte al 2012: 3.432; Q1)
- Escudero-González, J.; López-Jiménez, P.A. Pendent de publicació. Redox Cell Hydrodynamics Modelling. Towards a Real Improved Geometry based on CFD Analysis. Article acceptat a la revista i en proccés d´edició a la revista Engineering Applications of Computational Fluid Mechanics. (Factor de Impacte al 2012: 1.144; Q2).

Tabla de contenidos

Capítulo 1:

Introducción

El panorama energético en España está delimitado por las medidas impuestas para reducir las emisiones de CO_2 y la dependencia tanto de los combustibles fósiles como de los suministros de otros países [1]. Así pues, la producción energética generada a partir de fuentes renovables cobra una importancia especial en ese contexto. Sin embargo, la aplicabilidad de esta energía está ligada a la capacidad de almacenamiento para que pueda distribuirse con calidad. En el marco del desarrollo de estas tecnologías de almacenamiento de energía se encuentra el presente trabajo de investigación.

La producción de energía mediante fuentes renovables tiene la ventaja de que no emite CO_2 a la atmósfera y, además, utiliza recursos autóctonos permitiendo reducir la dependencia de los combustibles fósiles. Estos combustibles, en el caso de España, además, son en su mayor parte importados. Por ello, uno de los principales objetivos de la política energética europea es el de acrecentar la utilización de fuentes renovables en la producción de energía. El 9 de marzo de 2007 el Consejo Europeo de Primavera, con el apoyo del Parlamento Europeo y de los Estados miembros, acordó establecer un objetivo vinculante para que el 20 % de su consumo energético de 2020 [2] proceda de fuentes renovables teniendo en cuenta la situación específica de cada Estado Miembro. También adoptó el compromiso de reducir al menos un 20 % sus emisiones de gases de efecto invernadero en 2020 respecto a las de 1990, lograr un ahorro energético en ese año del 20 % y que los biocombustibles alcancen el 10 % del conjunto de los combustibles (gasóleo y gasolina) de transporte consumidos en la UE. El porcentaje asignado a España representaba, exactamente, el 20 % del consumo de energía final.

Se reconoce que la producción y el uso de la energía de hoy en día no es sostenible a largo plazo como consecuencia del previsible agotamiento de los combustibles fósiles y de la amenaza que

representa su uso para el medio ambiente, principalmente debido a las emisiones de gases invernadero (CO_2) y sus consecuencias en el cambio climático. Es por ello que los países industrializados están legislando y apoyando nuevas tecnologías que permitan conseguir que sus energías sean sostenibles en un futuro. Esta sostenibilidad equivale a mantener el crecimiento económico al mismo tiempo que se provee de seguridad energética y se aumenta la protección medioambiental.

El carácter no controlable de las energías renovables da lugar a las crecientes dificultades para operar con seguridad en el sistema eléctrico ya que la aportación de estas energías no ofrece potencia firme, pero sí son de uso inmediato. Esto supone un porcentaje significativo de la capacidad instalada.

La generación de electricidad de origen renovable no presenta firmeza en el suministro ni presta garantía de potencia, aunque sí contribuye a la cobertura de la demanda en términos de energía anual suministrada. En otras palabras, no podemos contar con potencia renovable firme para una hora determinada en el futuro, pero sí podemos saber que al cabo de un largo periodo de tiempo, por ejemplo, un año, habremos producido una cierta cantidad de energía eléctrica. Esta falta de garantía de potencia supone un problema para la operación del sistema ya que ésta requiere potencia firme. Adicionalmente, existen otros problemas ligados a la particular generación de energías renovables. Así, en zonas de mucho consumo y poca generación pueden existir problemas de congestión de la red debido a la saturación de las líneas de transporte.

Las tecnologías de almacenamiento de energía van a desempeñar un papel fundamental en un futuro próximo dentro del marco del aprovechamiento de las fuentes de energía eficiente y renovable como la eólica y solar, que, por lo general, sufren problemas de intermitencia en sistemas de generación distribuida. Las investigaciones más avanzadas van en la dirección de desarrollar elementos que permitan el almacenamiento de energía para su liberación conforme los sistemas de consumo la necesiten [3], [4]. A gran escala, este almacenamiento de energía podría aliviar la imprevisibilidad que tienen las fuentes de energía al favorecer su acumulación en el tiempo [5], [6].

Entre estas tecnologías una de las más prometedoras es la batería redox, como candidata para el almacenamiento de energía a media y gran escala [7]. Estas baterías almacenan energía en soluciones que contienen diferentes parejas redox; los procesos electródicos, reversibles, se llevan a cabo en las superficies de los electrodos (porosos o no) que, a su vez, pueden ser inertes o catalizar la reacción electródica. Las tecnologías redox son excelentes candidatas para grandes almacenamientos de energía y las semi-redox para cantidades intermedias, como podrían ser los sistemas destinados a usos domésticos [8].

La cantidad de energía que almacenan estos dispositivos depende de la cantidad de electrolito que acumulan, mientras que, su potencia es función de la superficie electródica. No se puede separar la etapa de potencia (directamente relacionada con la masa activa del electrodo) de la de acumulación de energía, ya que, el reactivo limitante para la acumulación es el mismo electrodo [9].

Por lo tanto, este tipo de baterías permiten modular sus voltajes de salida y capacidades de almacenamiento conectando múltiples celdas y usando depósitos de diferentes tamaños. Esta circunstancia las hace ideales como potenciales sistemas de almacenamiento de energía de generación distribuida cuyos requisitos dependen de las necesidades de distribución de cada sistema.

Para almacenamientos de ciertas energías renovables las soluciones electroquímicas son muy adecuadas ya que tienen entradas y salidas exclusivamente eléctricas, su potencia y capacidad de almacenamiento pueden cambiarse de forma modular y pueden instalarse relativamente cerca de los puntos de consumo [9]. Así, en la década de los años 70, aparecen los primeros tipos de acumuladores electrolíticos. Las primeras baterías eran de zinc como material anódico, combinados con oxígeno y pronto con cloro o bromo. En 1974 Thaller propone el primer concepto de celdas redox [10]. En 1980 Hagedorn y colaboradores publicaron los primeros resultados obtenidos en este tipo de prototipos [11]. Desde entonces, se han sucedido los diferentes prototipos de celdas destacando, entre otros, el paso a los acumuladores redox Fe/Cr [12].

En la actualidad, estos prototipos se siguen utilizando. En el desarrollo que se realiza para dichos prototipos, el estudio hidrodinámico (relación del flujo con la eficiencia) adopta especial importancia con el desarrollo del CFD, encontrando ciertos precursores del presente trabajo en el pasado reciente [9], [13]. Un interesante resumen de las baterías redox es presentado en Weber y colaboradores [8] que indican, entre sus conclusiones, que el futuro de la presente tecnología pasa por la modelación de la mecánica del flujo optimizando los diseños: flujo y transporte.

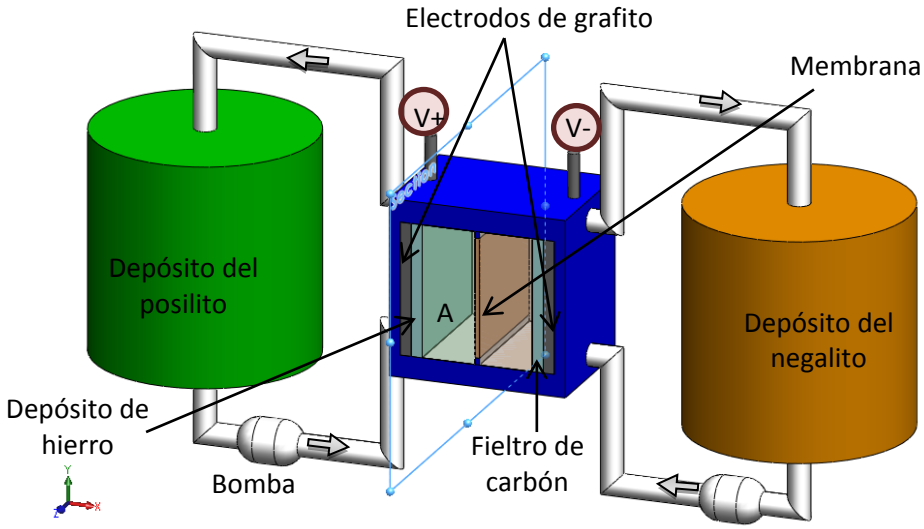

Figura 1. Esquema típico de un reactor electroquímico genérico.

La Figura 1 muestra el diagrama conceptual de un reactor electroquímico redox. Los dos tanques de almacenamiento de electrolito se representan como dos cilindros a los lados de la figura. El depósito sobre el electrodo negativo mantiene uno de los pares redox en disolución y el tanque positivo mantiene el segundo par redox en disolución. Hay dos bombas, una en cada lado de la celda (Figura 1). Éstas obligan a circular a través de la celda el electrolito con el fin de permitir que tengan lugar las semi-reacciones redox y se produzca una transferencia de carga.

La estructura de la celda está rodeada por placas bipolares: apoyo estructural y conductor eléctrico. Por el lado de cada placa bipolar se encuentra los electrodos. Estos no forman parte de las reacciones electroquímicas, pero proporcionan una superficie que facilita el camino de los electrones. Entre los dos lados de la celda se ubica la membrana: separación física entre los dos electrolitos para que no se mezclen, preservando la electro-neutralidad.

El volumen indicado como "A" (Figura 1) está ocupado por el electrolito. El prototipo analiza el flujo indicado de forma horizontal, con una geometría y caudal similares a la celda real.

Muchos son los aspectos de interés. Materiales clave: electrolito, electrodo y membrana [14], siendo las baterías de Vanadio las más conocidas, con análisis más profundos tanto en el campo teórico como de la modelación [15], [16].

La uniformidad de flujo tiene una influencia notable en el área eficaz del electrodo, la resistencia y la eficiencia, la vida útil de la batería y la polarización electroquímica, especialmente, bajo la alta variación de densidad de corriente.

Las referencias consultadas [5] proponen que el flujo del electrolito a través de la capa activa tiene una gran inferencia en el rendimiento del mismo. Moyabayashi y sus colaboradores [17] concluyen

que la distribución uniforme de electrolito es fundamental a fin de aumentar la eficiencia energética. No obstante, aunque el flujo sea homogéneo, hay importantes variaciones locales en la superficie de los electrodos, entre otras, fuertes cambios de pH. El análisis entre diferentes geometrías y las condiciones de flujo en la celda redox han sido consideradas en la bibliografía para conocer y mejorar el funcionamiento del conjunto de la celda [18], [19].

A causa del sistema de batería totalmente compacto, de que los materiales clave son completamente opacos y de la fuerte acidez del electrolito, la distribución del fluido dentro de la batería suele ser difícil de determinar y (más importante) de visualizar, medir y cuantificar. Sin embargo, todas las investigaciones coinciden en que es fundamental [20], [21].

Capítulo 2:

Objetivos

La presente tesis propone una metodología para optimizar la hidrodinámica en las celdas de reactores electroquímicos, por tanto, los objetivos están relacionados con la implementación de técnicas numéricas con validación experimental para avalar la metodología que se propone. En consecuencia, el propósito de la presente tesis es analizar y revelar los estados de flujo del electrolito dentro de la batería utilizando un código numérico que resuelva con exactitud, en la geometría que nos ocupa, la mecánica del flujo del mismo.

Ello permite determinar unos parámetros cuantificables que indiquen la bondad de los diseños en aras de tener visualizaciones de los flujos e indicadores que permitan la optimización de los diseños.

De esta forma, el objetivo fundamental de la tesis es el desarrollo y aplicación de las técnicas CFD para la optimización eficiente de un reactor electroquímico. Este objetivo de carácter general puede dividirse en una serie de objetivos más específicos que se detallan a continuación:

- Obtener una geometría óptima en función de los parámetros de diseño para la construcción de una celda a escala real para proponer una geometría final optimizada.
- Realizar un estudio de la viabilidad económica basado en el caso de España para este tipo de baterías.
- Realizar un estudio detallado acerca de las investigaciones realizadas hasta la fecha relativa a la optimización mediante técnicas CFD del interior de un reactor electroquímico redox, ya sea mediante metodologías funcionales o mediante otro tipo de técnicas de diseño.

- Evaluar la bondad de los distintos modelos desarrollados mediante las técnicas CFD frente a modelos experimentales, observando la adecuación de los modelos computacionales frente a los modelos físicos.
- Proponer parámetros propios en este campo para la cuantificación de la eficiencia del reactor en base a la velocidad a la que circula el fluido en el interior de la celda.
- Definir el ajuste más adecuado de los distintos operadores de diseño para cada una de las propuestas de optimización realizadas.
- Obtener una geometría óptima en función de los parámetros de diseño para la construcción de una celda a escala real.

En términos generales, el desarrollo de la tesis puede dividirse en cuatro grandes bloques interconectados entre sí: en primer lugar, un primer análisis del estado del arte, la situación y posible rol de la presente tecnología en el panorama energético Español; en segundo lugar estudio de una celda prototipo sin geometría real industrializable, basado en celdas existentes; en tercer lugar, las posibilidades de la tecnología de la modelación del flujo y las deficiencias observadas en prototipos previos, propuesta de un procedimiento de diseño basado en la propuesta de parámetros indicadores de la eficiencia en el papel que juega el flujo del electrolito de una batería a escala real; por último la implementación de la metodología propuesta en un caso a escala real para la validación de la propuesta metodológica previamente indicada constatándose a través de la medición experimental los parámetros que se han propuesto para el análisis del funcionamiento hidráulico del conjunto de la celda diseñada, verificando la mejora en dicho diseño con respecto a prototipos anteriores.

Capítulo 3:

Resultados y discusión

Los resultados de la presente investigación se obtienen en base a las etapas propuestas para la consecución de los objetivos de este trabajo. Cada etapa corresponde a una de las cuatro publicaciones que se han realizado en el marco de esta tesis.

Como denominador común en todos los artículos, a excepción de aquel que tiene por objetivo un análisis de las diferentes alternativas y de la viabilidad económica de la batería estudiada, se tiene el uso de un software comercial de CFD a través de un modelo validado y calibrado según mediciones experimentales. Como introducción en este capítulo dedicado al análisis de resultados, se presentan las características generales del modelo implementado y la estrategia utilizada para establecer la sensibilidad de la malla. La calibración y validación de los casos concretos se detallan en cada uno de sus correspondientes anexos.

En la primera etapa de la presente tesis se presenta una visión general de los sistemas de almacenamiento electroquímicos teniendo en cuenta las diferentes aplicaciones, ventajas y desventajas. En base a la revisión y a las posibles aplicaciones de cada tecnología se ha seleccionado la batería redox en base hierro y se ha analizado desde un punto de vista económico la determinación de aspectos tan importantes como la recuperación de la inversión o la tasa de retorno en el marco del panorama energético español (ANEXO I).

A continuación, en una segunda etapa, desarrollada de forma casi paralela con la anterior, se ha realizado un primer estudio de caracterización de prototipo de reactores electroquímicos con celdas montadas en paralelo. El objeto de esta etapa inicial ha consistido, básicamente, en obtener una visión general de los diversos aspectos que intervienen en la hidrodinámica de la celda.

Se han estudiado aquí los fenómenos entrada/salida, de especial relevancia en reactores de dimensiones reducidas en los que no se puede llegar a desarrollar un patrón de flujo definido, así como las variaciones en la hidrodinámica de los sistemas a escala prototipo para pasar en siguientes etapas de esta escala inferior de trabajo a una superior (ANEXO II).

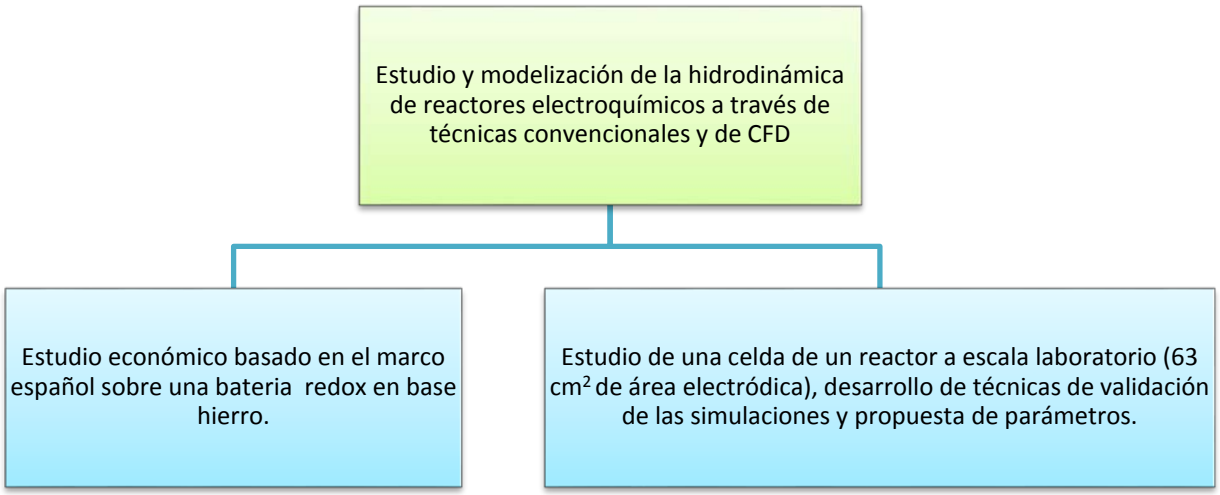

Figura 2. Esquema del presente trabajo. Primera y segunda etapas.

Esta etapa sirve para tener un conocimiento bastante pormenorizado de la hidrodinámica de estos sistemas, así como, para poner a punto diversas técnicas de caracterización y estudio de reactores a través de la modelación computacional validada con las mediciones desarrolladas en el laboratorio del Departamento de Electroquímica de la Universidad de Alicante.

En la tercera etapa del trabajo, a la vista de las aplicaciones posibles de la batería analizada y de la forma de analizar el prototipo propuesto, se ha propuesto una metodología para el análisis y la optimización de este tipo de estructuras basado en el flujo del electrolito (ANEXO III).

En esta etapa se abordó un caso de optimización concreto iniciándose un estudio mediante técnicas numéricas de simulación computacional de una celda de un reactor a escala real.

En este estudio de investigación se aportan varios parámetros para realizar la toma de decisiones en el rediseño y la optimización de reactores electroquímicos, de difícil acceso de otra forma, en base a su hidrodinámica y se contrastan de forma experimental en una geometría construida a escala real.

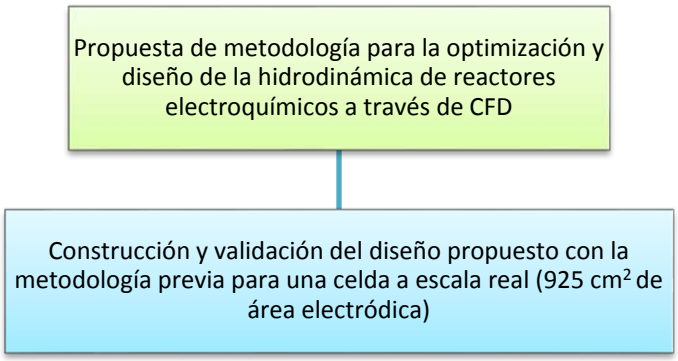

Figura 3. Esquema del presente trabajo. Tercera y cuarta etapas.

Finalmente, se ha aplicado la estrategia de optimización propuesta en la tercera etapa a través de los indicadores de un buen diseño hidrodinámico para obtener y construir un diseño mejorado de celda. Con ello se ha validado la propuesta metodológica empleada basada en estudios de CFD y se ha contrastado experimentalmente la bondad de dicho diseño en referencia a la uniformidad y simetría de las velocidades del fluido del electrolito (ANEXO IV).

Uno de los resultados más importantes de la presente investigación es la propuesta metodológica basada en la aplicación de la CFD para buscar la uniformidad de velocidades en el fluido del electrolito descrita en la tercera etapa de esta tesis. La figura 4 describe en mayor detalle esta metodología (ANEXO III) en base a los parámetros propuestos: coeficiente de simetría evaluado a la entrada de la celda; coeficiente de uniformidad evaluado a la salida de los últimos canales de uniformización del flujo y coeficiente del rango de velocidades evaluado el inicio de la membrana.

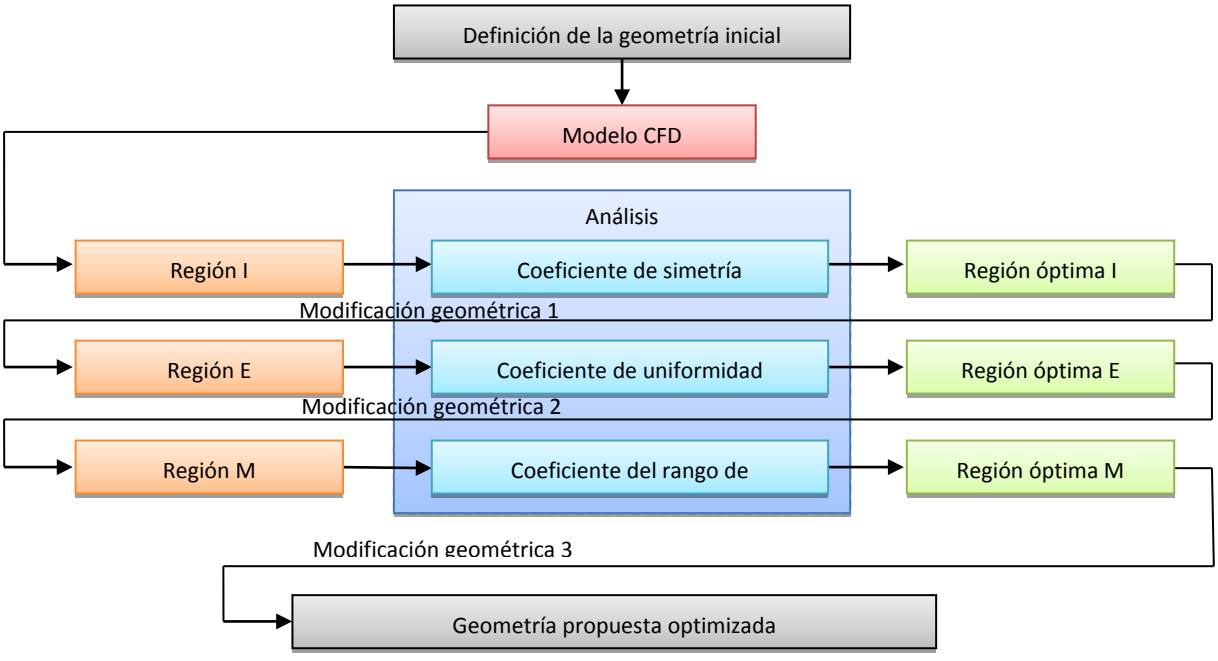

Figura 4. Metodología desarrollada en la etapa tercera de la presente tesis (ANEXO III).

Finalmente, la metodología descrita en la Figura 4 basada en la definición de parámetros indicadores de la uniformidad y simetría del flujo, así como la experiencia adquirida en la modelación y diseño de baterías redox sirven al doctorando para proponer una estructura de batería basada la metodología y en los parámetros indicadores desarrollados. Esta celda ha podido implementarse de forma física y las magnitudes hidrodinámicas han sido medidas de manera experimental en el laboratorio Justo Nieto de Mecánica de Fluidos de la Universidad Politécnica de Valencia, con lo que se ha validado la metodología y el diseño propuestos.

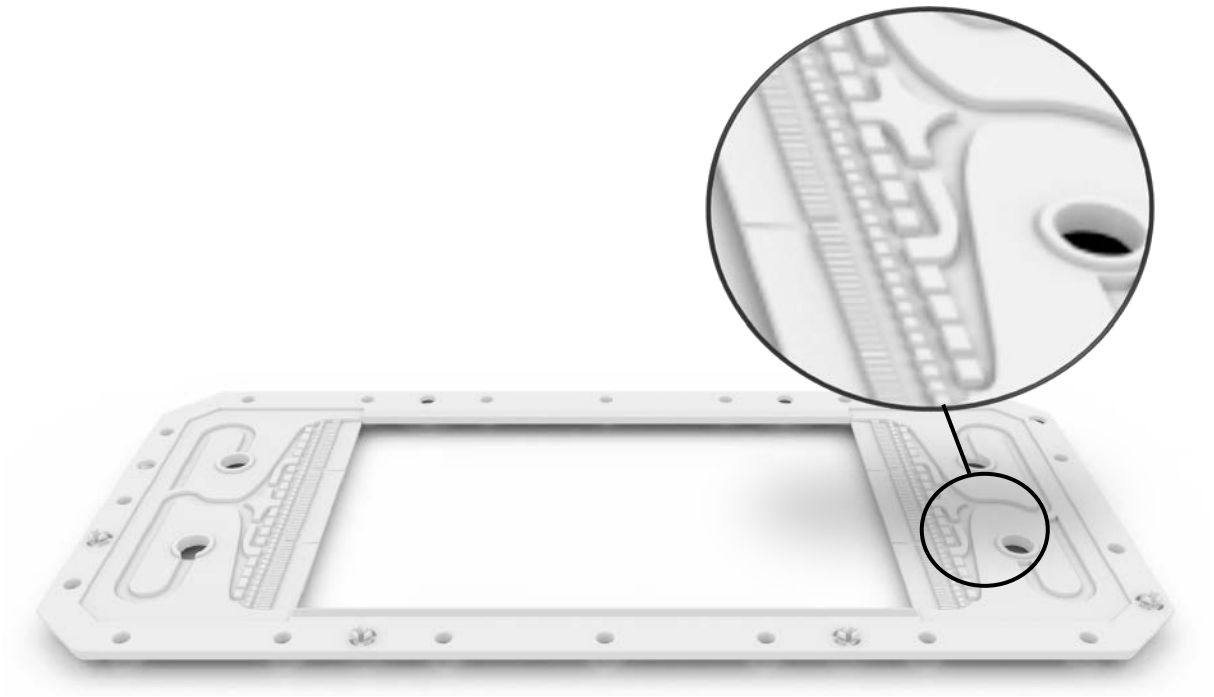

Figura 5. Diseño final de la celda redox propuesta en la presente tesis de un reactor.

A continuación se detallan los principales hitos de los artículos que avalan la presente investigación.

3.1. El modelo CFD

La fluidodinámica computacional es una técnica bien conocida desde hace algunas décadas, que permite la resolución numérica de las ecuaciones representativas del movimiento de fluidos en volúmenes de control bajo ciertas condiciones de contorno. Una vez se dispone de las condiciones de frontera bien definidas y una malla adecuada en toda la extensión del modelo, los códigos computacionales implementados resuelven las ecuaciones del movimiento (conservación de la masa o continuidad; y conservación de la cantidad de movimiento o Navier Stokes).

En la presente tesis, se han realizado simulaciones tridimensionales utilizando el software STAR-CCM+. El código empleado está basado en el método de volúmenes finitos (FVM) para resolver la ecuación de la conservación de la masa y las ecuaciones promediadas de Navier-Stokes en un

mallado curvilíneo, no teniendo en cuenta los efectos de la temperatura. Con el fin de cumplir la condición de conservación de la masa se usa un algoritmo de corrección de presión estándar (SIMPLE). De esta forma, el código resuelve algebraica e iterativamente las ecuaciones hasta que los valores de los residuos numéricos son suficientemente bajos (menores de 10^{-3}) y se considera que la resolución ha convergido. Se ha utilizado el modelo de flujo segregado ya que este resuelve las ecuaciones de flujo (uno para cada componente de la velocidad, y uno para cada componente de la presión) de manera separada. El vínculo entre las ecuaciones de movimiento y la continuidad se logra con un enfoque predictor-corrector. La formulación completa se puede describir como el uso de un arreglo de variables yuxtapuestas y un acoplamiento presión-velocidad resuelto en la conocida interpolación *Rhie-Chow*.

En régimen turbulento, al no anularse las tensiones de Reynolds, se necesitan soluciones de cierre que aporten las ecuaciones suficientes para conocer las velocidades instantáneas en todo el dominio. En este caso, la turbulencia aparece en todas las geometrías estudiadas en la entra y salida del reactor. Se ha utilizado el modelo *realizable (o RNG) k-Ɛ* que a bajos números de Reynolds funciona bien. Este es un modelo semi-empírico basado en las ecuaciones de transporte de la energía cinética turbulenta (*k*) y del rango de disipación (*Ɛ*).

Una hipótesis de trabajo importante ha sido asumir que el fluido electrolítico no produce ninguna deposición dentro del reactor así como tampoco produce ninguna fase gaseosa dentro del mismo. Otra premisa que se ha supuesto es referente a la densidad del fluido. Se considera una densidad constante para todo el flujo. La viscosidad del fluido electrolítico a 40ºC es la misma que la del agua a 20ºC, por ello, junto con la facilidad de manejo del agua, es conveniente el uso de la misma como fluido de trabajo en el modelo experimental, sin considerar otras variaciones que ocurrirán con el fluido real, como el pH y la conductividad.

En general, se ha definido una velocidad de entrada que corresponde al caudal de entrada al modelo, una condición de contorno correspondiente a la presión de salida del modelo y una condición de pared para todas las demás fronteras. La condición de pared que utiliza el código computacional se asimila a la llamada '*rugosidad de tubo liso'* que se adecua bien a las características del material del que se ha construido los prototipos.

Para el mallado volumétrico se ha escogido los elementos hexaédricos adaptados a la superficie, se ha aplicado un refinamiento de la malla en la superficie para que la malla se adapte correctamente a la misma. En todas las simulaciones se realizado un análisis de sensibilidad de la malla para verificar la independencia de la de malla. Se han simulado diferentes tamaños de malla y se han comparado las predicciones en las celdas entre sí. La condición para que se cumpla la independencia de la malla

es: la diferencia de presión entre la entrada y la de salida del reactor (malla primera) respecto al mismo parámetro evaluado en una segunda malla sea inferior al 1 %.

3.2. La batería redox en base hierro como sistema de almacenamiento eléctrico en el marco energético español

Este primer punto está basado en el artículo:

> *Escudero-González, E.; López Jiménez, P.A. 2014. Iron redox battery as electrical energy storage system in the Spanish energetic framework. International Journal of Electrical Power & Energy Systems. Volume 61, October 2014, Pages 421–428*.

Esta revista tiene un factor de impacto en 2012 de 3,432, en el área Engineering, Electrical & Electronic. En esta área ocupa la posición 13 de 243 revistas indexadas, perteneciendo claramente al primer cuartil de su clasificación (Q1).

Resumen del artículo aportado

Los dispositivos de acumulación son necesarios en el marco de un aprovechamiento energético de fuentes alternativas, ya que son imprescindibles para que la energía que se produce en situaciones punta temporalmente localizadas puedan utilizarse en otros momentos en los que la demanda sea adecuada; y, sin embargo, no haya producción. En este sentido en el artículo descrito en el Anexo I se presenta una panorámica de los dispositivos de acumulación en el marco del sistema eléctrico español; y, dentro de ellos, se ubica la batería redox en base hierro como una alternativa viable y con grandes beneficios económicos, sociales y ambientales para la sostenibilidad que hace que sea una tecnología muy recomendable. La presente afirmación se acompaña de un análisis numérico que permite establecer de forma inicial un estudio económico del dispositivo que se presenta.

La capacidad mundial de almacenamiento de la red eléctrica es de aproximadamente de 127 GW y esta aumenta cada año, por lo que un sistema de almacenamiento de energía es más que nunca una necesidad. En la actualidad muchos tipos diferentes de dispositivos pueden ser utilizados para almacenar electricidad. Esta necesidad de almacenar energía aumenta a medida que el uso de las energías renovables se vuelve más importante en los balances nacionales.

Las baterías electroquímicas son una de las tecnologías más utilizadas para el almacenaje de la energía. Éstas son muy convenientes y se pueden adaptar fácilmente a las necesidades de la red proporcionando un buen rendimiento. Diferentes tecnologías de baterías electroquímicas han sido desarrollado en los últimos años: las baterías de plomo, baterías de sodio/azufre, baterías de níquel-cadmio, baterías de litio y la batería redox en base hierro.

En el artículo descrito en el Anexo I se han citado y descrito los beneficios de las alternativas presentadas anteriormente. Estos beneficios se basan en aspectos tanto operativos como económicos. Comparando todas estas posibles soluciones se ha observado que la batería redox en base hierro se posiciona como una alternativa prometedora para el sistema ya que se trata de una batería con un alto número de ciclos de vida y con un coste menor que otras baterías. Este tipo de baterías son de larga duración (aproximadamente 25 años) siendo muy beneficioso para aplicaciones donde la energía se debe almacenar durante mucho tiempo.

Sobre la base del análisis comparativo se ha hecho un estudio para el caso particular de la batería redox en base hierro aplicado al sistema español de tarifas eléctricas. La batería que se ha utilizado para el análisis tiene las siguientes características: una capacidad de almacenamiento de 21 kW h, una potencia de 3 kW y una eficiencia de ciclo del 70 %.

En este caso concreto la amortización de la inversión de esta batería se produce entre el octavo y noveno año. Este es un plazo muy razonable para el retorno de la inversión ya que la vida útil de esta batería es de 25 años.

3.3. Estudio hidrodinámico de una celda a escala de laboratorio: simulación y validación

Este segundo punto está basado en el artículo:

> *Escudero Gonzalez, J.; Alberola, A.; López-Jiménez, P. A. 2013. Redox Cell Hydrodynamics Modelling. Simulation and Experimental Validation. Engineering Applications of Computational Fluid Mechanics. Vol 7. N 2. pp 168-181. June 2013.*

Esta revista se encuentra indexada en la base de datos de Journal Citation reports, en la que tiene un factor de impacto en 2012 de 1,144, indexada en las áreas "Engineering, Multidisciplinary" y "Engineering, Mechanical" ocupando la posición 26 de un total de 90 revistas indexadas y la posición 40 de 125 revistas, en ambas áreas respectivamente. Se encuentra por tanto en el segundo cuartil, (Q2), pero primer tercio en las dos materias en que se indexa.

Resumen del artículo aportado

Un reactor electroquímico es un ensamblaje de celdas capaces de soportar una reacción electroquímica para una aplicación dada. Básicamente se compone de electrodos rodeados por un volumen de electrolito líquido. La mayor dificultad de modelar y simular este tipo de reactores es el

hecho de que los fluidos que circulan por el interior tienen un pH muy bajo y por lo tanto son muy ácidos. Para superar esta problemática se ha propuesto un modelo de cálculo adecuado para ser utilizado como un laboratorio virtual. Esta es una gran herramienta para los diseñadores de baterías redox ya que pueden realizar multitud de experimentos sin la necesidad de fabricar una infinidad de reactores prototipos.

En este artículo se ha propuesto un modelo numérico para analizar el flujo del electrolito líquido en una celda de un reactor electroquímico a escala laboratorio. Además, se ha validado experimentalmente la celda prototipo pudiendo calibrar el modelo computacional. Para poder medir la presión se ha utilizado 5 tubos piezométricos distribuidos equitativamente por toda la celda. Se ha utilizado metacrilato translúcido para cerrar la celda y así poder visualizar las líneas de corriente del flujo mediante un tinte. De este modo, se muestra el comportamiento hidráulico en toda la celda observándose zonas prácticamente sin velocidad o con recirculaciones.

En este segundo artículo se ha desarrollado un modelo numérico sobre la base de un código comercial utilizado para resolver las ecuaciones de la mecánica de fluidos (Star CCM+ de Adapco©). Por medio de la resolución de las ecuaciones de presiones, velocidades y líneas de corriente se ha conocido en todo el volumen el comportamiento del fluido en el interior de la celda. Con una geometría similar a la del modelo computacional se ha construido un modelo físico y se han desarrollado las mediciones de presión en los mismos puntos del prototipo real y en los mismos instantes de tiempo en el laboratorio del Departamento de Electroquímica de la Universidad de Alicante. Estos análisis muestran una gran concordancia entre los valores modelados y medidos. Para poder cuantificar las bondades del CFD se ha utilizado el error cuadrático medio (RMSE) para la comparación entre las diferentes medidas de presión. El RMSE ha variado desde 0,69 % para un caudal de 70 l/h hasta un 2,22 % para un caudal de 100 l/h. Este valor aumenta según crece el número de Reynolds.

En este artículo se ha propuesto un parámetro para cuantificar la laminaridad y dirección del fluido en el interior de la celda estudiada: volumen de fluido en la dirección principal. Un valor grande de este parámetro representa la uniformidad del fluido, evitando caminos preferenciales y la aparición de turbulencia en el interior de la celda. En el prototipo considerado, este valor es de alrededor de 83 %, lo que permite la posibilidad de realizar mejoras de diseño. Este parámetro permite al diseñador poder comparar diferentes geometrías basándose en la uniformidad del flujo mediante las técnicas de CFD. El modelo simplificado arroja luz sobre el comportamiento hidrodinámico del flujo completo en la celda prototipo.

La posibilidad de contar con un modelo numérico versátil como un laboratorio virtual como el aquí realizado, permite facilitar la toma de decisiones al diseñador. Como resultado de la investigación se postula la aplicación de técnicas de CFD como una herramienta clave para futuros desarrollos en este campo.

3.4. Metodología para optimizar el flujo en el interior de una celda redox

Este tercer punto está basado en el artículo:

> *Escudero-González, J.; López-Jiménez, P. A. 2014. Methodology to Optimize Fluid-Dynamic Design in a Redox Cell. Journal of Power Sources. Volume 251, 1 April 2014, Pages 243–253.*

Esta revista se encuentra indexada en la base de datos de Journal Citation reports, en la que tiene un factor de impacto en 2012 de 4,675 en las áreas de Electrochemistry y Energy and Fuels. Ocupan la posición: 3 de 26 revistas y 9 de 81 revistas respectivamente, estando en ambas claramente en el primer cuartil (Q1).

Resumen del artículo aportado

La batería redox estudiada en este tercer artículo consiste en un dispositivo diseñado para convertir la energía de los reactivos en energía eléctrica mediante la reacción de un electrolito líquido en el electrodo. En este tipo particular de celdas, los dos electrolitos están presentes circulando por el interior de la celda separados por una membrana de intercambio de protones. Por tanto, el flujo del electrolito y la interacción con la membrana tiene una importancia primordial para el rendimiento del conjunto de la batería.

En este artículo (Anexo III) se ha descrito la metodología para el diseño de la parte de entrada de la celda en base a la optimización de la uniformidad del flujo y la posición inicial de la membrana. Del modelo de CFD junto con el estudio estadístico se han obtenido varias conclusiones prácticas sobre la manera de mejorar la construcción de la geometría final.

La metodología utilizada se ha basado en la definición de tres indicadores: el coeficiente de simetría, el coeficiente de uniformidad y el coeficiente del rango de velocidades. Estos parámetros pueden ayudar a cuantificar la uniformidad de flujo en el diseño final de las celdas de un reactor.

El coeficiente de simetría indica la diferencia de caudal que circula por ambas partes de la celda en la dirección longitudinal. Se ha desarrollado un profundo análisis CFD con el fin de conseguir los caudales circulantes por ambas partes de la celda.

El coeficiente de uniformidad evalúa la velocidad media de cada canal. En este caso en particular, el objetivo es mantener una velocidad constante dentro de la celda. Con el fin de definir este coeficiente se ha desarrollado un test de hipótesis sobre la base de las velocidades obtenidas de los resultados de CFD para comparar los perfiles de velocidad.

Finalmente se propone el coeficiente del rango de velocidades. Este analiza la diferencia de velocidad en un punto específico determinando la variabilidad del frente de velocidad. Mediante este parámetro se pretende encontrar la posición más conveniente para la colocación de la membrana en donde el frente de velocidad es lo más uniforme posible estando lo más cerca posible de los últimos canales de la geometría.

El estudio de estos tres parámetros permite al diseñador determinar el número de canales de entrada, la forma de estos canales, la distancia entre ellos y la configuración de la geometría de entrada con el fin de obtener una velocidad uniforme en el contacto entre la membrana y el fluido del electrolito.

Se ha estudiado un caso particular para ilustrar la capacidad de la metodología descrita. Se ha diseñado una geometría óptima de una celda para un caudal de diseño de 150 l/h. En este caso, los parámetros propuestos se han utilizado para determinar la geometría más conveniente entre muchas alternativas diferentes. Se ha propuesto un diseño final, en la que sólo el 4,8 % de los canales tiene un valor diferente entre sí, por lo que el frente de velocidades al contacto con la membrana es muy uniforme.

Este caso de estudio es una propuesta que se construye y valida en la siguiente etapa de la presente tesis. En posteriores investigaciones, esta geometría se construye con el fin de validar la distribución de velocidades proporcionada por el CFD y la metodología que aquí se propone.

3.5. Validación experimental de la metodología propuesta basándose en un análisis CFD

Por último este cuarto epígrafe está basado en el artículo en proceso de publicación *'Redox Cell Hydrodynamics Modelling – Towards a Real Improved Geometry based on CFD Analysis*' (Anexo IV) aceptado para su publicación y en proceso de edición en la revista: *'Engineering Applications of Computational Fluid Mechanics'* el cual en 2012 tiene un índice de impacto de 1,144.

Resumen del artículo aportado

Una celda redox es un conjunto que consta de electrodos rodeados por un volumen de electrolito (líquido). El dispositivo almacena energía eléctrica en el líquido que está en constante movimiento. Este fluido es muy ácido y esta acidez provoca grandes dificultades para el diseño físico. Para superar este problema se ha desarrollado un análisis numérico y experimental del fluido en una celda redox real. Se propone una validación de la metodología anteriormente descrita para mejorar el rendimiento de las celdas redox basado en el análisis del flujo del electrolito.

En este artículo se ha descrito una geometría de una celda redox desarrollada y mejorada previamente diseñada por los autores. Para realizar estas mejoras en esta celda redox real la metodología se basa en un análisis CFD previamente validado con datos experimentales.

Los parámetros cuantificados y validados en esta geometría han sido: coeficiente de simetría, coeficiente de uniformidad, el coeficiente del rango de velocidades y el volumen de fluido en la dirección principal. Este diseño ha sido construido y ensayado en el Laboratorio de Mecánica de Fluidos de la Universidad Politécnica de Valencia (España) mediante un material transparente y se ha utilizado un tinte para el análisis de velocidades.

Se ha propuesto una metodología para la validación del modelo experimental para un caudal de 50 l/h. Se ha validado el modelo computacional con el modelo experimental mediante la presión y la velocidad obteniendo una convergencia aceptable entre ellos. Esto conduce a dos conclusiones: el diseño propuesto es adecuado para mejoras y los parámetros de la geometría considerados son una herramienta poderosa para los diseños de celdas similares.

Los parámetros propuestos se refieren a la uniformidad de la velocidad en diferentes regiones de la celda. En este caso particular, el coeficiente de simetría muestra una diferencia de flujo de 4 % entre ambos lados de la geometría. El coeficiente de uniformidad indica que un 8 % de los canales son estadísticamente diferentes entre sí en base a sus velocidades. El coeficiente del rango de velocidades es de 0,015 m/s; esto asegura un flujo uniforme en toda la membrana. Se ha verificado que en la zona de la membrana no aparecerán zonas muertas ni turbulencias. Estos tres parámetros

descritos anteriormente garantizan mejoras significativas y uniformidad de flujo por toda la superficie de la membrana.

El modelo validado permite a los diseñadores poder analizar las velocidades dentro de toda la geometría. En este caso el volumen en las que el fluido circula en la dirección predominante del flujo en la sección de la membrana es del 0 %. Este hecho mejora considerablemente los diseños anteriores en los que este valor rondaba el 83 %.

Analizando estos cuatro parámetros, en este artículo se ha mejorado sustancialmente la superficie de la membrana útil para favorecer el mejor intercambio iónico disminuyendo las zonas problemáticas. Así, se da validez a la metodología basada en el uso de CFD para diseñar celdas redox y se dispone de un modelo mejorado para el reactor electroquímico.

Capítulo 4:

Conclusiones y aportaciones

La presente tesis describe la metodología del diseño de celdas de reactores electroquímicos basada en los parámetros de la hidrodinámica del flujo del electrolito en su interior. Las conclusiones y aportaciones de este trabajo conjunto se detallan y analizan a continuación.

- **La hidrodinámica del flujo del electrolito es fundamental en la eficiencia del conjunto del reactor: la uniformidad y simetría del campo de velocidades determinan de forma directa el funcionamiento de la celda.**

  Si la velocidad del fluido del electrolito es uniforme, el intercambio iónico que ocurre a través de la membrana existente en la celda, se realiza simultáneamente y las deposiciones de hierro son homogéneas en todo el electrodo. En cambio, si dicha velocidad no es uniforme aparecen deposiciones locales de hierro pudiendo romper la membrana y favoreciendo el incremento sucesivo de la turbulencia. Esto hace que disminuya el rendimiento del reactor.

  El parámetro crítico en este análisis es el campo de velocidades del fluido del electrolito en la celda del reactor. El análisis detallado de este parámetro solamente se puede realizar a través de técnicas de fluidodinámica computacional al ser imposible realizar un ensayo con fluido del electrolito real con ese gran nivel de detalle.

  Por tanto, la velocidad debe ser lo más uniforme posible en todo el conjunto de la celda, para lo cual, dada la distribución lateral de las entradas y salidas diseñadas para la posterior industrialización del reactor, este campo de velocidades debe asegurarse una simetría a lo

largo de su eje longitudinal. Los parámetros que se refieran a la uniformidad y simetría del flujo serán determinantes para conseguir un buen diseño final.

- **Es necesario proponer parámetros que permitan la cuantificación de esta uniformidad en el interior de la geometría de las celdas del reactor para permitir la comparación entre diferentes celdas de reactores similares.**

  Para ello en la presente tesis se aportan los siguientes parámetros de diseño:

  COEFICIENTE DE SIMETRIA

  Este parámetro se propone para evitar el problema de un mal reparo de caudales en el interior del reactor derivado del hecho de tener las entradas y salidas de los fluidos en los laterales. Para solucionar esa asimetría se ha decidido diseñar una geometría que permita compensar la inercia del fluido. Este coeficiente se define como la diferencia en porcentaje del caudal que circula por un lado de la geometría y por el otro, evaluado en la primera bifurcación del canal de entrada o salida (región I). El flujo será completamente simétrico cuando este parámetro tienda a 0.

  El coeficiente de simetría es:

$$C_{Simmetry}(\%) = \frac{|Q_{x>0}| - |Q_{x<0}|}{|Q_{x>0}| + |Q_{x<0}|} \cdot 100$$

  donde:

  $Q_{x>0}$: caudal en el lado derecho de la geometría.

  $Q_{x<0}$: caudal en el lado izquierdo de la geometría.

  COEFICIENTE DE UNIFORMIDAD

  Para analizar la posible presencia de caminos preferenciales en el interior de la celda se propone el coeficiente de uniformidad. Este coeficiente tiene el objetivo de igualar todas la velocidades en el miso eje transversal. Para resolver el problema de la no uniformidad del campo de velocidades, se ha decido realizar un diseño en forma de peine que vaya igualando todas las velocidades en el interior de la celda. Este coeficiente se evalúa en la última zona de canales (región E).

Para evaluar este coeficiente es necesario realizar un test de hipótesis sobre los resultados obtenidos de la CFD para el campo de velocidades del flujo electrolito en la zona de los canales.

El coeficiente de uniformidad se define como la diferencia entre que se cumpla la hipótesis nula o que se cumpla la hipótesis alternativa. La hipótesis nula es cierta cuando la velocidad de un canal es igual a la velocidad de otro canal. En caso contrario la hipótesis es falsa. Se comparan todos los canales uno a uno evaluando la hipótesis nula. Para este caso en particular se han evaluado 3486 hipótesis.

Una geometría será más uniforme cuando este coeficiente tienda a cero. El coeficiente de uniformidad se define como:

$$C_{uniformity}(\%) = \frac{\sum\left(-z_{\alpha/2} \le Z \le z_{\alpha/2}\right)}{\sum(Z)} \cdot 100$$

donde:

α: 0,05 (nivel de significación).

$(-z_{(\alpha/2)} \le Z \le z_{(\alpha/2)})$ es la región de aceptación.

Z es el estadístico de contrate utilizado (t-Student).

COEFICIENTE DEL RANGO DE VELOCIDADES

Una problemática de este tipo de tecnologías es que la parte económica asociada a la membrana es muy elevada. A su vez, esta zona es donde se produce el intercambio iónico por lo que se intenta maximizar la zona útil de la membrana. Es por ello que el nivel de detalle en el análisis del campo de velocidades en esta región de estudio es fundamental para un buen diseño. Este coeficiente se usa para determinar la posición de la membrana dentro de la celda intentado homogeneizar el fluido en toda la superficie de la membrana. Este coeficiente del rango de velocidades se obtiene de la resta de la velocidad máxima y mínima en el primer contacto del fluido con la membrana (región M). Cuanto menor sea este coeficiente menor es la variabilidad de velocidades y mejor es el comportamiento hidráulico en el interior de la celda.

Este coeficiente se define como:

$$R_i\ (\mathrm{m/s}) = V_{\max} - V_{\min}$$

donde:

V_{max}: velocidad máxima evaluada en la región M.

V_{min}: velocidad mínima evaluada en la región M.

VOLUMEN DE FLUIDO EN LA DIRECCIÓN PRINCIPAL

Es necesario saber cuánto fluido avanza en la dirección principal y cuanto fluido se opone a esta o tiene una velocidad nula ya que indicará zonas de turbulencia o remolinos. Para poder evaluar esto último se define el parámetro de volumen de fluido en la dirección principal. Este se define como el volumen que circula en la dirección favorable del fluido respecto al volumen total evaluado de manera porcentual. Este parámetro se puede evaluar en toda la celda o en zonas de interés como puede ser la membrana.

Por lo tanto el porcentaje de volumen que circula en la dirección predominante es:

$$V_{upwards}(\%) = \frac{V_{v+}}{V_{TOTAL}} \cdot 100$$

donde:

V_{v+}: Volumen total de fluido circulando en la dirección principal.

V_{TOTAL}: Volumen total de fluido.

En cambio el volumen que circula provocando un funcionamiento de la celda inadecuado se define como:

$$V_{downwards}(\%) = \frac{V_{v-} + V_{dead\_zones}}{V_{TOTAL}} \cdot 100$$

donde:

V_{v-}: Volumen total de fluido circulando en la oposición al flujo principal.

V_{dead_zones}: Volumen total de fluido con velocidad nulas.

V_{TOTAL}: Volumen total de fluido.

Estos 4 coeficientes se aplican de manera secuencial para el diseño de la celda (metodología propuesta). Primero se intenta minimizar el coeficiente de simetría, llegando al óptimo

asumible, a continuación se minimiza el coeficiente de uniformidad hasta el objetivo fijado y, por último, se optimiza el coeficiente del rango de velocidades.

Para poder comparar diseños se utiliza el parámetro de volumen de fluido en la dirección principal.

- **La estimación de los parámetros previamente presentada solamente puede hacerse con un nivel de detalle ajustado basándose en la fluidodinámica computacional debidamente validada.**

  Para la modelación de la celda se ha realizado una serie de hipótesis. La más importante ha sido suponer que el fluido electrolítico no produce ninguna deposición dentro de la célula ni ninguna fase gaseosa. Esta hipótesis es completamente cierta cuando la reacción redox es 100 % eficiente. Otra hipótesis que se ha supuesto es referente a la características del fluido; la viscosidad y densidad del fluido electrolítico a 40ºC es la misma que la del agua a 20ºC, por ello, junto con la facilidad de manejo del agua, se ha usado el agua como fluido de trabajo en los modelos experimentales.

  Se ha aplicado un modelo estacionario para el análisis de la presión y para el cálculo del tiempo de residencia mediante formulación. Para el análisis de velocidades se ha aplicado un modelo transitorio. Otra hipótesis es utilizar el modelo de flujo segregado ya que este resuelve las ecuaciones (uno para cada componente de la velocidad, y uno para cada componente de la presión) de manera separada. El vínculo entre las ecuaciones de movimiento y la continuidad se logra con un enfoque predictor-corrector.

  El nivel de detalle del modelo numérico para la realización de la presente modelación computacional de la mecánica del flujo resuelve las ecuaciones de conservación de cantidad de movimiento (o Navier-Stokes) y de continuidad, a través de sus parámetros promediados. El análisis del problema que nos ocupa permite la promediación de las variables de las ecuaciones tradicionalmente denominada RANS (Reynolds Averaged Navier Stokes) con ecuaciones de cierre para la turbulencia comúnmente aceptadas. El modelo de turbulencia utilizado es el modelo k-ε realizable, este es un modelo semi-empírico basado en la ecuaciones de transporte de la energía turbulenta cinética (k) y del rango de disipación (ε).

  En todas las simulaciones se ha comprado la independencia de la malla con la solución final. Esta independencia se calcula cuando la diferencia de presión (entre la entrada y la salida) de la celda varia menos del 1 % con la malla anterior y posterior.

Comparando el modelo experimental con el modelo computacional se ha obtenido una diferencia de presiones del 2,22 % para la celda prototipo y del 3% para la celda real. Estos valores garantizan una buena aproximación y permitirán realizar simulaciones futuras. La validación del modelo permite a los diseñadores analizar los campos de velocidad en el interior de la celda y estimar las zonas muertas o de recirculación en diferentes zonas de la celda.

- **La metodología basada en la propuesta de parámetros de diseño y optimización de cada uno de ellos para diseñar una celda real se ha llevado a cabo en una geometría de celda concreta para un reactor electroquímico industrializable.**

  Se aporta un caso de estudio de diseño basado en la propuesta del uso metodológico de los indicadores previamente presentados, mejorando una geometría anterior cuyo campo de velocidades y presiones se ha validado en laboratorio.

  La geometría propuesta se ha validado para un caudal de 50 l/h. Las medidas de la celda son 0,73 m x 0,34 m y tiene una zona útil de membrana de 925 cm^2. El número de canales antes de que el fluido llegue a la zona de la membrana son de 84 canales con una separación de 1 mm entre ellos.

  Los valores de los parámetros de diseño para esta celda real son:

  - Coeficiente de simetría: 4 %.
  - Coeficiente de uniformidad: 8 %.
  - Coeficiente de del rango de velocidades: 0,015 m/s.
  - Volumen de fluido en la dirección principal para toda la celda es 91,17 % y para la zona de la membrana del 100 %.

  En este caso particular, en la zona de la membrana se tiene un porcentaje de zonas de recirculación o zonas muertas del 0 % que es considerablemente menor al 17 % obtenido en diseños previos. Esto significa que la propuesta de estos parámetros mejora sustancialmente el flujo en la zona de la membrana favoreciendo que el intercambio iónico se produzca en el 100 x 100 de la superficie posible.

  La celda final optimiza todos los parámetros propuestos frente a muchas otras geometrías analizadas de forma secuencial aportando el mejor de los diseños que se ha encontrado en este cada caso y validando la aplicabilidad de la metodología propuesta**.**

- **En el panorama energético español la tecnología que aquí se analiza es viable.**

  En esta tesis se ha desarrollado una visión general de los roles que juega esta tecnología dentro de los sistemas de almacenamiento electroquímico. Este tipo de batería tiene una vida útil elevada (alrededor de los 25 años) y unos costes iniciales relativamente bajos (13.312 € en el caso del reactor diseñado).

  Asimismo, se ha comparado la batería electroquímica en base hierro con las otras baterías electroquímicas obteniendo buenos resultados tantos en aspectos económicos como de sostenibilidad.

  Se ha comprobado la viabilidad económica de esta batería en el marco tarifario español, teniendo como resultado que el retorno económico de esta batería es en ocho años y medio. Se asegura así la viabilidad económica de la tecnología diseñada con la metodología propuesta.

Como conclusión final, cabe indicar que, en la presente tesis se ha aportado un análisis del estado del arte en este tipo de tecnologías, una proposición de procedimiento metodológico para el diseño de reactores electroquímicos en lo que al flujo hidrodinámico del electrolito basado en la fluidodinámica computacional se refiere, una validación práctica de dicho procedimiento y un análisis de viabilidad económica en el marco español que no se ha encontrado descrito en investigaciones previas. Prueba de ello es la rapidez con la que se han publicado los resultados aquí obtenidos en revistas de alto impacto y la posibilidad de desarrollos e implementaciones futuras de la presente tecnología en relación al desarrollo de las técnicas numéricas de la fluidodinámica computacional.

Capítulo 5:

Referencias

[1] P. Gonzalez, «Ten years of renewable electricity policies in Spain: an analysis of successive feed-in tariff reforms,» *Energy Policicy,* vol. 36, pp. 2917-2929, 2008.

[2] SEC, «The support of electricity from renewable energy sources,» 2005.

[3] M. Rychcik and M. Skyllas Kazacos, "Characterist of a new all-vanadium redox flow battery," vol. 22, no. 59-67, May 1987.

[4] R. Dell and D. Rand, "Energy storage-a key technology for global energy sustainability," vol. 100, no. 2-17, November 2001.

[5] L. Joerissen, J. Garche, C. Fabjan y G. Tomazix, «Possible use of vanadium redox-flow batteries for energy storage in small grids and stand-alone photovoltaic systems,» vol. 127, nº 98-104, March 2004.

[6] Z. Yang, J. Zhang, M. Kintner Meyer, X. Lu, D. Choi, J. Lemmon y J. Liu, «Electrochemical Energy Storage for Green Grid,» vol. 111, nº 716-732, 2011.

[7] C. Ponce de Leon, A. Frias Ferrer, J. González García, D. Szanto y F. Walsh, «Redox flow cells for energy conversion,» vol. 160, nº 716-732, 2006.

[8] A. Weber, M. Mench, J. Meyers, P. Ross, J. Gostick y Q. Liu, «Redox flow batteries: a review,» vol. 41, nº 1137-1164, 2011.

[9] A. Frías Ferrer, Optimización de la hidrodinámica de reactores electroquímicos: empleo de métodos experimentales y númericos, Universidad de Alicante: Tesis Doctoral, 2004.

[10] L. Thaller, «Electrically Rechargeable Redox Flow Cells,» nº 924-928, 1974.

[11] Hagedorn, H. Norman y L. Thaller, «Redox Storage Systems for Solar Applications,» *NASA TM-81464,* 1980.

[12] K. Nozaki, H. Kaneko, A. Negishi, K. Kanari y T. Ozaka, vol. 2, nº 844-894, 1984.

[13] G. Codina, Desarrollo de una planta de acumulacón de nergía eléctrica basada en el acumulador redox Fe/Cr, Universidad de Alicante: Tesis Doctoral, 1992.

[14] V. Estahanian, H. Mahmoodi, H. Babazadeh, M. Aghvami, R. Pasandeh, F. Torabi y G. Ahmadi, «Numerical simulation of electrolyte particles trajectory to investigate battery cover design characteristics,» vol. 191, nº 139-143, 2009.

[15] M. Secanell, J. Wishartb y P. Dobson, «Computacional design and optimization of fuel cells and fuel cells systems: A review,» vol. 196, April 2011.

[16] X. Ma, H. Zhang y F. Xing, «A three-dimensional model for negative half cell of the vanadium redox flow battery,» vol. 58, nº 238-246, 2011.

[17] M. Moyabayashi, T. Tayama, Y. Kageyama y H. Oyama.Patente 5.851.694, 1998.

[18] C. Bengoa, A. Montillet, P. Legentilhomme y J. Legrand, «Flow visualization and modelling of a filter-press type electrochemical reactor,» vol. 27, nº 1313-1322, 1997.

[19] A. Wragg y A. Leontaritis, «Local mass transfer and current distribution in baffled and unbaffled parallel plate electrochemical reactor,» vol. 66, nº 1-10, 1997.

[20] J. Cheng, B. Wang y J. Yang, «Solvent Extraction and Ion Exchange,» vol. 27, nº 302, 2009.

[21] J. Cheng, B. Wang y L. Hong-Ling, «Numerical Simularion and Experiment on the Electrolyte Flow Distribution for All Vanadium Redox Flow Battery,» Vols. %1 de %2236-238, nº 604-607, May 2011.

Anexos

ANEXO I:

IRON REDOX BATTERY AS ELECTRICAL ENERGY STORAGE SYSTEM IN THE SPANISH ENERGETIC FRAMEWORK

ANEXO II:

REDOX CELL HYDRODYNAMIC MODELLING. SIMULATION AND EXPERIMENTAL VALIDATION

ANEXO III:

METHODOLOGY TO OPTIMIZE FLUID-DYNAMIC DESIGN IN A REDOX CELL

ANEXO IV:

REDOX CELL HYDRODYNAMIC MODELLING: TOWARDS A REAL IMPROVED GEOMETRY BASED ON CFD ANALYSIS

ANEXO I: IRON REDOX BATTERY AS ELECTRICAL ENERGY STORAGE SYSTEM IN THE SPANISH ENERGETIC FRAMEWORK

ABSTRACT

The energy storage technologies will play a crucial role in the near future under the use of efficient electric energy sources and renewable energies such as wind and solar energy. This sort of energy usually suffers from intermittent problems in distributed generation systems. To overcome this problem, electricity storage systems provide solutions to improve dispatchability and reliability. The different electrochemical storage systems are presented when considering their applications and comparing advantages and disadvantages. Based on this description and the possible applications of each technology, a particular case is considered in the framework of the Spanish energetic system. An iron redox battery (one of the most promising technologies) is analyzed from an economic point of view determining important aspects as the payback of the investment or the IRR.

Keywords. Electrical energy storage, Renewable energy, Economic assessment

1. INTRODUCTION

1.1 General scope

The energy situation in Europe is determined by measures to reduce the CO_2 emissions and the dependence on fossil fuels from other countries. For these reasons, the energy production from renewable sources becomes especially important. However, the large energy distribution leads to a benefit for the renewable energy which will be unviable without an appropriate storage capacity system.

The produced energy from renewable sources has the advantage of not emitting CO_2 to the atmosphere. Renewable energy allows managers to use local energy sources and to reduce the energy dependency on foreign energy sources, especially fossil fuels, which are mostly imported to Spain and the European Union [1]. Therefore, one of the main objectives of European Authorities is to increase the use of renewable sources in energy production. On March 9, 2007, the Spring European Council, with the support of the European Parliament and the Member States agreed that at least 20 % of its energy consumption must be produced with renewable energy sources by 2020 [2]. Nevertheless, the energy situation of each specific European country must be taken into account. The European Council also adopted a commitment to reduce by at least 20 % its greenhouse effect gases emissions to achieve energy savings of 20 %. Furthermore, biofuels reach 10 % within fuels consumed in the EU transport. In this sense, Spain was encouraged to reduce exactly 20 % of its energy consumption.

1.2 Renewable energy integration in the whole energy system

It is recognized that the energy production and consumption as known nowadays is not sustainable. It means that, fossil fuels could be finished in the long term besides the threat which supposes its use for the environment, mainly due to greenhouse effect gases emissions and its impact on climate change [3], [4].This is why, industrialized countries are supporting and legislating new technologies to ensure that their energy will be sustainable in the future. This sustainability aims to maintain the economical growth of the country while increasing energy security and environmental protection.

The renewable energy sources and its application, especially to produce electricity, have been supported by all the Governments of Spain. In 2011 the Renewable Energy Plan 2011-2020 (or 20-20-20 package) was published to indicate the commitment of the Spanish Government to cover at least 20 % of total primary energy consumption by renewable energy sources in 2010 [5].

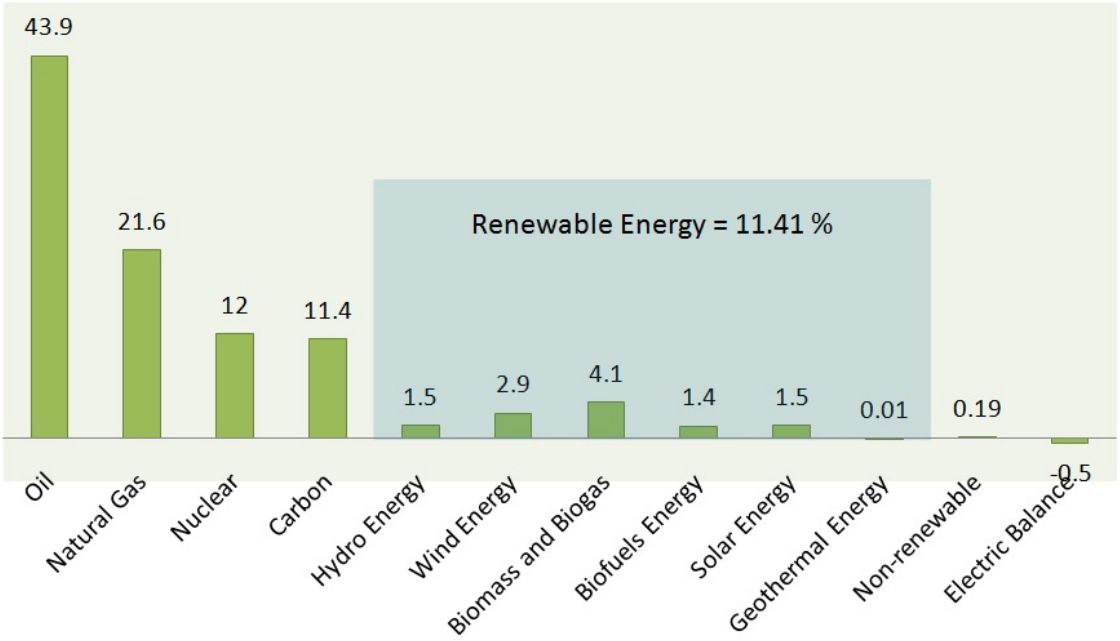

Fig. 1 Primary energy sources, the case of Spain. Adapted from (IDAE [6]).

Nevertheless, it is still a long way to reach the target rates set in 2020 regarding the proportion of renewable energy in final energy consumption. The power sector has to greater contribute to achieve this goal in the case of Spain [7]. According to recent studies carried out by the Spanish Government, 40 % of renewable energy source is required in the power (electricity) sector to reach a renewable energy integration of 20 % in the whole system. To achieve this desirable goal is not easy. While fossil fuels can be easily transported and can perform as energy stores, most of renewable energy sources cannot be stored or transported without being converted first to electricity [8]. This is why, energy storage strategies and technologies are necessary to contribute to sustainable development [9]. It is necessary to store energy when it is produced by renewable sources (such solar and wind power) to be consumed when required. Nowadays, there are many storage systems [10]. However, its industrial implementation and regulations [11] are still being under development. It is very important to have a positive balance between benefits obtained from the use of storage systems compared with the economical investment [12]. In this contribution a simplified analysis about one of these new storage devices is presented: the Electro-Chemical Energy Storage Semi-Redox Iron Flow. The aim of the study is

to quantify the functionality and the economical viability of the storage device in the Spanish energy scope.

1.3 The need to store energy

The uncontrollable nature of some renewable energy sources leads to increase the difficulties to safely operate power systems. This kind of energy will represent a significant percentage of the power installed capacity in the future. Electricity generation from renewable sources does not firmly contribute to the power supply warranty. Nevertheless, it contributes to cover the power demands in terms of annual energy supply. This lack of power guaranteed is a problem for the operation of the power system because it requires a stable power generation. Additionally, there are problems associated with the particular renewable energy generation and problems of network congestion in areas with high consumption and low generation rates, due to the saturation of the transmission lines.

The extent of regenerative electricity involving a disparity between power production and consumption can lead to the loss of electricity produced if the presence of electricity storage systems is not ensured. Every country has its own necessities of storage systems related to the precedence of the energy in the national system, as the case of Japan [13] or Saudi Arabia [14], [4]. The growing of renewable energy in Spain [15] is considered in all the forecasted scenarios (Fig. 2).

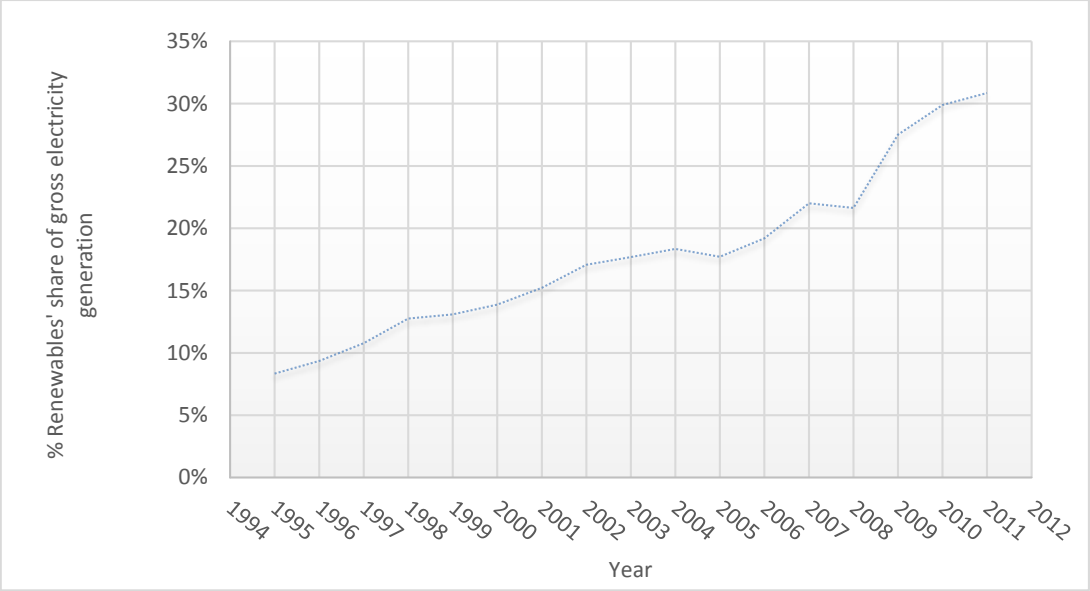

Fig. 2 Renewables´ share of gross electricity generation (Source ForoNuclear.org [15]).

2. ELECTRICITY STORAGE SYSTEMS

Worldwide electrical grid storage capacity is about at 127 GW and it increasing each year [16]. Electric Energy Store Systems (EES) are crucial for future developments in national energy grids [17]. In general, an energy storage system is more than ever a necessity [18], [19] and many different sorts of devices can be applied to storage electricity [20], [21]. This necessity increases as the use of renewable energy gets more important in national balances of electricity [22]. Economic implications of these devices attract great interest in recent times [23] , [24].

Two categories of EES can be considered related to their applications [25]: Energy Management applications (long-duration discharge applied to decouple generation and consumption of electric energy), and Power Management Applications (short duration discharge applied to deliver power in real time).

Energy Management applications involve different scales of time, since daily up to several times per month along a year (long duration storage up to hours or more). Power management applications involve short-duration with a big number of discharges over a year involved (short fractions of time up to some minutes).

2.1 An overview on the more efficient Electrochemical Storage Systems Batteries

Electrochemical batteries are one of the most used technologies for store energy [26].They are very convenient for many sort of uses and adaptable to grid necessities providing very good efficiency, in some cases up to 95%. Different technologies have been developed in the recent years [14]: Lead-acid batteries, Sodium/Sulfur batteries and Flow batteries, Nickel-Cadmium and Lithium Ion. Apart of them, the Iron flow battery will be presented in this article as one of the most interesting ones based on economic and technological factors. A short description of the general types of batteries is provided.

2.1.1 Lead-acid batteries

These are the oldest and most mature battery technology currently in use. These battery cells consist of spongy lead anode and lead acid cathode immersed in a dilute sulfuric acid electrolyte, using lead as the current collector [27].

2.1.2 Sodium/Sulfur batteries

Sodium/Sulfur (Na/S) batteries are based on a high-temperature electrochemical reaction between sodium and sulfur separated by a beta alumina ceramic electrolyte. The active materials in a Na/S battery are molten sulfur as the positive electrode and molten sodium as the negative one [28].

2.1.3 Nickel Cadmium batteries

Nickel Cadmium (NiCad) batteries are a rechargeable batteries using nickel oxide hydroxide and metallic cadmium as electrodes. Sealed Ni-Cd batteries require no maintenance, as described on [29].

2.1.4 Lithium Ion batteries

Lithium Ion (Li-ion) batteries are batteries where the cathode is a lithiated metal oxide and the anode is made of layers of graphitic carbon. Lithium ions move between the anode and cathode to generate current flow. At the carbon anode the lithium ions combine with external electrons and they are deposited between carbon layers as lithium atoms. This process is reversed during discharge [30].

2.1.5 Flow batteries

Flow batteries are electrochemical devices that convert chemical energy into electrical energy during battery discharge and, during battery charge, batteries convert the electrical energy back into chemical energy for long-term storage [31].The fundamental building block of a battery is a single electrochemical cell. Cells are connected together in variety of configurations to provide the necessary voltage, energy and power for their application [32], [33].

Every cell has two separate chemical reactions occurring—one involving the release of the electrons during battery discharge (at the negative electrode material, or anode) and one involving the take-up of the electrons during battery discharge (at the positive electrode material, or cathode). When the cell is charged the electrochemical reactions occur in the reverse directions, taking electrons out of the material at the positive electrode and putting them back into the negative electrode material.

Electrolyte solution is crucial, as it allows balancing of the negatively charged electron that is moving from one electrode to the other. The materials in redox batteries (electrolyte, positive and negative electrode materials) are housed in a separate container and they are actively pumped into the container where the electrochemical reactions occur.

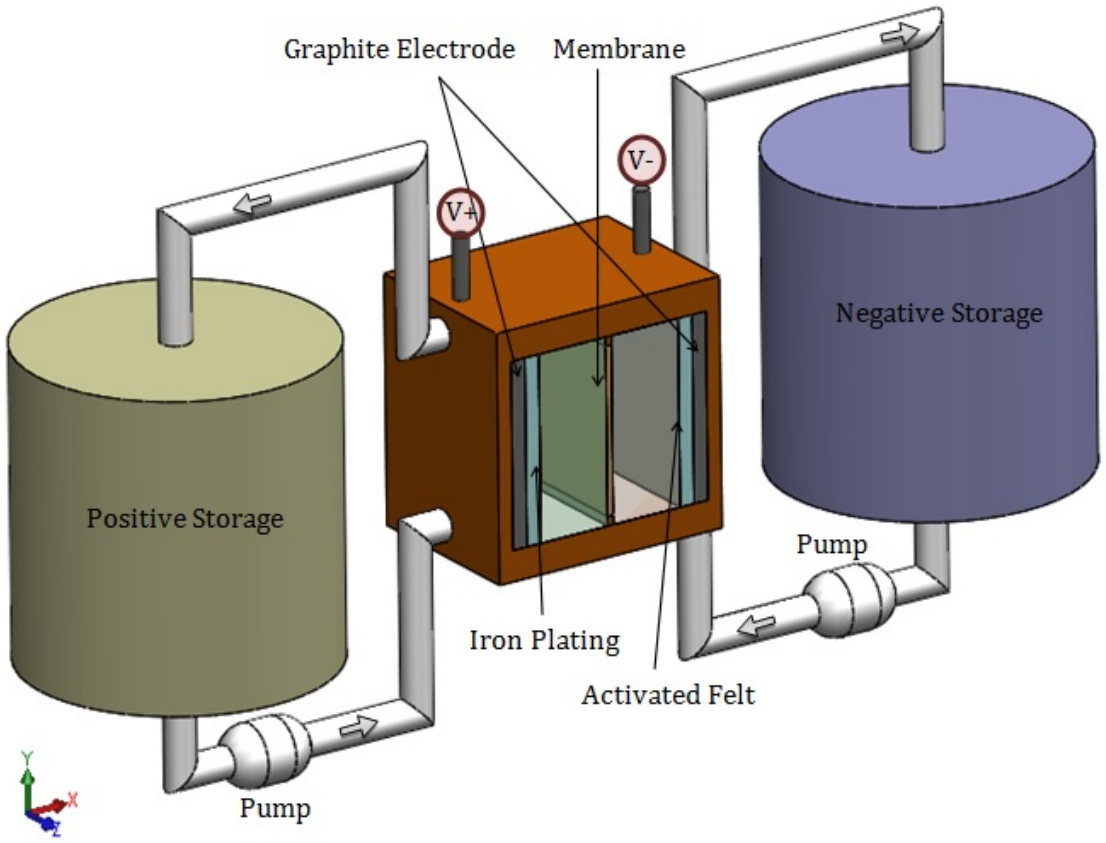

Fig. 3 Typical battery scheme.

The first class of electrolyte batteries appeared in the 70s. The first batteries were made in Zinc as anodic material, combined with Oxygen, Chlorine or Brome. In 1974 Thaler proposed the actual redox prototype [34]. In 1980 Hagedorn [35] published the first results obtained on prototypes. Since then, different cell prototypes have been proposed highlighting redox batteries of Fe/Cr [36].

An interesting summary of the Redox battery is presented in Weber et al. [37] who highlighted this main idea: the future of this technology goes through optimizing the design modeling: flow and transport.

Different sort of flow batteries can be found used as accumulators depending on the nature of the electrolyte:

- Vanadium redox batteries (VRB). VRB store energy by employing vanadium redox couples dissolved in mild sulfuric acid solutions (electrolytes). Hydrogen ions are exchanged between the two electrolyte tanks through a hydrogen-ion-permeable polymer membrane along charge and discharge processes [38], [39], [40].

- Zinc/Bromine (Zn/Br) batteries. In each cell of a Zn/Br battery there are two cells of a Zn/Br battery with two different electrolytes flow past carbon-plastic composite electrodes in two compartments separated by a micro porous polyolefin membrane.
- Iron redox batteries (FeRB). This is the new type of battery proposed in this contribution. It uses a ferrous chloride salt in aqueous solution with ammonium chloride as the supporting electrolyte. On the negative side of the battery, ferrous ions are reduced during charge, plating as iron metal onto a graphite electrode. On the positive side of the battery, ferrous ions are oxidized to ferric ions during charge, remaining in solution. These reactions are the opposite upon discharge. To preserve electroneutrality, chloride ions (Cl-) travel across the micro porous membrane separator in the opposite direction as the electrons [41], [42], [43], [44], [45].

2.2 Assessment and comparison of the electrochemical energy storage technologies

Power and energy storage technology are the essential difference in each energy storage technology. These capacities are key indicators of what applications a medium storage might be able to fulfill. Efficiency and cycle life are other two of the most interesting aspects to be considered before and along selecting a storage technology. Both of these parameters affect the overall storage cost. Low efficiency increases the effective energy cost by diminishing the performance of the whole system. Low cycle life also increases the total cost, as the technology needs to be replaced more often. Both parameters should be considered together in the economic balance of the investment in this storage technology, to compare different possible choices.

Furthermore, every device is more suitable to different applications: most technologies are not practical or economical suitable for both power and energy applications. Table 1 shows the suitability of some of the described technologies for electrochemical energy storage applications [10]. It can be observed than the FeRB battery has the same advantages than VRB but with a lower capital cost.

Technology	Power rating	Discharge time (second, minute and hour)	Cycle life to 80% DOD	Efficiency (%)	Capital Cost		Advantages	Disadvantages
					Current cost $/kWh	Future cost $/kWh		
Lead Acid	0-20 MW	s-h	600 - 500	70/80	100 - 150	100	Low cost, spill resistant (Sealed batteries). Useful for automobiles. No liquid parts.	Limited low temperature. Performance. Cost and cycle life.
NaS	50kW-8MW	s-h	2000	80/90	500	500	High energy and power density. Relatively high efficiency. Long cycle life. Relatively well-established	Relatively expensive (still small volume manufacturing). High temperature produces unique safety issues.
NiCd	0-40MW	s-h	2000	60/65	300	300	Excellent cycle life. Flat discharge curve. Good high- and low temperature performance. High resistance to shock and vibration	High initial cost. Only fair charge retention- Memory effect.
Li-ion	0-100 kW	m-h	1200	85/90	600	250	Limited high-rate capacities; safety concerns.	High initial cost, relative high rate of self-discharge
VRB	30kW-3MW	s- 10 h	10000	75/85	1450	1000	Do not directly engage electrodes in the electron transfer process nor involve them in solid-state reactions. Neither energy storage nor power capacity is dependent on their dimensions. can be stored indefinitely at any state-of-charge with only negligible self-discharge	High initial cost. Base don't raw materials
ZnBr	50kW-2MW	s- 10 h	8000	75/85	300	100	High energy density in small cells. Flat discharge rate.	Dries out quickly. Cannot be stored for more than 2 months when charged.
FeRB	30kW-3MW	s- 10 h	10000	75/85	1130	850	Can be stored indefinitely at any state-of-charge with only negligible self-discharge. Almost unlimited cycles. Cheap an widely available starting materials	Energy storage and power capacity not independent

Table 1 Energy applications for different electricity storage systems. Adapted from Chen et al. [10].

3. ELECTRICITY STORAGE SYSTEMS BENEFITS

The benefits of the electricity storage systems must be considered as a whole: energy operation and economic sustainability [46]. The basic question to be examined is whether the investments will be recovered. In this case, to analyze the return, a particular case of Flow Iron battery of 3 kW and 21 kWh is presented, in the framework of the Spanish electric system, with an initial cost of 13,352.15 €.

3.1 Operational Benefits

Apart from an economic analysis, the benefits in the operation of a national electric system of the storage devices are important: The final objective is the integration of the renewable sources of electricity generation. They are experiencing dynamic growth but are also subject to relatively strong fluctuations. Some of these benefits are here detailed.

- Support for renewable energy. The electricity storage system can reduce fluctuations in power output of wind and photovoltaic installations allowing dispatchability.
- Reliability and quality of supply.
- Active and reactive power control. The power interfaces provide the ability to change rapidly between active and reactive power absorbed and / or assigned to the network.
- Load leveling. The electricity storage devices are recharged during off peak periods using lower-cost energy generation plants from base and are downloaded during periods of high demand improving the load factor of the whole system.
- Load following. The electricity storage devices can accept changes in demanded power level very quickly.
- Help in the energy management.
- Tertiary Reserve.
- System stability. Power and frequency variations are attenuated more rapidly varying output active or reactive power in the system.
- Automatic control in the generation. The stored energy in the system can be used for minimizing the area control error.

- Reducing the use of fossil fuels to improve overall system efficiency.
- Reduction of transmission and distribution losses if the location of the storage system is optimized against the consumption points.
- Increased efficiency and reduce maintenance of plants carrying the machines operating points with lower variation around its optimum performance.

3.2 Economic Benefits

To analyze the feasibility of these elements, the need is justified as part of an energy system that seeks to optimize the use of renewable energy, an Iron Flow battery is presented as electricity storage efficient system, introduced in Table 1 as one of the most convenient among all the considered examples.

- *Time-shift.* Storage can be used to time-shift electric energy generated. Users are able to buy and sell the energy. Usually it is stored when demand and price for power are low, so the energy can be used when power demand and price are high. Those who invest in this kind of battery receive the benefits of this previously explained concept.
- *Load following*. This service, individually provided by each one of the batteries has a benefit for the global electricity system as a whole. Since this concept reduces the need for human resources dedicated to the management of the system, thus reducing the risk of human failure and endowing it with flexibility in excess or in default of electrical generation.
- *Spinning reserve*. Another service provided by batteries with active management is acting as storage generators to face unexpected demand changes or unexpected mistakes in the generation of alternative energy sources.
- *Integration of not controllable power sources: nuclear and renewable.* The not controllable sources of energy are those that receive the benefit of an implantation of batteries allow the not controllable sources still growing. Moreover, this system also facilitates its management as it has the capacity of becoming automatic and allowing a greater input of renewable. These two aspects are very positive as they guarantee a gradually stabilization of the energy cost.
- *Regulation of power.* This service is constantly adapting energy changes to offer and demand profile. The frequency is the indicator of the balance condition between offer

and demand where values over 50Hz (for the EU) indicate an excess of offer and values under 50Hz represent an excess of demand.

- *Compensation for reactive power.* The electrical engines inject reactive energy to the grid. This type of energy is not useful, it is a disturbance that loads the grid, occupies it, prejudices the main energy use and it is penalized by the electrical companies. The most extended solution to avoid this kind of penalization is to transform this useless energy into a useful one by means of AC/DC reversible transformers, that is to say, make it pass through a battery system. The owner of the accumulator obtains benefits from three main concepts:
  - The user is able to avoid the penalization for the reactive energy generated in its facilities.
  - The user decreases costs by making the most of the recovered energy and by decreasing the quantity purchased.
  - The user will be rewarded with a cleaned grid by the action of consuming the reactive energy of the grid.

4. CASE STUDY: IRON FLOW BATTERY ANALYSIS IN THE SPANISH ENERGETIC FRAMEWORK

The Spanish electricity system recognizes the need of introducing efficient storage energy systems. This is crucial to integrate renewable energy sources into the whole system. Therefore, different strategies are being used in order to achieve this storage.

The electrical energy can be generated, transported and easily processed. However, it is difficult to store it in large quantities. But, even if it is complicated, the Spanish electricity system accepts various methods of energy storage along the supply chain:

- Big Scale (GW): reversible hydro-electrical (Pumped Hydro Energy Storage, PHES)
- Grid Storage and final user (MW and KW): batteries, capacitors, superconductors and flywheels.

New energy storage technologies will become key elements of the future electrical systems so that, the electrical storage can add value to the chain of electricity supply. Particularly, Iron flow battery is an economic and robust alternative in the MW and KW scale. It is a promising solution as it is one of the most durable and reliable batteries.

The renewable energy storing not only covers the gaps between supply and demand, it also allows households to consume their own generated electricity and sell the surplus to the network. In the case of the Spanish legislation, this Iron flow battery technology will be applied to grid storage systems. Nowadays, this technology is very new but, as here depicted, it is a real future alternative.

The current law estimates that the percentage from renewable energies in Spain (especially in wind and solar energy) that need to be stored and regulated would be 4.4% of the total energy. In this grid store systems, the Iron redox batteries must play a key role.

In this section the economic balance of each concept previously presented is explained. The characteristics of the studied battery are: storage capacity (C) (21kW h), rated power (P) (3kW), depth of discharge (DOC) (80%) and full cycle efficiency (η) (70%). To evaluate the economic values from a selected storage, it is necessary to decide a main purpose of the storage then, the calculation of the benefit from its major application and additional returns, from various synergy effects, can be done. In this particular case, all the possible benefits from the use of the storage system are analyzed.

Different aspects have to be considered separately: time shift, services offered to the grid and compensation for reactive power. Finally, the total contribution of them is considered as a whole. To make a numerical quantification of the benefits, the methodology proposed by [47] has been used and adapted to the Spanish energetic system (values for 2013).

4.1 Economic benefits of Iron flow battery in the system: partial economic analysis

4.1.1 Time-shift

In the present framework, time-shift concept represents the benefit based on the time specific prices paid under terms of different tariff prices. The most common practice In the Spain market it is to buy energy according to two different pricing, an off-peak pricing (0.067 €/kW h) and a standard pricing (0.181 €/kW h). The value of the power term in Spain is 1.82443 €/kW/month. With these pricing on mind and the specific characteristics of this battery, the proposed storage battery system gets through this concept a saving of 1.472 € / d.

$$Return\ (€/year) = Saving/day\ (€) - Cost/day\ (€) \cdot 365 \quad (1)$$

$$Saving/day\ (€) = P \cdot C \cdot DOC \cdot \eta \cdot Standard\ Pricing + Power\ Term\ (P/30) \quad (2)$$

$$Cost/day\ (€) = C \cdot DOC \cdot Off\ Peak\ Pricing \quad (3)$$

Fig. 4 shows the evolution of this concept throughout the life of the battery, constantly increasing with time. Expression 1 considers this benefit.

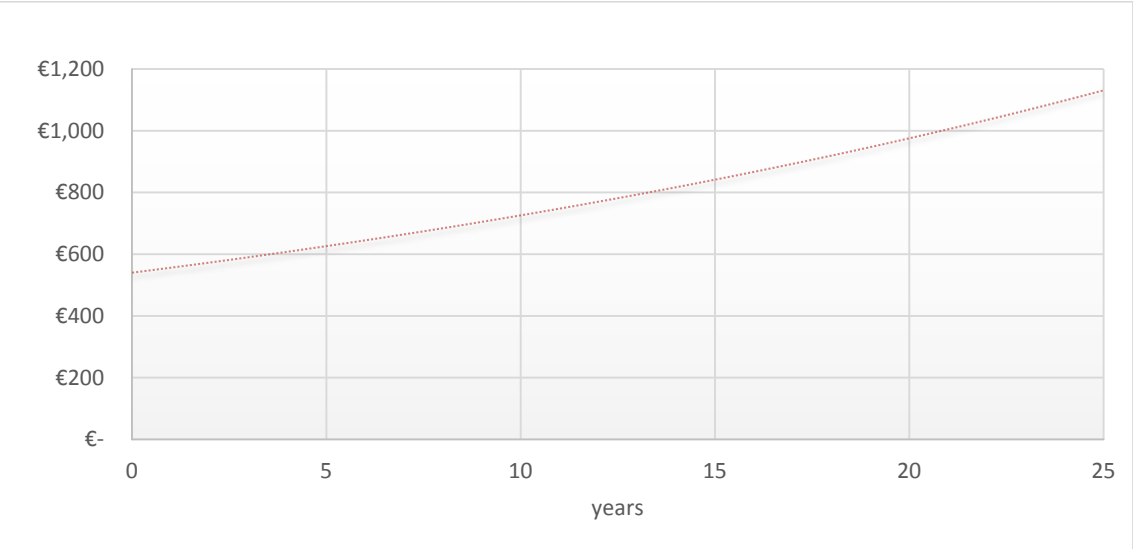

Fig. 4 Temporal evolution of the concept time shifting.

4.1.2 Services offered to the grid

This concept includes the investment returns due to: load following, spinning reserves, integration of not controllable power sources and power control.

Load following. It is considered that a system of electrical build-up may be working 2,500 h / y in load following service so, for each nominal kW available 2,500 kW h / y. can be managed The average price of energy in Spain is taken as references at low pool prices of 20 €/MW h (hydroelectric generation) and at high pool prices of 50 € / MW h (generation in combined cycles). With this price difference, when 2 MW h / y are managed, the returns arises up to 75 € / y / kW based on this service offered (4).

$$Returns\ (€/year) = (High\ Pool\ Prices - Low\ Pool\ Prices) \cdot Energy\ Managed \quad (4)$$

Spinning reserves. To evaluate these benefits that the system receives, the service is consider to provide 2,500 hour to an average price between 3 € / MW h and 6 € / MW h. Maintaining the same assumptions described in the previous concept, annual returns arise up to between 7.5 € / kW / y and 15 € / kW / y obtained in terms of installed rated power (5).

$$Returns\ (€/year) = Energy\ Prices \cdot Energy\ Managed \quad (5)$$

Integration of not controllable power sources: nuclear and renewable. A system of batteries that manages 204.4 kW h / kW h / y of energy with the same characteristics previously described are considered. In the Spanish energy mix around half of this energy comes from non-controllable power sources. The cost of managing the grid is the difference between the price that the final consumer pays (0.142 € / kW h) and the pool price (0.05 € / kW h). Operating with all these values, the income that a system of accumulation must obtain for the integration of not controllable power sources it is 4,730.43 € / kW h / y (6).

$$Returns\ (€/year) = Energy\ Managed \cdot (1 - d)^{year} \cdot r \cdot (1 + i)^{year} \cdot (End\ User\ Energy\ Prices - Pool\ Energy\ Price) \cdot (1 + Energy\ Price\ Increment)^{year} \cdot l \cdot C \quad (6)$$

- Degradation (d) = 0.5 % per year
- Increment of Energy from Non Controllable Sources (i)= 2 %
- Rated Energy from Non Controllable Sources (r) = 0.5
- Distribution Lines (l)= 0.5

Regulation of power. An annual service of 2,500 h / y in this concept is assumed. Therefore each KW manages around 2.5 MW h/y. The cost to manage this energy may be regarded as the cost difference between peak hours and off-peak hours, but at the point of the final consumer.

Therefore, according to the Spanish electricity pricing, the benefits under this point are in between 160 € / MW h and 60 € / MW h, which is equivalent to 100 € / W h. This gives as a returns by the regulation power of 250 € / kW / y (7), similar to (4).

$$Returns\ (€/year) = (High\ Pool\ Prices - Low\ Pool\ Prices) \cdot Energy\ Managed \qquad (7)$$

Fig. 5 shows the value of the returns provided by each of these four concepts throughout the 25 years of battery life.

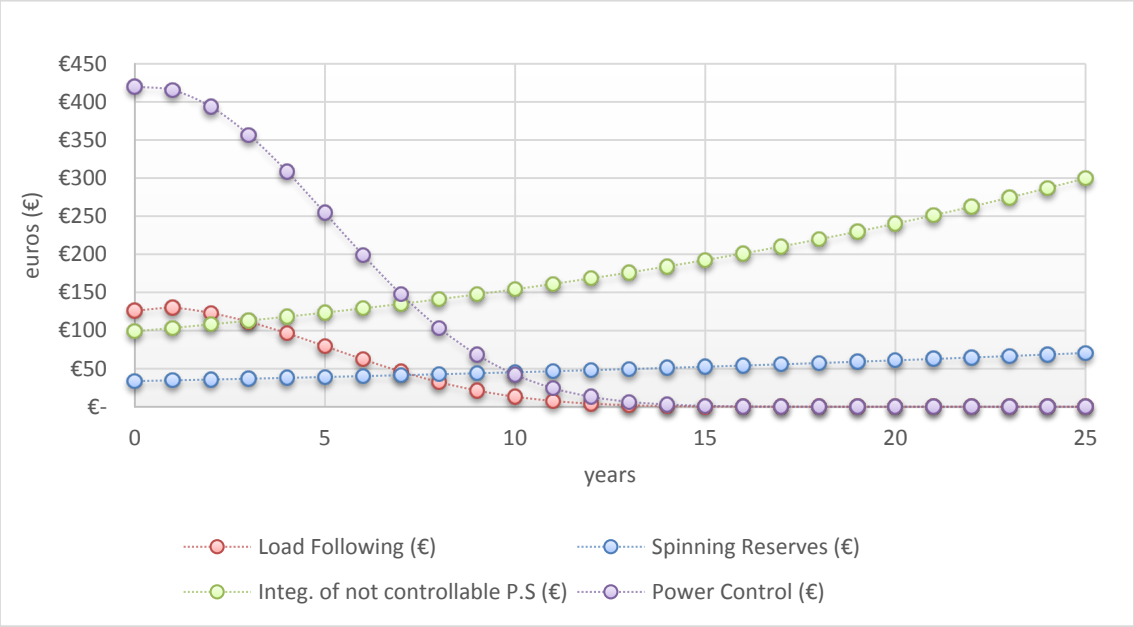

Fig. 5 Value of the returns: load following, spinning reserves, integration of not controllable power sources and the power control.

4.1.3 Compensation for reactive power

In order to quantify this benefit a medium company is considered. On the basis of the information provided, this company can generate about 54 kVarh per kW hired per month. In the Spanish market the compensation when generating a reactive energy with the cos ϕ greater than 0.8 is 0.041554 € / kVarh. With all these data this concept produces savings in penalties and save 46.06 € / kW/ y because of the lack of energy purchase (8).

$$Returns\ (€/year) = Reactive\ Power\ Generated \cdot \eta \cdot (0.45 \cdot Standard\ Pricing + 0.55 \cdot Low\ Pricing) \cdot 12 \cdot DOC \qquad (8)$$

Fig. 6 shows the shape of this temporal evolution of income by this concept.

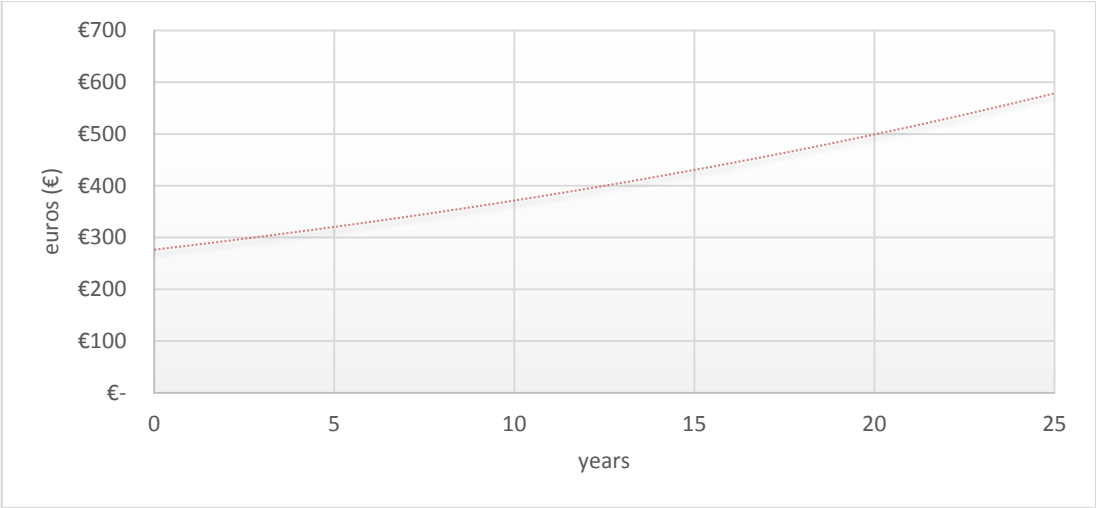

Fig. 6 Income from the concept of compensation for reactive power.

4.2 Integration of total benefits

The weight of the six concepts studied in the previous point regarding the battery global benefit will be analyzed in this section. As Fig. 7 shows, the greatest economic return is produced by the time shift concept. It contributes more than a half (51%) of all revenues over the 25 years of the battery life. The following more important concept is due to compensation for reactive power which generates 26% of the total benefit. The remaining 23 % of the benefits come from the next concepts: load following, spinning reserve, integration of not controllable power sources and power control.

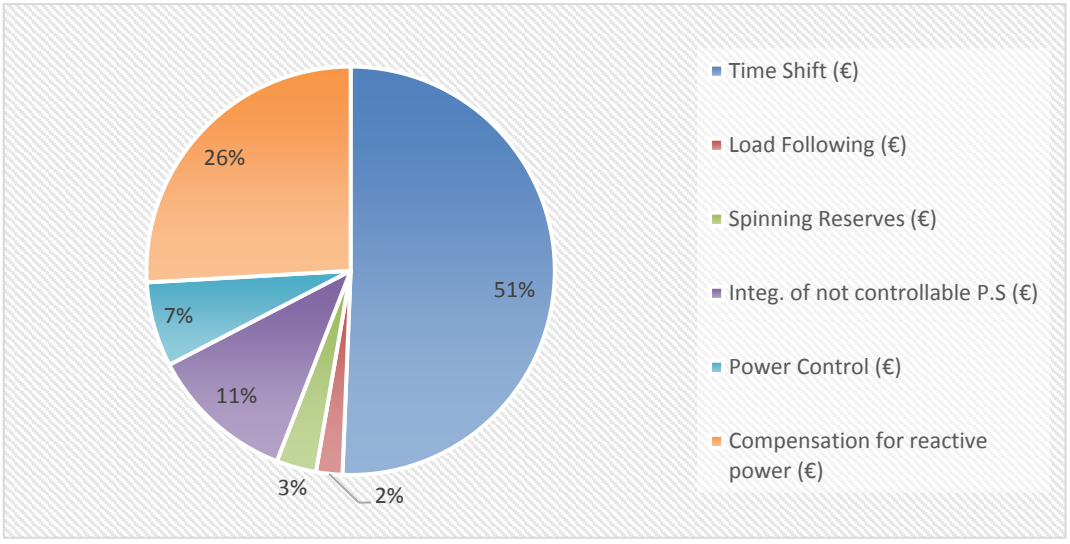

Fig. 7 Integration of different benefits in the total economic balance.

Fig. 8 shows the accumulated returns according to a combination of all concepts analyzed in the previous point. This Fig. illustrates all the sum of all the considered incomes. These increasing returns are the reason why an electrical accumulation system (in this case, a flow battery in iron base) is economically so convenient.

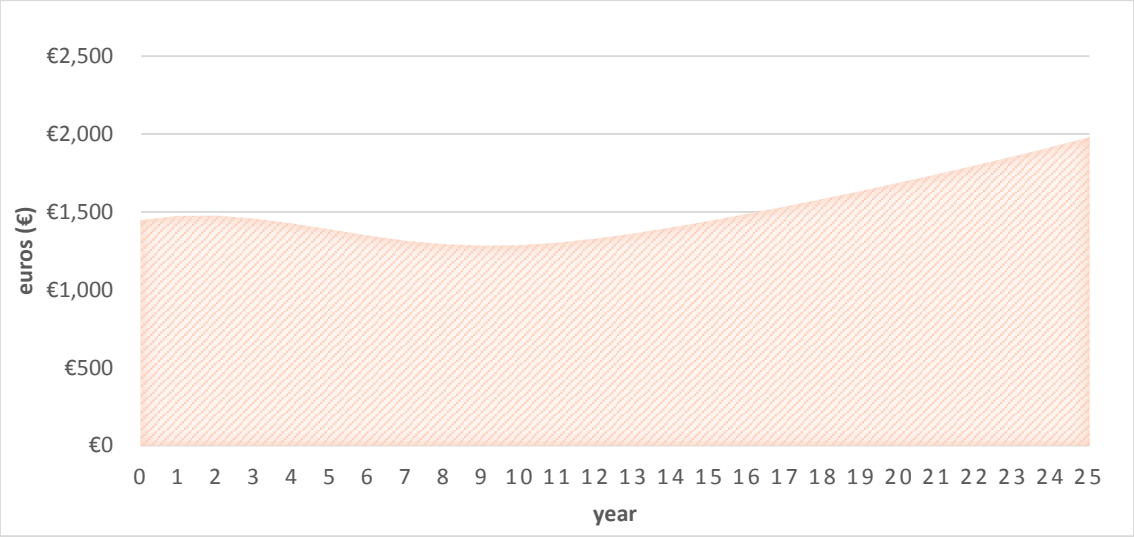

Fig. 8 Incomes per year of the different concepts (Year vs. €).

In Fig. 9 the cash flow is shown. The maintenance costs considered are the consulted references which arise up to 0.008 €/kW h. As it can be observed, a payback of the investment occurs in the eighth year of the battery. Therefore, it is considered an investment with a very reasonable redeemable deadline. In the present case an IRR of 12% is obtained where the value of the investment is 13,312 € with the specified returns.

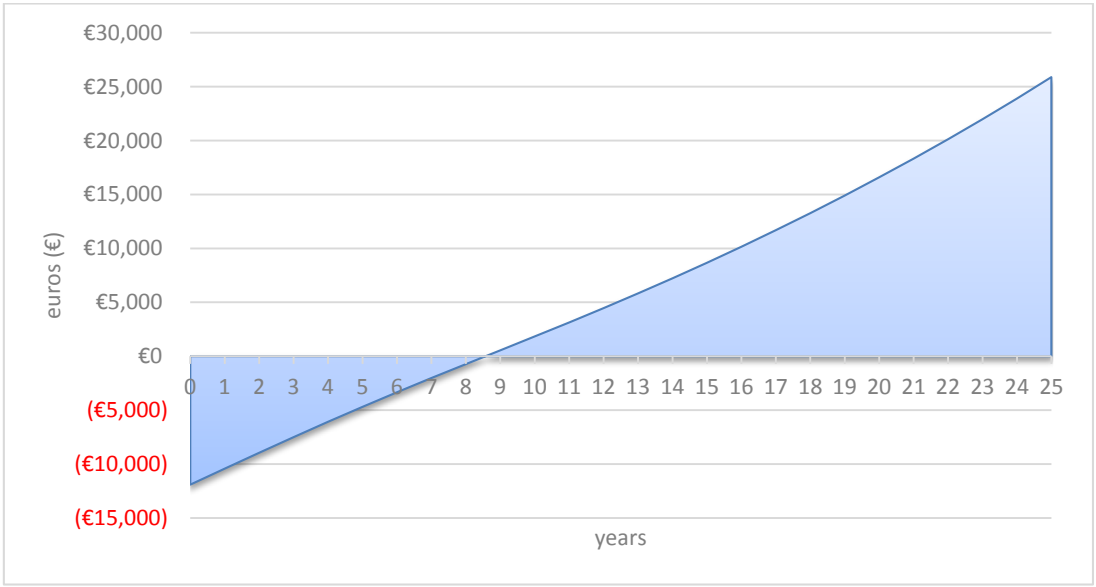

Fig. 9 Cash flow.

5. CONCLUSIONS

In this paper, a general vision of the role played by electrochemical energy storage systems is presented.

It can be concluded, comparing all these possible solutions, that among all of them, iron redox battery is considered as one of the most promising options: according to Table 1, this is the battery with the biggest number of life cycles and the smallest current and future costs. Additionally, this is a long duration battery with a lifespan of approximately 25 years. This is beneficial for long duration applications especially when it must be stored for a long time.

The benefits of the presented alternatives have been depicted focusing on operational and economic aspects. Based on the previously comparative analysis, a particular case study of the iron redox battery has been widely described, particularly applied to Spanish electrical tariff system. As a conclusion, with the applied methodology, the payback of the investment in the battery occurs at the eight year and a half. This is a very reasonable deadline for the return of the investment.

Apart from these economic considerations, electrochemical devices and in particular Iron redox batteries will be of paramount importance in future management of Energetic System.

6. REFERENCES

[1] P. Gonzalez, «Ten years of renewable electricity policies in Spain: an analysis of successive feed-in tariff reforms,» *Energy Policicy,* vol. 36, pp. 2917-2929, 2008.

[2] SEC, «The support of electricity from renewable energy sources,» 2005.

[3] K. Hanjalić, R. Van de Krol y A. Lekić, Sustainable Energy Technologies. Options and Prospects, Springer, 2008.

[4] A. Evans, V. Strezov y J. Tim, «Assessment of utility energy storage options for increased renewable energy penetration,» *Renewable and Sustainable Energy Reviews,* vol. 16, pp. 4141-4147, 2012.

[5] «Plan de energías renovables 2011-2020,» 2013. [En línea]. Available: http://www.idae.es. [Último acceso: 2012].

[6] 2013. [En línea]. Available: http://www.idae.es. [Último acceso: 2012].

[7] R. Cossent, T. Gómez y L. Olmos, «Large-scale integration of renewable and distributed generation of electricity in Spain: Current situation and future needs,» *Energy Policy,* vol. 39, pp. 8078-8087, 2011.

[8] I. Serban y C. Marinescu, «Battery energy storage system for frequency support in microgrids,» *Electrical Power and Energy Systems,* vol. 54, pp. 432-441, 2014.

[9] A. Arabali, M. Ghofrani y M. Etezadi-Amoli, «Cost analysis of a power system using probabilistic optimal power flow,» *Electrical Power and Energy Systems,* vol. 53, pp. 832-841, 2013.

[10] H. Chen, T. Ngoc-Cong, W. Yang, C. Tan, Y. Li y Y. Ding, «Progress in electrical energy storage system: A critical review,» *Progress in Natural Science,* vol. 19, nº 3, pp. 291-312, 2009.

[11] P. Frias, T. Gomez, R. Cossent and J. Rivier, "Improvements in current European network regulation to facilitate the integration of ditributed generation," *Electrical power and Energy Systems,* pp. 445-451, 2009.

[12] G. Krajacic, N. Duic, A. Tsikalakis, M. Zoulias, G. Caralis, E. Panteri y M. Carvalh, «Feed-in tariffs for promotion of energy storage technologies,» *Energy Policy,* vol. 39, pp. 1410-1425, 2011.

[13] M. Esteban, Q. Zhang y A. Utama, «Estimation of the energy storage requirement of a future 100% renewable energy system in Japan,» *Energy Policy,* vol. 47, pp. 22-31, 2012.

[14] F. Rahman, S. Rehman y M. Abdul-Majeed, «Overview of energy storage systems for storing electricity from renewable energy sources in Saudi Arabia,» *Renewable and Sustainable Energy Reviews,* vol. 16, pp. 274-283, 2012.

[15] 2013. [En línea]. Available: http://www.foronuclear.org/energia. [Último acceso: 2012].

[16] «Electric Energy Storage Technology Options: A White Paper Primer on Applications, Costs, and Beneffits,» 1020676, California, 2010.

[17] Eyer, M. James, Corey, P. Garth, Iannucci y J. Joseph, «Sponsoring Organization: USDOE 2004,» 2004.

[18] E. Raducan y L. Moraru, «Energy Storage Systems,» *Journal of Science and Arts,* vol. 14, nº 1, pp. 103-108, 2011.

[19] H. Ibrahim, A. Ilinca y J. Perron, «Energy storage systems-Characteristics and comparisons,» *Renewable and Sustainable Energy Reviews,* vol. 12, pp. 1221-1250, 2008.

[20] J. Kondoh, I. Ishii, H. Yamaguchi, A. Murata y K. Otani, «Electrical energy storage systems for energy networks,» *Energy Conversion and Management,* vol. 41, pp. 1863-1874, 2010.

[21] L. Jörissen, «Energy Storage,» *Encyclopedia of Electrochemical Power Sources,* pp. 215-231, 2009.

[22] C. Schaber , P. Mazza y R. Hammerschlag, «Utility-Scale Storage of Renewable Energy,» *The Electricity Journal,* vol. 17, pp. 21-29, 2004.

[23] J. Mellentine, «Performance Characterization and Cost Assessment of an Iron Hybrid Flow Battery,» *Thesis. University of Iceland,* 2011.

[24] L. Rong-Ceng, «An economic analysis model for the energy storage system applied,» *Electrical Power and Energy Systems,* vol. 34, pp. 132-137, 2012.

[25] P. Georgilakis, «Technical challenges associated with the integration of wind power into power systems,» *Renewable and Sustainable Energy Reviews,* vol. 12, pp. 852-863, 2008.

[26] D. Linden y T. Reddy, Handbook of Batteries, Third ed., McGraw-Hill Professional.

[27] S. Vazquez, S. Lukic, E. Galvan, L. Franquelo y J. Carrasco, «Energy storage systems for transport and grid applications,» *IEEE Trans Ind Electron,* vol. 57, pp. 3881-3895, 2010.

[28] R. Walawalkar y J. Apt, «Market Analysis of Emerging Electric Energy Storage System,» DOE/NETL-2008/1330, 2008.

[29] A. Shukla, S. Venugopalan y B. Hariprakash, «Nickel-based rechargeable batteries,» *Jounal Power Sources,* vol. 100, pp. 122-148, 2001.

[30] M. Yoshio, R. Brodd y A. Kozawa, Lithium-Ion Batteries, ISBN:978-0-387-34444-7 ed., Springer, 2009.

[31] T. Nguyen y R. Savinell, «Flow batteries,» *Electrochemical Society Interface,* vol. 19, pp. 54-56, 2010.

[32] J. Leadbetter y L. Swan, «Selection of battery technology to support grid-integrated renewable electricity,» *Journal of Power Sources,* vol. 296, pp. 376-386, 2012.

[33] C. Parker, «Energy Storage Systems: Batteries,» *Encyclopedia of Electrochemical Power Sources,* pp. 53-64, 2009.

[34] L. Thaller, «Electrically Rechargeable Redox Flow Cells,» de 9th Intersociety Energy Conversion Engineering Conference, Proceedings, 1974.

[35] Hagedorn, H. Norman y L. Thaller, «Redox Storage Systems for Solar Applications,» *NASA TM-81464,* 1980.

[36] K. Nozaki, H. Kaneko , A. Negishi, K. Kanari y T. Ozaka, *Proc. 19th Intersoc. Energy Conv. Eng. Conf.,* vol. 2, pp. 844-894, 1984.

[37] A. Weber, M. Mench, J. Meyers, P. Ross, J. Gostick y Liu, «Redox flow batteries: a review,» *Journal of Applied Electrochemistry,* vol. 41, p. 1137–1164, 2011.

[38] F. Rahman y M. Skyllas-Kazacos, «Solubility of vanadyl sulfate in concentrated sulfuric acid solutions,» *Journal of Power Sources,* vol. 72, pp. 105-110, 1998.

[39] F. Rahman y M. Skyllas-Kazacos, «Optimization of supersaturated vanadium electrolyte for high energy density vanadium redox battery,» de *4th international conference and exhibition on chemistry in industry*, 2000.

[40] M. Vynnycky, «Analysis of a model for the operation of a vanadium redox battery,» *Energy,* vol. 36, pp. 2242-2256, 2011.

[41] C. Ponce de Leon, A. Frias Ferrer, J. González García, D. Szanto y F. Walsh, «Redox flow cells for energy conversion,» *Journal of Power Sources,* vol. 160, p. 716–732, 2006.

[42] G. Codina, «Desarrollo de una planta de acumulación de energía eléctrica basada en el acumulador redox Fe/Cr,» *Thesis Universidad de Alicante,* 1992.

[43] A. Frias-Ferrer, «Optimización de la hidrodinámica de reactores electroquímicos: empleo de métodos experimentales y numéricos,» *Thesis. Universidad de Alicante,* 2004.

[44] J. Escudero-González, A. Alberola y P. López-Jiménez, «Redox Cell Hydrodynamic Modelling. Simulation And Experimental Validation,» *Engineering Applications of Computational Fluid Mechanics,* vol. 7, nº 2, pp. 168-181, 2013.

[45] J. Escudero-González y P. López-Jiménez, «Methodology to optimize fluid-dynamic design in a redox cell,» *Journal of Power Sources,* vol. 251, pp. 243-253, 2014.

[46] N. Wade, P. Taylor, P. Lang y P. Jones, «Evaluating the benefits of an electrical energy storage system in a future smart grid,» *Energy Policy,* vol. 38, pp. 780-7188, 2010.

[47] Electricity Storage Association, «ESA,» 2013. [En línea]. Available: http://www.electricitystorage.org. [Último acceso: 2012].

ANEXO II: REDOX CELL HYDRODYNAMIC MODELLING. SIMULATION AND EXPERIMENTAL VALIDATION

ABSTRACT

An electrochemical reactor is an assembly capable of withstanding an electrochemical reaction of practical application. It consists of electrodes surrounded by a volume of liquid electrolyte. Major difficulty and challenge involved in this modeling is the fact that real experimentation with high acid flows is extremely difficult to perform: to overcome them, some assumptions are proposed in order to achieve a computational model suitable to be used as virtual laboratory for redox batteries designers.

A model is proposed to analyze the flow of the liquid electrolyte in an electrochemical reactor. Numerical and experimental analysis of such flow in a prototype of a real reactor are proposed. Good hydraulic behaviors will be shown in the majority of the volume, even if there are zones with practically no velocities or with recirculations. These volumes are used to define the parameters that indicate the hydraulic operation.

This article describes the experimental and numerical modeling applied to a particular Iron Flow Cell prototype. The experimental validation has shown little numerical errors, smaller that 2.25%. This methodological research provides a very powerful calibrated tool which will help engineers in a future in the decision-making in order to optimize real designs.

Keywords. Computational Fluid Mechanics, Hydraulic Experiment, Electrolyte Distribution, Electrolytic Reactor, Redox Iron Flow Cell.

1. Introduction

The energy storage technologies will play a crucial role in the near future under the use of efficient energy sources and renewable energy such as wind and solar. This sort of energy usually suffers from intermittent problems in distributed generation systems. Actual researches are achieving elements for storing energy to be released as consumer will need it [1] , [2]. In a large scale, this energy storage could alleviate the unpredictability of energy sources by promoting its accumulation over time [3], [4].

One of the most promising among these technologies is the redox flow battery (RFB), as a candidate for the energy storage medium and large scale [5]. These batteries store energy in solutions containing different redox couples. The electrodic processes, reversible, are carried out on the surfaces of the electrodes (porous or not) which in turn can be inert or catalyze the electrode reaction. Redox technologies are excellent candidates for large energy storage and semi-redox for medium quantities, as domestic uses [6].

The amount of energy stored by these devices depends on the amount of accumulated electrolyte, while the power is dependent on the electrode surface. The power stage cannot be separated by the stage of energy storage, as it is directly related to the active mass of the electrode, as the limiting reagent for accumulation is the same electrode [7].

Therefore, this sort of batteries let users modulate their output voltages and capacities by connecting multiple storage cells and using different sized reservoirs. This makes them very appropriated as potential system for distributed energy storage, whose requirements depend on the distribution needs of each system.

For certain renewable energy storage, electrochemical solutions are well suited: they are exclusively electrical inputs and outputs, power and storage capacity can be modularly changed and can be installed relatively close to the consumption points [7]. Furthermore, in the 70s appeared the first class of electrolyte batteries. The first batteries were made in Zinc as anodic material, combined with Oxygen, Chlorine or Brome. In 1974 Thaler proposed the actual redox prototype [8]. In 1980 Hagedorn et al. [9] published the first results obtained on prototypes. Since then, different cell prototypes have been proposed highlighting, among others redox batteries of Fe/Cr [10].

Actually, these prototypes are in use. Furthermore, the hydrodynamic study (relating flow with efficiency) gets special importance with the development of computational fluid dynamics techniques, finding certain precursors of the present work [7], [11], [12]. An interesting

summary of the Redox battery is presented in Weber et al. [6] who highlights this main idea: the future of this technology goes through optimizing the design modeling: flow and transport.

Fig. 1 describes the conceptual diagram of the redox cell. In this particular case, an iron flow cell is represented. The two electrolyte storage tanks are represented as two cylinders on the sides of the Fig. 1. The tank located on the negative electrode maintains one of the redox pairs in solution, and the positive tank maintains the second redox pair in solution. Two pumps are installed: one in each side of the reactor (Fig. 1). These pumps move the electrolyte across the cell in order to allow the redox semi-reactions and achieve the charge transfer.

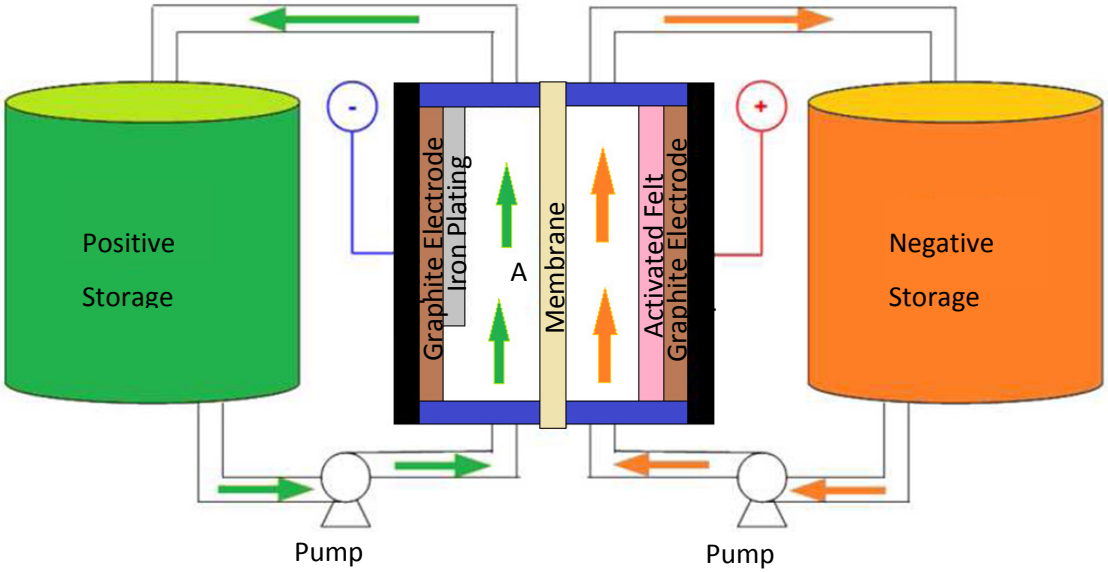

Fig. 1 Typical scheme of a generic reactor.

The cell structure is surrounded by bipolar plates: structural support and electrical conductor. The electrodes are located on the side of each bipolar plate. These are not part of the electrochemical reactions, but provide a surface which facilitates the path of the electrons. Between the two sides of the reactor a membrane is located, acting as physical separation between the two electrolytes, preserving the electroneutrality. The named volume “A” in Fig. 1 is occupied by electrolyte. The here developed prototype represents the flow horizontally, with a geometry and flow similar to a real iron flow battery cell.

There are many interesting aspects in the design of the cell: key materials, electrode and membrane [13]. Vanadium batteries are the most known ones, with deeper analysis reported in the references [14], [15]. The uniformity of flow has a significant influence on the effective area of the electrode, the strength and efficiency, the lifetime of the battery and electrochemical polarization; especially under high current density variation

The consulted references [3] also highlight that the flow of electrolyte through the active layer has a high performance inference in the same. Moyabayashi et al. [16] conclude that the uniform distribution of electrolyte is essential to increase energy efficiency. Nevertheless, even when the flow is homogeneous, some important variations of velocity can be found in the electrode surfaces that can lead, among other effects, to strong changes in pH. The importance of this velocity analysis has also been reported in the references [17], [18]. The reverse flow zones will be located mainly around the entrance of the flow. According to the reviewed literature, as pointed out in Bengoa et al [17], the flow distribution is asymmetric due to the design of the inlet system in the active zone, as this is the less uniform part of the flow. As demonstrated by Wragg and Leontaritis [18] the local mass value coefficient measured in different geometries of cells with baffles (to uniformize the flow) and without them, was critically affected by the complex hydrodynamic effects associated with phenomena such as cell inlet and exit and flow reversal near baffles ends. This effect was also observed and furthermore, quantified in this case.

Flow distribution inside the battery is a difficult parameter to determine and visualize. It is caused by different factors, i.e.: the compact structure of the battery, the opaque materials and the strong acidity of the electrolyte. Nevertheless, all the consulted researches indicate the paramount importance of a correct distribution for the efficiency of the whole system [19], [20]. In this framework, the purpose of this research is to analyze and reveal the movement of the electrolyte inside the cell by means of CFD techniques, solving the equations applied to the mechanism of movement of electrolyte inside the redox cell. The numerical analysis will provide some quantifiable parameters describing the performance of the system. This methodology has been validated on an experimental facility in laboratory scale.

2. Materials and methods

This research was performed in two complementary phases. On one side, a laboratory-scale prototype is developed in Electrochemical Department in Alicante University (Spain) [12]; on the other side, a commercial code for CFD modeling (STAR-CCM+ [21]) is used for the computational analysis of the cell.

2.1 Experimental device; taking measurements in the laboratory

Fig. 2 represents the developed laboratory device. A prototype of the redox cell has been built with a power of 5 W and a capacity of 0.1 kWh, with an area of 63 cm^2. The cathode is made of graphite or carbon felt. The anode is made in carbon felt and a selective membrane as separator. Two peristaltic pumps are used, equipped with jacketed tanks for the negative and positive compartments [22] [11]. The prototype has also an electronic resistance and a data logger for electrical parameters. The viscosity of the electrolyte has been measured at the working temperature (40ºC), which is the same than water at 20ºC.

In this case study, the more interesting variables to be considered are the pressures in five different points of the prototype. To measure such values of pressure, a set of piezometers have been installed in the interesting points, as observed in Fig. 2.

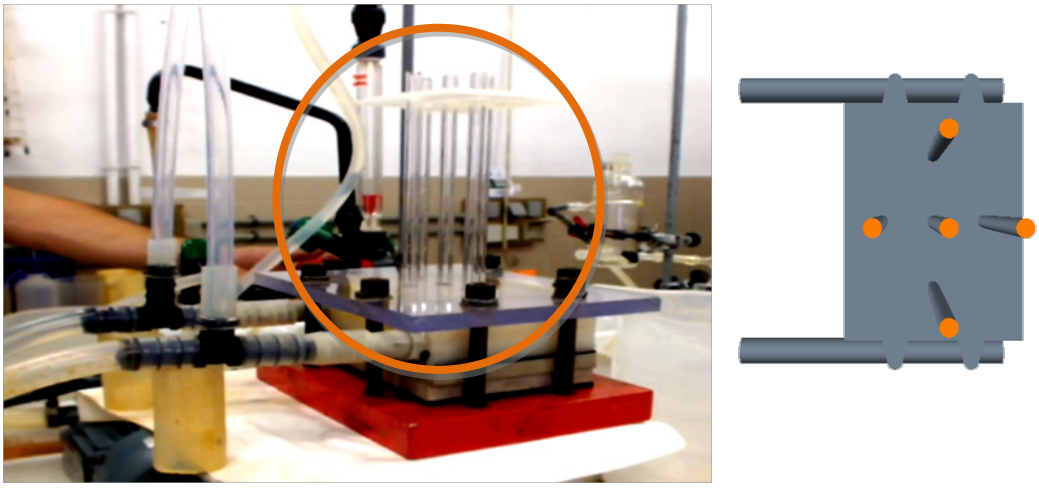

Fig. 2 Experimental prototype installations and view of interest points.

A high definition camera and a tracer dye have been used for velocity measurements. Preferential paths will be thus observed in the flow within the cell, as the prototype is built in transparent material.

2.2 The computational model: solving the flow equations

Computational Fluid Dynamics (CFD) is a parallel approach in hydrodynamic modeling. Throughout the twentieth century the study and practice of fluid dynamics, both in the science of physics and engineering is based on theoretical tools on one side and experimental tools in the other side [23]

Since 1960s, the emergence and development of computers along with the development of accurate numerical algorithms revolutionized the way in which fluid dynamics had been treated until then. Thus, the CFD (defined as "a set of numerical computational methods based on the equation of conservation of mass and the Navier-Stokes equations") is presented today as a powerful tool in research and engineering design. CFD techniques are a virtual laboratory for the knowledge of pressures and velocities at any point of a considered geometry, comparing it with experimental measurements used in the validation process.

This work was carried out using commercial software specialized in solving fluid dynamics equations: STAR-CCM +. This is interactive software for the simulation of physical processes in engineering (fluid or solid). This platform is an interface that has implemented various models and algorithms allowing developing computational simulations from conceptual models previously conceived. Fig. 3 shows the methodology to be followed in the numerical modeling.

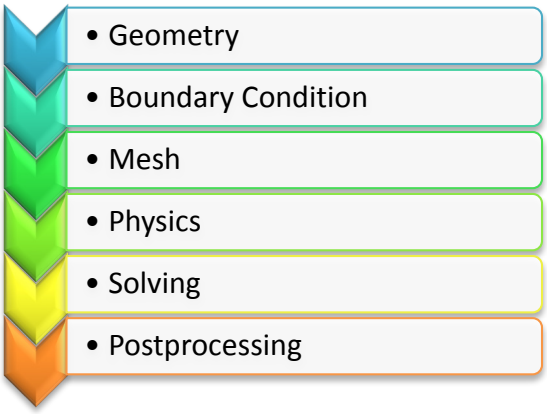

Fig. 3 CFD methodologies.

2.2.1 Real geometry and mesh of the fluid model

Before introducing the geometry in the calculation software, the geometry must be properly prepared. To do this, the geometry of the experiment has been modeled using the SolidWorks software. Once the geometry of the reactor is represented, it is imported to the calculation software and the meshing process is performed on the fluid domain. Hexahedral elements

adapted to the surface have been chosen for the volumetric mesh, by applying a mesh refinement. Fig. 4 shows the general geometry considered in the modeling process.

To verify that the results are independent of the number of cells, several simulations with different meshes have been performed: that is, reducing the cell size. The objective is find out the more convenient mesh size, after considering the affection of different mesh numbers on the computation results. Five different meshes were proposed by changing the relative minimum size (mm) and the relative target size (mm), resulting in different number of elements. The main parameters of these five meshes are described in Table 1 with simulations for 70 l/h.

FLOW (70l/h)	mesh 1	mesh 2	mesh 3	mesh 4
Relative minimum size (MM)	0.3	0.15	0.05	0.05
Relative target size (mm)	1.2	0.8	0.4	0.3
Volume mesh cells	85,172	143,481	357,252	581,964

Table 1 Different mesh parameters considered for comparison.

In order to choose the more convenient mesh, achieving a compromise between size and accuracy, a comparison of the influence in pressure predictions is performed. Comparison between the pressure simulations (in the interest points) with all meshes has been done. Differences in RMSE for these pressures are depicted in table 2 for all the performed meshes.

Difference in RMS for pressure predictions	mesh 1	mesh 2	mesh 3	mesh 4
mesh 1	- - -	1.6	1.8	1.9
mesh 2	1.6	- - -	0.4	0.4
mesh 3	1.8	0.4	- - -	0.2
mesh 4	1.9	0.4	0.2	- - -

Table 2 Comparison of RMSE predictions for pressure between pairs of meshes (%).

Regarding table 2, optimized mesh number is mesh 3. It has been considered a good mesh when the error (in simulated pressure) by comparing simulation results with another mesh is less than 1 %. On the one hand, coarser meshes than mesh 3 give poorer results in pressure; on the other hand, mesh 4 (finer than mesh 3, with more cells and a bigger computational time), increase the accuracy of the results only in 0.2%. As a consequence, mesh 3 is finally implemented for all the simulations. Optimized mesh main parameters are described in table 3.

Base size (mm)	1.6	Surface curvature (pts./circle)	60
Relative minimum size (mm)	0.05	Maximum cells size (mm)	4.8
Relative target size (mm)	0.4	Remeshed surface (FACES)	411,556
Volume mesh (cells)	357,252		

Table 2 Optimized mesh features.

Fig. 4 gives some details about the resultant optimized mesh.

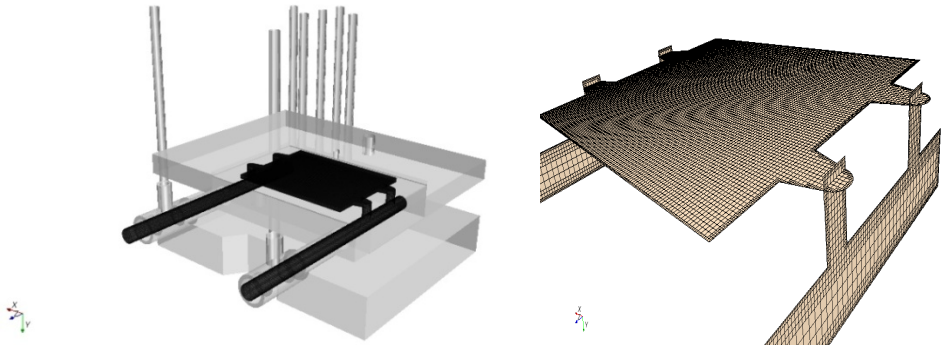

Fig. 4 Geometry and mesh detail.

2.2.2 Boundary Conditions

An input speed and an output pressure of the model have been designed. The other boundaries are represented by a condition of wall, the one used by the computational code is similar to the one called "smooth tube roughness" [24] that is well suited to the material properties of the prototype. Initial readings in the experimental prototype indicate that the pressure at the outlet of the model is lower than the atmospheric value used to calibrate the model (table 4). In Fig. 5 the five measurement points and the input and output boundary conditions are shown.

The selective membrane does not affect the hydrodynamic movement of the fluid, as there is no pass of fluid across the membrane; only electronic transfer occurs in this process. As this does not affect velocity, pressure or turbulence, the boundary condition implemented for the membrane is wall.

FLOW (l/h)	PRESSURE OUTLET (mmca)
70	-4
80	-4
90	-7
100	-10

Table 3 Outlet pressure conditions according to the flow.

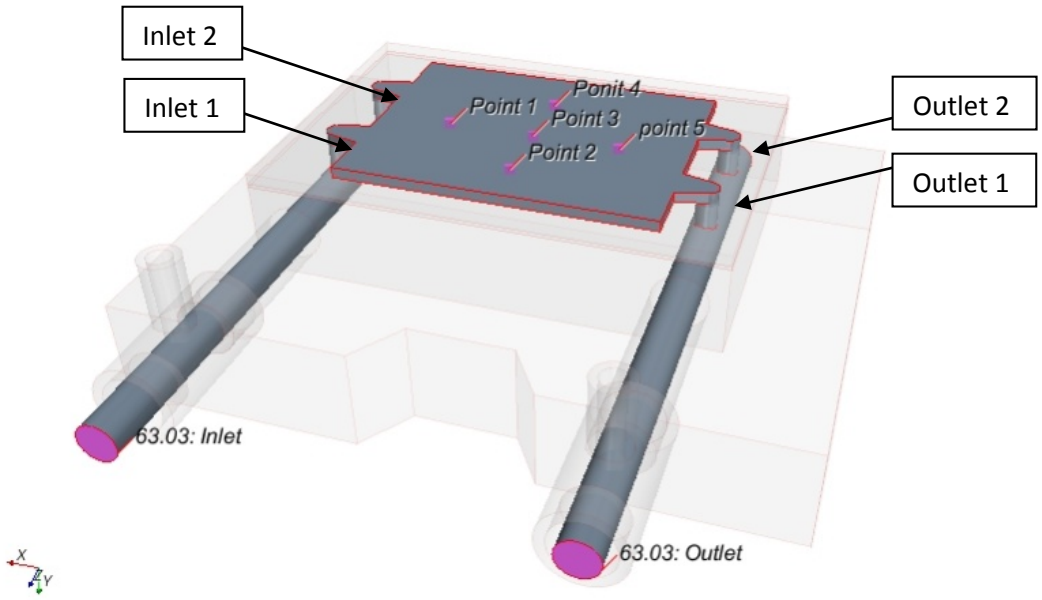

Fig. 5 Boundary conditions and measurement points.

2.2.3 Physics

A series of hypotheses have been made for the modeling of the cell, applied to this prototype of iron flow battery. The most important one has been the fact of assuming that the electrolytic fluid produces no deposition within the cell as well as it does not produce any gas phase. This hypothesis would be completely true if the redox reaction was 100% efficient. In reality other competing reactions can occur with little gas production, which are disregarded as hypothesis [25]. Another assumed hypothesis is the one concerning the density of the fluid. Density is considered constant for all flow and we work with piezometric pressures. The viscosity of the electrolytic fluid at 40 ° C is the same as the viscosity of the water at 20 ° C. Therefore, together with the easy management of the water, it is convenient the use of the water as working fluid in the experimental model, despite of disregarding other variations which occur with the actual fluid, such as pH and conductivity [7], [11].

Unlike the velocity analysis which is transient, the analysis of the pressure is steady-state. The segregated flow model is used; it solves the equations (one for each velocity component and one for each pressure component) separately. The link between the equations of motion and continuity is achieved by a corrector-predictor approach. The complete formulation can be described the use of an array of juxtaposed variables and a velocity-pressure coupling solved in the Rhie-Chow interpolation known [26].

It is assumed that turbulence occurs in the simulation due to the input and output effects. It is generally considered that the transition from laminar to turbulent is performed by passing from Reynolds Number 2000 and 2300 to 4000. From this value, the flow begins to accelerate and certain turbulent parameters can appear in the movement, in the so-called transition zone, which reaches the value of 4000. In the case of the here described simulations, despite the low Reynolds Numbers in the cell, there may be local turbulences. This has already been reported in bibliography [27], [28], so as the Reynolds Number grows, the hypothesis of laminar flow loses representation and solutions should be found for the turbulence.

The model of turbulence used is the realizable k-epsilon model developed by Shih et al. [29], this is a semi-empirical model based on transport equations of the kinetic turbulent energy (k) and the range of dissipation (ε). This model contains a new transport equation for the turbulent dissipation rate. Also, a critical coefficient of the model, is expressed as a function of mean flow and turbulence properties, rather than assumed to be constant as in the standard model. This allows the model to satisfy certain mathematical constraints on the normal stresses consistent with the physics of turbulence (realizability). The concept of a variable is also consistent with experimental observations in boundary layers.

The Transport Equations:

$$\frac{\partial}{\partial t}(\rho k) + \frac{\partial}{\partial x_j}(\rho k u_j) = \frac{\partial}{\partial x_j}\left[\left((\mu + \frac{\mu_t}{\sigma_k}\right)\frac{\partial k}{\partial x_j}\right] + P_k + P_b - \rho\epsilon - Y_M + S_k \quad (1)$$

$$\frac{\partial}{\partial t}(\rho \epsilon) + \frac{\partial}{\partial x_j}(\rho \epsilon u_j) = \frac{\partial}{\partial x_j}\left[\left((\mu + \frac{\mu_t}{\sigma_\epsilon}\right)\frac{\partial \epsilon}{\partial x_j}\right] + \rho C_1 S\epsilon - \rho C_2 \frac{\epsilon^2}{k+\sqrt{\upsilon\epsilon}} + C_{1\epsilon}\frac{\epsilon}{k}C_{3\epsilon}P_b + S_\epsilon \quad (2)$$

Where:

$$C_1 = max\left[0.43, \frac{\eta}{\eta+5}\right], \qquad \eta = S\frac{k}{\epsilon}, \qquad S = \sqrt{2S_{ij}S_{ij}} \quad (3)$$

In these equations, P_k represents the generation of turbulence kinetic energy due to the mean velocity gradients, calculated in same manner as standard k-epsilon model. P_b is the generation of turbulence kinetic energy due to buoyancy, calculated in same way as standard k-epsilon model.

The modeling turbulent viscosity is:

$$\mu_t = \rho C_\mu \frac{k^2}{\epsilon} \tag{4}$$

Where:

$$C_\mu = \frac{1}{A_0 + A_S \frac{kU^*}{\epsilon}} \tag{5}$$

$$U^* \equiv \sqrt{S_{ij}S_{ij} + \widetilde{\Omega}_{ij}\widetilde{\Omega}_{ij}} \tag{6}$$

$$\widetilde{\Omega}_{ij} = \Omega_{ij} - 2\epsilon_{ijk}\omega_k \tag{7}$$

$$\Omega_{ij} = \overline{\Omega_{\iota J}} - \epsilon_{ijk}\omega_k \tag{8}$$

Where $\overline{\Omega_{\iota J}}$ is the mean rate-of-rotation tensor viewed in a rotating reference frame with the angular velocityω_k. The model constants A_0 and A_S are given by:

$$A_0 = 4.04, \quad A_S = \sqrt{6}\, cos\phi$$
$$\phi = \frac{1}{3} cos^{-1}\left(\sqrt{6}\ W\right), \quad W = \frac{S_{ij}S_{jk}S_{ki}}{\tilde{S}^3}, \quad S = \sqrt{S_{ij}S_{ij}}, \quad S_{ij} = \frac{1}{2}\left(\frac{\partial u_j}{\partial x_i} + \frac{\partial u_i}{\partial x_j}\right) \tag{9}$$

Model Constants:

$$C_{1\epsilon} = 1.44, \quad C_2 = 1.9, \quad \sigma_k = 1.0, \quad \sigma_\epsilon = 1.2$$

2.2.4 Solving equations and postprocessing

Once the boundary conditions have been well defined and a suitable mesh in the full model is implemented, the computer code solves the equations of movement (conservation of mass or continuity (10), and conservation of movement quantity or Navier Stokes (11)).

$$\nabla \overline{U} = 0 \tag{10}$$

$$\frac{\partial \overline{U}}{\partial t} + \nabla\left(\overline{UU}\right) - \nabla\left(\nu \nabla \overline{U}\right) = -\nabla \overline{p} + \overline{U'U'} \tag{11}$$

Where U represents the velocity vector, U 'indicates fluctuations around the value of the mean velocity, p is the dynamic pressure, ν is the kinematic viscosity and $\overline{U'U'}$ represents the so-called Reynolds stresses. In laminar flow conditions, the average velocities coincide with the snapshots and the Reynolds term vanishes, leading to a closed system of equations, which requires no turbulent solutions. In turbulent flow, as Reynolds stresses are not canceled, close

solutions are needed which provide the sufficient equations to know the instantaneous velocities throughout the domain. At low Reynolds Numbers, the most indicated solutions are k-epsilon [30], [31], [32]. The bibliography is profuse in the use of these techniques in similar engineering problems [33], [34], [35] even in modeling environments close to the here described technique [36], [37].

In this modeling, three-dimensional simulations were performed using the STAR-CCM + software. This is based on the finite volume method (FVM) to solve the conservation of mass equation and the Navier-Stokes averaged equations in a curvilinear mesh, not taking into account the effects of temperature. Second order upwind scheme is used in this case for discretization. The advantage of this scheme over the first-order upwind scheme is that it is nominally second-order accurate. In order to meet the mass conservation condition a correction algorithm standard pressure (SIMPLE) is used. Thus, the code solves algebraic and iteratively equations considering gravity at all times until the residue numbers values are sufficiently low (less than 10^{-3}) considering that the resolution has converged.

3. Results and discussion

3.1 Steady

A steady flow is characterized by constant values of all flow variables at any location in space. If $\emptyset$ is any flow quantity like velocity, pressure, etc., then in steady flow

$$\frac{\partial \emptyset}{\partial t}(x, y, z, t) \equiv 0 \quad (12)$$

Hence all flow quantities depend only on the spatial location

$$\emptyset(x, y, z, t) = \emptyset(x, y, z) \quad (13)$$

Where as a flow in which flow/fluid properties keep on changing with time, is termed as unsteady flow.

3.1.1 Pressure

Fig. 6 shows measurements taken in the device for flows 70, 80, 90 y 100 l/h. In the same figure, simulations performed for the same flows are depicted, observing very little deviation between them.

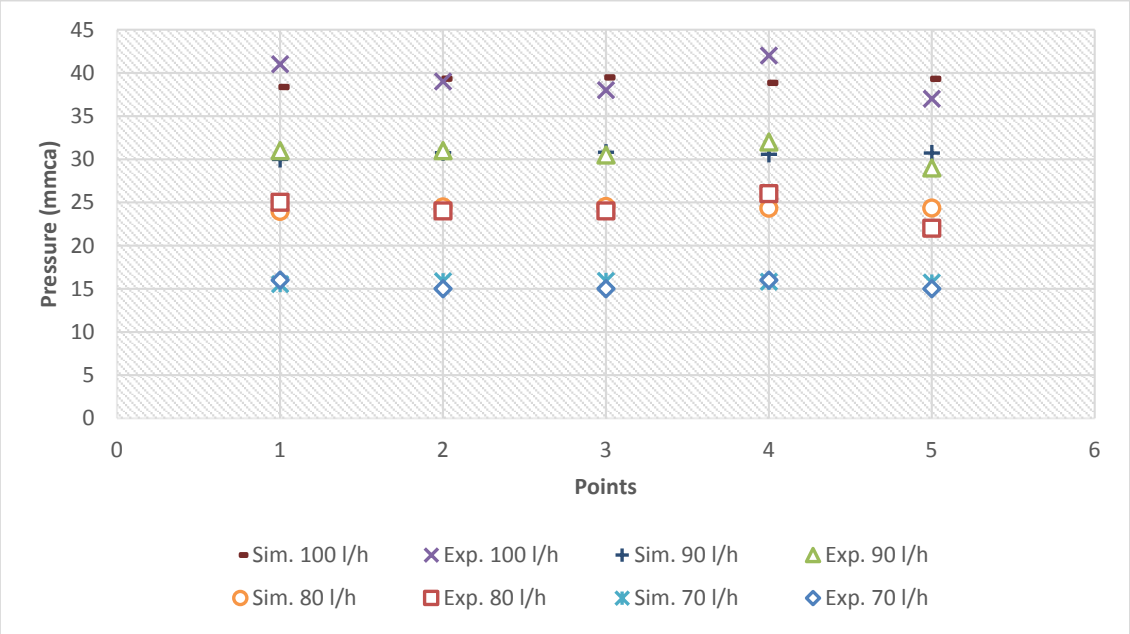

Fig. 6 Experimental measurements versus computational model of pressures.

To quantify the accuracy of the performed measurements, the root mean squared error is proposed to be used (RMSE) [38]. This is defined by the expression:

$$RMSE = \sqrt{\sum_{i=1}^{N} \frac{(\emptyset_i - \emptyset_{i,obs})^2}{N}} \quad (14)$$

where:

$\emptyset_i$ is the predicted value for i cell.

$\emptyset_{i,obs}$ is the observed value for i cell

N is the number of analyzed cases: 5.

The RSME for each flow (Reynolds Number in table 5) is depicted in table 6.

FLOW (l/h)	Nº REYNOLDS
70	1612
80	1842
90	2072
100	2303

Table 4 Reynolds Number for each flow.

FLOW (l/h)	RMSE (%)
70	0.69
80	1.41
90	1.12
100	2.22

Table 5 RMSE for modeled flow.

The deviation in relative terms is very small. Discordances between measurements and models are smaller than 2.25%. This accuracy in these sorts of models represents a clear success. The slower the flow is the smaller the errors; as it can be observed in table 6.

3.2 Implicit unsteadiness

In the implicit unsteady approach each physical time-step involves some number of inner iterations to converge the solution for that given instant of time. These inner iterations may be accomplished using the same implicit integration or explicit integration schemes used for steady analysis. The physical time-step size used in the outer loop is specified by you, whereas the inner

iterations are marched by the integration scheme using optimal local steps as determined by the Courant number. For temporal discretization, the Euler method is used in an implicit way.

The explicit unsteady approach is effectively the same as the explicit integration scheme available for steady-state simulations, but using a constant time-step for all cells in the domain (rather than local time-stepping). In this case the size of the time-step is determined automatically by the solver such that one value satisfies the Courant condition at all points (that is, the minimum allowable time-step is used everywhere). Thus each iteration becomes a time-accurate advancement of the solution. In this case the Courant number should be 1 or less, resulting in a physical time-step that varies from one iteration to the next as the flow field changes. Furthermore, preconditioning of the governing equations is omitted, thus making the explicit unsteady approach unsuited for incompressible flow simulations.

For implicit unsteady computations, the time-step is specified by the user (0.01s). However, a local pseudo time-step associated with the iterations within a time-step is computed using the same Courant numbers as follows:

$$Courant\ Number = \frac{u}{u_n} = \frac{u\Delta t}{\Delta x} \quad (15)$$

Where:

Δx = base size.

Δt = time-step.

u = velocity.

3.2.1 Velocity

Flow analysis requires a transient simulation in order to compare velocities between model and experimental device. Velocity field for 70 l/h has been analyzed by means of a HD video. A comparison has been performed for each instant, observing in a qualitative way the coupled tendency between both models. Fig. 7 shows three instantaneous comparison of velocity contours as described. In this Fig. both computational and experimental models show a trend to asymmetry in the velocity distribution along the whole device: inlet and outlet 1 have more flow that inlet and outlet 2.

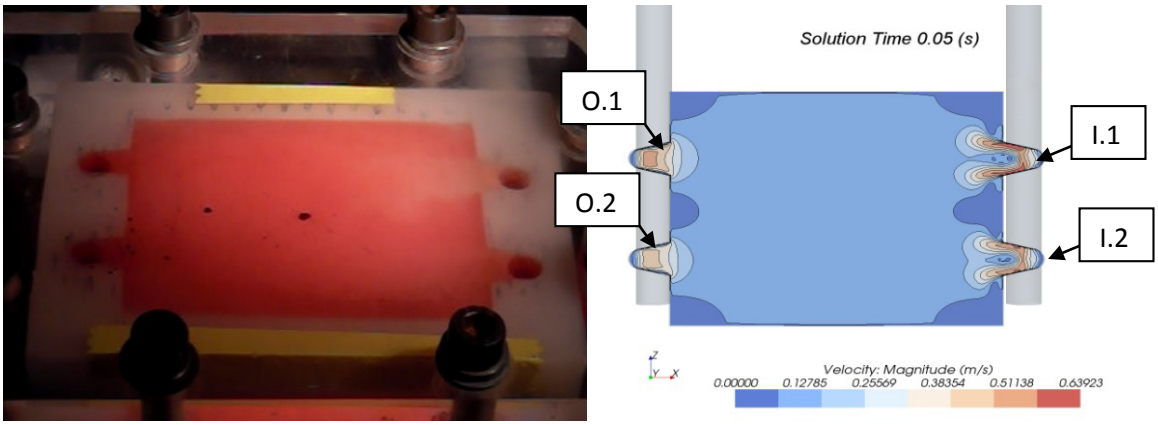

Experiment versus computational model of velocity at time 0.05 seconds.

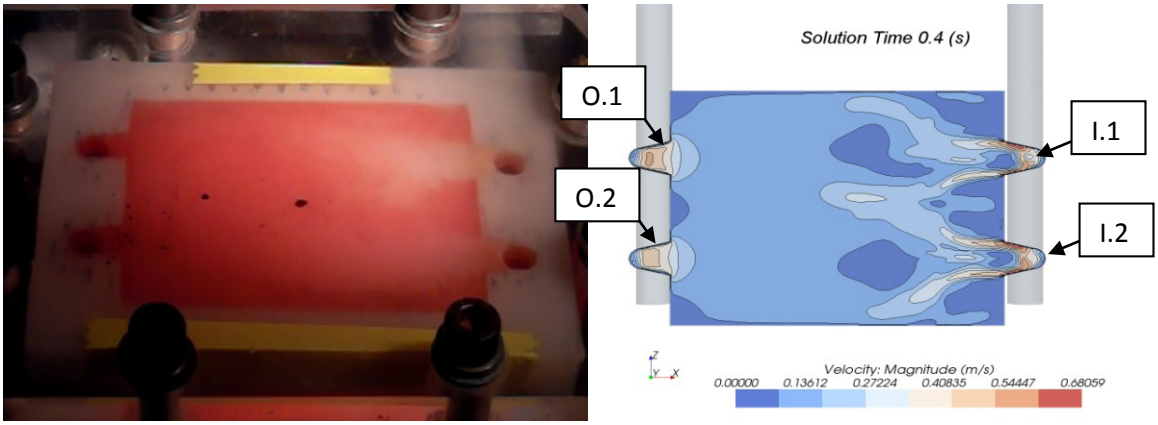

Experiment versus computational model of velocity at time 0.4 seconds.

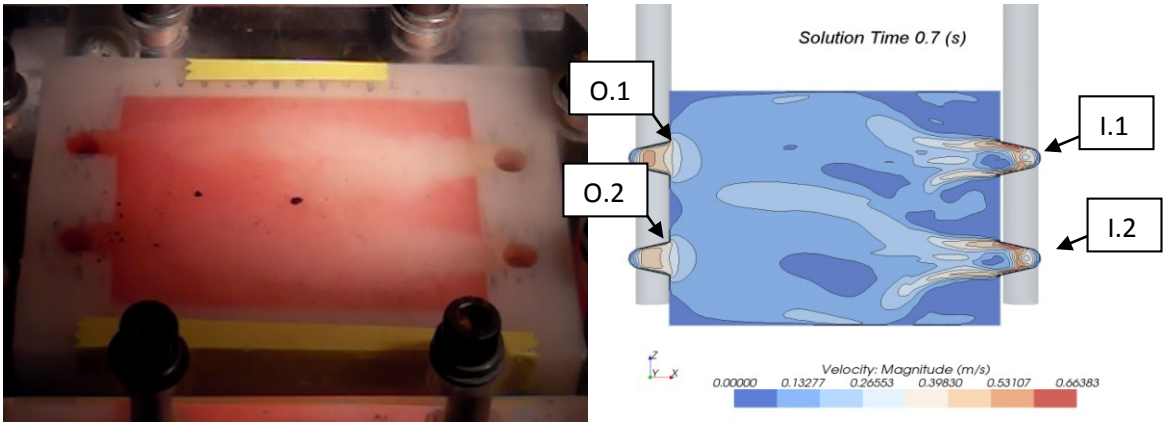

Experiment versus computational model of velocity at time 0.7 seconds.

Fig. 7 contour for velocity field, visual calibration.

3.3 Postprocessing, parameters to quantify the flow behaviour: steady state conditions

Under the calibration process performed, the computational model is considered valid for representing the hydraulic performance of the system. Furthermore, the flow is fully analyzed in the steady state model by means of the computational simulation for 70 l/h. Therefore, the parameters proposed in this analysis for determining the flow behavior are:

- Pressure, evaluated in the XZ central point of the reactor.
- Streamlines, following the inlet conditions, let the modeler visualize possible recirculations and their location.
- Percent volume analysis: considering the number of cells occupied by flow moving in the main direction of the flow and opposite to this direction. This parameter allows the modeler to know partial recirculations.
- Velocities, analyzed as vectors in the mean plane of the reactor in the main current direction.

Fig. 8 and 9 make reference to pressure analysis. Fig. 8 shows the pressure contours inside the reactor. Limits in the observed values determine the total head loss inside the device. Fig. 9 depicts the pressure distribution in the tridimensional model and in exes X and Y (expressed in meters) in the mean plane described in Fig. 8.

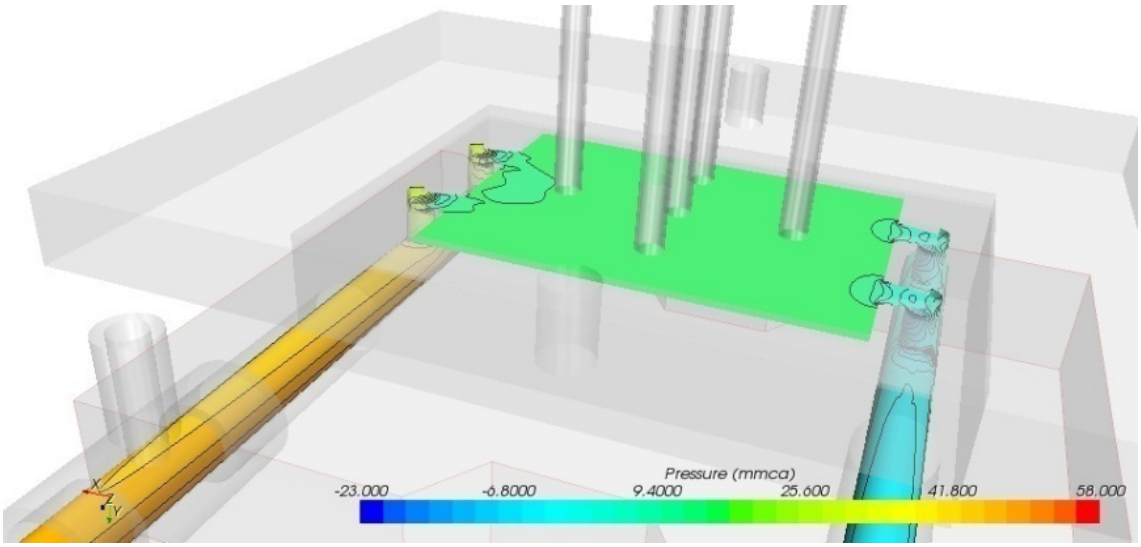

Fig. 8 Pressure contours.

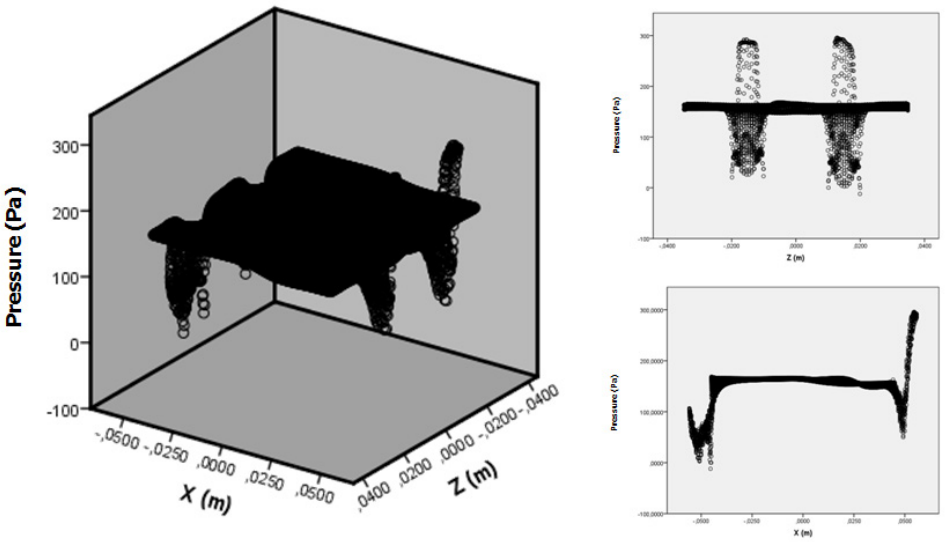

Fig. 9 Pressure distribution 3-D, X and Z.

Fig. 10 shows the streamlines inside the considered reactor. As it can be observed, different turbulences appear in the whole control volume.

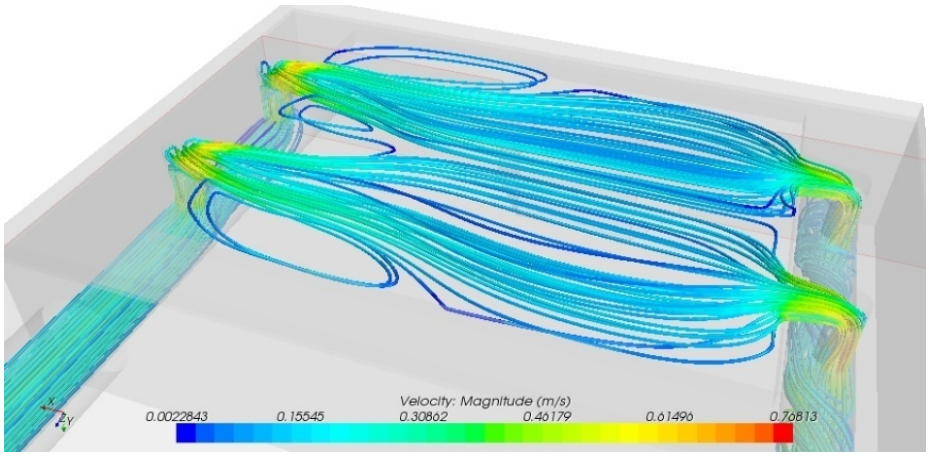

Fig. 10 streamlines inside the cell.

Fig. 11 shows the volume occupied by fluid moving in the same direction that main flow (A) and the volume occupied by fluid moving in an opposite direction to the main flow (B).

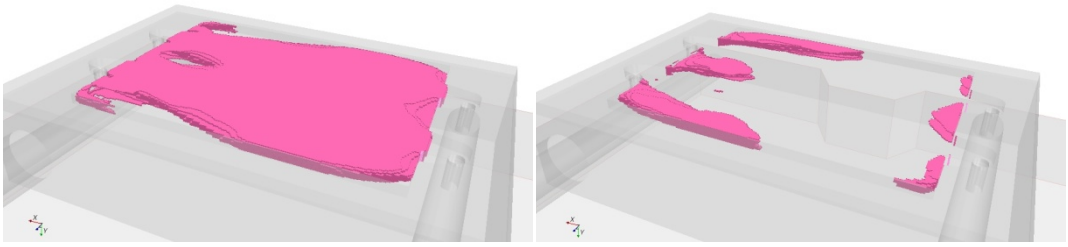

Fig. 11 (A) Volume occupied by cells with flow in the main direction; (B) Volume occupied by cells with flow opposite to the main direction.

Table 7 quantifies this percent volume. On one hand, a big value of the percent volume of flow moving in the main direction of the flow indicates a more uniform distribution in the electrolyte. This uniformity is of paramount importance for the good behavior of the system. On the other hand, the volume in which the velocity is opposite to main current increases as flow does. This tendency is a consequence of the upcoming value of Reynolds Number; and therefore turbulence and recirculation.

Flow (l/h)	% Volume in the mean current	% Volume opposite to main current
70	84.3	15.7
80	83.6	16.4
90	82.9	17.1
100	82.3	17.7

Table 6 results of Volume percent with velocity parallel and opposite to the main current.

This parameter is related to recirculations that influence the behavior of the flow. This volume should be as small as possible. In this sense, two observations are feasible: On one hand; related to the local position of these zones: mostly in the entrance of the cell. This is the most interesting zone to propose improvements in the design, in order to uniform the velocity vectors. Some improvements could be addressed to add a pre-chamber for acquiring uniformity or consider more than two inlet tubes: more longitudinal distribution of the inlet condition. On the other hand, this cell should be implemented for small flows. As the flows increases, the uniformity decreases. This parameter can quantify the optimum range of flow to be implemented for each cell, determining the maximum value of flow for designing future sizes of cells.

Regarding to velocities inside the cell, Fig. 12 depicts the tridimensional velocity contour. X and Z velocity module are also presented in the Fig. 12 as it can be observed, the velocity value is neither homogeneous, but with a little range of variation of 0.8m/s.

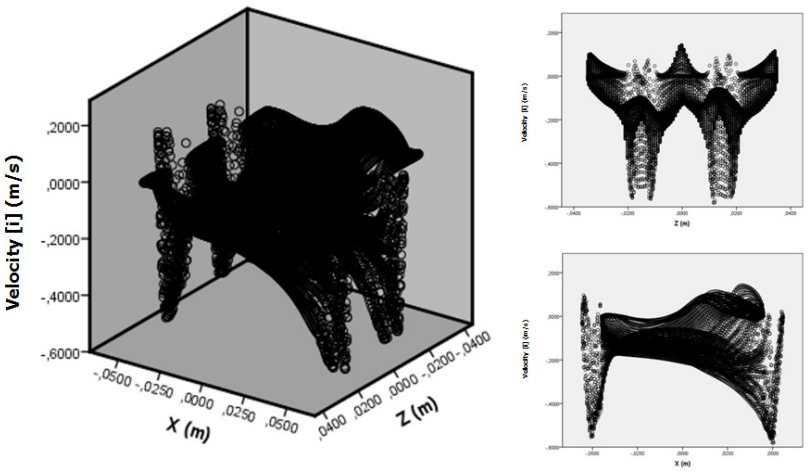

Fig. 12 Velocity distribution [i] 3-D view, X and Z.

Fig. 13 represents the velocity module in the mean plane. As it can be observed, very little volume of dead zones are present in the prototype. Velocity is not homogeneous, but volumes occupied by recirculation flow is small (15.55 to 17.7% for different modeled flows, increasing as Reynolds Number does).

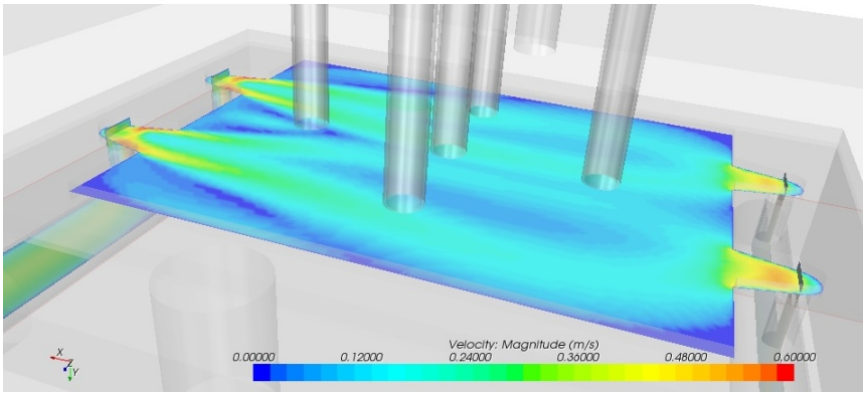

Fig. 13 Velocity modules in the mean plane.

These dead zone or recirculation volumes are mainly located in inlet (mainly) and outlet parts of the cell, as referred. Nevertheless, some improvements in the design can be performed to avoid dead zones and recirculations. A deeper analysis will be performed in this part of the cell, providing different geometries in order to minimize recirculations and quantify the effectiveness of the designs related to decrease the turbulence. Some possible improvements will be performed, among others: to increase the number of inlets; to use different diameters in each inlet to avoid asymmetries or to design a sort of strainer chamber before the main entrances to the cell in order to increase the laminarity of the flow.

4. CONCLUSIONS AND FUTURE WORKS

An experimental device for representing a prototype for redox cell has been presented. The electrolyte flow has also been numerically modeled for a geometry adapted to this device. A transparent material has been used for visualize the streamlines of the flow, while pressure have been measured with piezometers.

At the same time, a numerical model has been developed based on a commercial code used for solving the fluid mechanics equations. By means of the resolution of the equations, pressures, velocities and streamlines will be known in all the modeled volume. With a similar geometry, measurements of pressure have been performed in same points of the real prototype and time instant. These analyses depict a great agreement between modeled and measured values. RSME has been used for comparing both measurement and modeled velocities and pressures, varying from 0.69 until 2.22%, growing as the Reynolds Number does.

A parameter has been proposed for quantify the flow laminarity in a tridimensional study: the percent of volume in the main direction of the current and in the opposite direction to the current. A big value of volume of fluid advancing in the main direction of flow with similar value of velocity represents uniformity, avoiding preferential ways. In the considered prototype, this value is around 83%, allowing future enhancements for the designs. The main definition of this parameter is a contribution of this paper. This parameter will let the modeler to compare geometries by considering uniformity of the flow using CFD techniques.

In this particular case, the validation of the numerical model has also been presented. This validation process is an additional advantage, as the real electrolyte fluid is highly acidic and corrosive. The simplified model sheds light on its hydrodynamic behavior (despite not considering the chemical aspects under the assumptions made).

Actually, this research has been focused on modeling the hydrodynamic of the cell. In this sense some parameters have been processed to quantify the behavior of the flow. The analysis of these results makes some indications about future improvements in the design previously discussed, mainly based avoiding turbulences around entrances.

Future works will be consequent with the previous analysis: On one side, different scale models will be developed in order to apply improvements and similarity; On the other side, different parameters will be proposed to study the evolution of the flow.

The possibility of having a versatile numerical model as a virtual laboratory will allow the designer to make future decisions. Different configurations will be able to be analyzed,

quantifying information referred to hydrodynamics of the flow. As a result, the application of CFD techniques is postulated as a key tool for future developments in this field.

5. References

[1] M. Rychcik and M. Skyllas Kazacos, "Characterist of a new all-vanadium redox flow battery," vol. 22, pp. 59-67, 1987.

[2] R. Dell and D. Rand, "Energy storage-a key technology for global energy sustainability," vol. 100, pp. 2-17, 2001.

[3] L. Joerissen, J. Garche, C. Fabjan y G. Tomazix, «Possible use of vanadium redox-flow batteries for energy storage in small grids and stand-alone photovoltaic systems,» vol. 127, pp. 98-104, 2004.

[4] Z. Yang, J. Zhang, M. Kintner Meyer, X. Lu, D. Choi, J. Lemmon y J. Liu, «Electrochemical Energy Storage for Green Grid,» vol. 111, pp. 716-732, 2011.

[5] C. Ponce de Leon, A. Frias Ferrer, J. González García, D. Szanto y F. Walsh, «Redox flow cells for energy conversion,» *Journal of Power Sources,* vol. 160, p. 716–732, 2006.

[6] A. Weber, M. Mench, J. Meyers, P. Ross, J. Gostick y Liu, «Redox flow batteries: a review,» *Journal of Applied Electrochemistry,* vol. 41, p. 1137–1164, 2011.

[7] A. Frias-Ferrer, «Optimización de la hidrodinámica de reactores electroquímicos: empleo de métodos experimentales y numéricos,» *Thesis. Universidad de Alicante,* 2004.

[8] L. Thaller, «Electrically Rechargeable Redox Flow Cells,» de *9th Intersociety Energy Conversion Engineering Conference, Proceedings*, 1974.

[9] Hagedorn, H. Norman y L. Thaller, «Redox Storage Systems for Solar Applications,» *NASA TM-81464,* 1980.

[10] K. Nozaki, H. Kaneko , A. Negishi, K. Kanari y T. Ozaka, *Proc. 19th Intersoc. Energy Conv. Eng. Conf.,* vol. 2, pp. 844-894, 1984.

[11] G. Codina, «Desarrollo de una planta de acumulación de energía eléctrica basada en el acumulador redox Fe/Cr,» *Thesis Universidad de Alicante,* 1992.

[12] P. Frias, T. Gomez, R. Cossent and J. Rivier, "Improvements in current European network regulation to facilitate the integration of ditributed generation," *Electrical power and Energy Systems,* pp. 445-451, 2009.

[13] V. Estahanian, H. Mahmoodi, H. Babazadeh, M. Aghvami, R. Pasandeh, F. Torabi y G. Ahmadi, «Numerical simulation of electrolyte particles trajectory to investigate battery cover design characteristics,» vol. 191, pp. 139-143, 2009.

[14] X. Ma, H. Zhang y F. Xing, «A three-dimensional model for negative half cell of the vanadium redox flow battery,» vol. 58, pp. 238-246, 2011.

[15] M. Secanell, J. Wishartb y P. Dobson, «Computacional design and optimization of fuel cells and fuel cells systems: A review,» vol. 196, April 2011.

[16] M. Moyabayashi, T. Tayama, Y. Kageyama y H. Oyama.Patente 5.851.694, 1998.

[17] C. Bengoa, A. Montillet, P. Legentilhomme y J. Legrand, «Flow visualization and modelling of a filter-press type electrochemical reactor,» vol. 27, pp. 1313-1322, 1997.

[18] A. Wragg y A. Leontaritis, «Local mass transfer and current distribution in baffled and unbaffled parallel plate electrochemical reactor,» vol. 66, pp. 1-10, 1997.

[19] J. Cheng, B. Wang y J. Yang, «Adsorption and Diffusion of VO2+ and VO2 + across Cation Membrane for All-Vanadium Redox Flow Battery,» *Solvent Extraction and Ion Exchange,* vol. 27, pp. 312-327, 2009.

[20] J. Cheng, B. Wang y L. Hong-Ling, «Numerical Simularion and Experiment on the Electrolyte Flow Distribution for All Vanadium Redox Flow Battery,» *Advanced Materials Research,* Vols. %1 de %2236-238, pp. 604-607, 2011.

[21] STAR-CCM+, *User's Manual,* 2013.

[22] F. Walsh y G. Reade, «Design and performance of electrochemical reactors for efficient synthesis and environmental treatment. Part 2. Typical reactors and their performance,» *Analyst,* vol. 119, pp. 797-803, 1994.

[23] A. Date, Introduction to Computational Fluid Dynamics, Cambridge University Press, 2005.

[24] T. Cebeci y P. Bradshaw, Momentum Transfer in Boundary Layers, McGraw-Hill, 1997.

[25] A. Bard y L. Faulkner, Electrochemical methods, Wiley, 2001.

[26] I. Demirdzic y S. Muzaferija, «Numerical method for coupled Fluid Flow, heat transfer and stress analysis using unstructured moving meshes with cells of arbitrary topology,» *Computer Methods in Applied Mechanics and Engineering,* vol. 125, pp. 232-255, 1995.

[27] C. Brown, A. Montillet , P. Legentilhomme y J. Legrand, «Studies of space-averaged mass transport in FM01-LC laboratory electrolyser,» *Journal of Applied Electrochemistry,* vol. 23, pp. 38-43, 1993.

[28] A. Bannari, C. Cirtiu, F. Kerdouss, P. Proulx y H. Menard , «Turbulence intensity in an electrochemical cell: Effect on reactor performance,» *Chemical Engineering and Processing: Process Intensification,* vol. 45, pp. 471-480, 2006.

[29] T. Shih , W. Liou, A. Shabbir, Z. Yang y J. Zhu, «A new k-E eddy viscosity model for hight Reynolds number turbulent flows - Model developmente and validation,» *NASA TM 106721,* 1994.

[30] L. Norris y W. Reynolds, Turbulent channel flow with a moving wavy boundary., Department of Mechanical Engineering, Stanford University, USA., 1975.

[31] W. Xu, Q. Chen y F. Nieuwstadt, «A new turbulence model for near-wall natural convection.,» *International Journal of Heat and Mass Transfer,* vol. 21, nº 41, pp. 3161-3176, 1998.

[32] M. Wolfstein, «The velocity and temperature distribution in one-dimensional flow with turbulence augmentation and pressure gradient.,» *International Journal Of Heat And Mass Transfer,* vol. 3, nº 12, p. 301, 1969.

[33] H. Farjallah, H. Abbassi y S. Turki, «Vortex Shedding of Electrically Conducting Fluid Flow Behind Square Cylinder under Magnetic Field,» *Engineering Applications of Computational Fluid Mechanics,* vol. 5, p. 349–356., 2011.

[34] M. Sadiq Al-Baghdadi y H. Shahad Al-Janabi , «Effect of Design Parameters on the Hygro-Thermal Stresses in Proton Exchange Membranes of the Fuel Cells,» *Engineering Applications of Computational Fluid Mechanics,* vol. 1, pp. 71-87, 2007.

[35] L. Yu, G. Ren, M. Qin y X. Jiang, «Performance Influencing Factors Simulation of Proton Exchange Membrane Fuel Cells with Different Flow Modes,» *Engineering Applications of Computational Fluid Mechanics,* vol. 2, nº 3, p. 344–353, 2008.

[36] J. Joshi y V. Ranade, «Computational Fluid Dynamics for Designing Process Equipment: Expectations, Current Status, and Path Forward,» *Industrial Engineer Chemical Research,* vol. 42, pp. 1115-1128, 2003.

[37] J. Santos, J. Geraldes , S. Velizarova y J. Crespo, «Characterization of fluid dynamics and mass-transfer in an electrochemical oxidation cell by experimental and CFD studies,» *Chemical Engineering Journal 157:379–392,* vol. 157, p. 379–392, 2010.

[38] L. Castro y E. Villacampa, Estadística aplicada a la ingeniería civil., Club Universitario, 2000.

ANEXO III: METHODOLOGY TO OPTIMIZE FLUID-DYNAMIC DESIGN IN A REDOX CELL

ABSTRACT

The present work is aimed at the optimization of a redox cell design. The studied redox cell consists on a device designed to convert the energy of reactants into electrical energy when a liquid electrolyte reacts at the electrode in a conventional manner. In this particular sort of cells, the two electrolytes are present and separated by a proton exchange membrane. Therefore, the flow of the electrolyte and the interaction with the membrane takes a paramount importance for the general performance of the cell. A methodology for designing the inlet part of the cell based on optimizing the uniformity of the flow and the initial position of the membrane is presented in this study. This methodology, based on the definition and optimization of several parameters related to the electrolyte flow in different regions of the geometry, is depicted. The CFD (Computational Fluid Dynamics) model coupled with the statistical study pointed to several practical conclusions on how to improve the final geometry construction of the redox cell. A particular case study of redox cell is implemented in order to validate the proposed methodology.

Keywords. Redox cell, computational fluid mechanics, design optimization, statistical analysis.

1. INTRODUCTION

Redox Flow Cells are large stationary electricity storage systems. This sort of energy storage technologies will play a paramount role in the near future. The increasing use of efficient energy sources and renewable energy such as wind and solar, makes them necessary. These technologies usually suffer from experiencing intermittent generation [1] and the storage of energy is crucial to avoid the intermittency in the supply system.

The leading edge research impulses the development of energy storage to release the consumer system needs [2], [3], [4]. On a large scale, this energy storage could alleviate the unpredictability of energy sources to promote their accumulation over time [5].

Among these technologies, one of the most prominent is the redox flow battery (RFB). It is one of the best options for energy storage at medium and large scale [6]. The performance of these batteries is based on storing energy in solutions containing different redox couples. The electrodes surface makes possible the reversible electrodic processes. Redox and semi-redox technologies are good candidates for large stores of energy and medium domestic use storage, respectively [7].

On the one side, in this sort of batteries, the accumulated electrolyte determines the amount of energy stored. On the other side, the battery power depends on the electrode surface. The power stage is directly related to the active mass of the electrode, as the energy storage [8].

Accordingly, such batteries can modulate their output voltages and storage capabilities, and multiple cells can be interconnected using different sized reservoirs. Furthermore, they are very adequate as potential energy storage systems for distributed generation. In such cases the needs of each system determine their own requirements.

One of the first documented works on the redox flow cell was presented by Thaller in mid 1970s [9]. Since then, the redox flow cell concept has been implemented in different strategies, materials and chemical alternatives [10]. The numerically analysis of flow of electrolyte makes sense with the development of Computational Fluid Dynamics Technology (CFD), considering the precursors described in the papers of Frias-Ferrer [8], Codina [11] and Weber et al. [7] compile an interesting summary of redox batteries. In these research conclusions it is highlighted that the future of this technology goes through optimizing designs modeling, both: flow and transport. In this sense, different materials have been applied in redox batteries, with different geometries [6], [7], [12].

Fig. 1 shows the scheduled diagram of a redox cell. The two cylinders placed on the sides of the figure represent the two electrolyte storage tanks. The tank on the negative electrode storages a redox solution, this solution will be different from the tank on the positive electrode. There are two pumps,

one on each side of the reactor (Fig. 1). These pumps force the flow to circulate through the electrolyte in order to allow the semi-occurring redox reactions involving transfer of load.

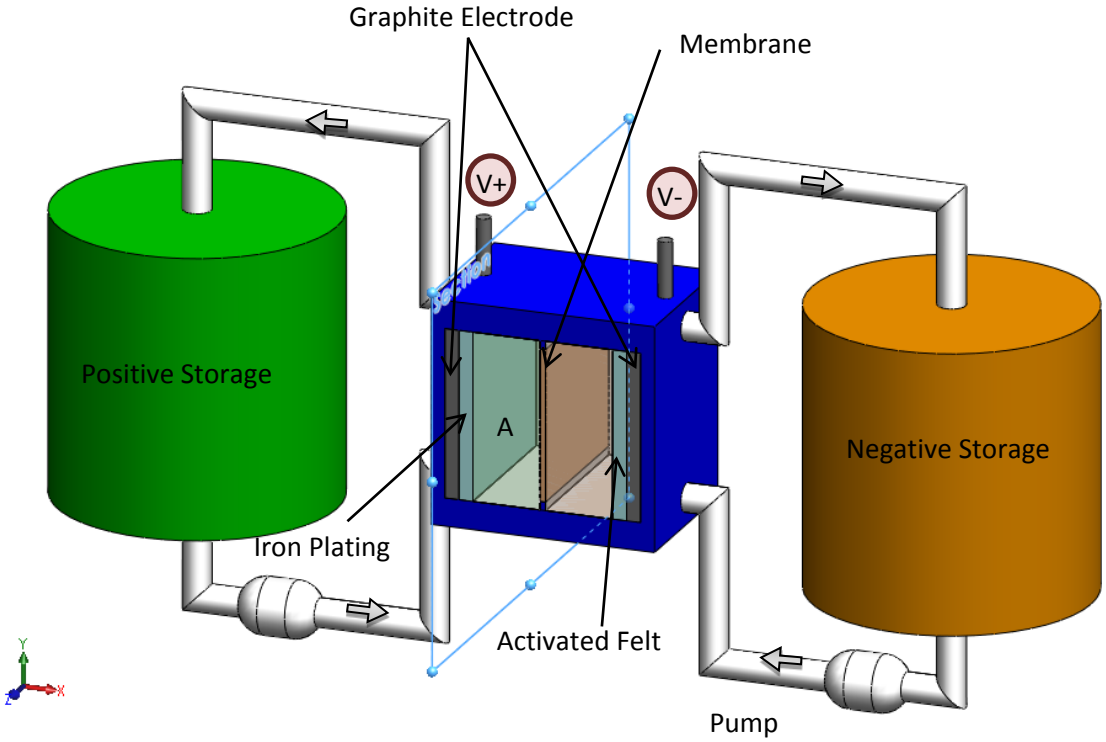

Fig. 1. Diagram of an iron flow battery (system components).

The cathode is made of graphite of carbon felt. The anode is also made of graphite or carbon felt with a selective membrane as separator. The membranes are made up of cross-linked linear polymer chains, which form a three-dimensional network. Without the cross-linking, the membrane would be dissolved in water forming a polyelectrolyte solution. Ion exchange membranes have fixed ion functional groups and oppositely charged counter ions, present in sufficient numbers to render the whole exchanger electrically neutral. The reactions achieved in the cell (considered as an all-iron redox cell) are:

- $2Fe^{2+} \rightarrow 2Fe^{3+} + 2Fe$, during the charge
- $2Fe^{3+} + 2Fe \rightarrow 2Fe^{2+}$, during the discharge

The electrolyte composition for this purpose is 2m FeCl2 + 0.5m NH4Cl in deionized water, as based on [13]. The working temperature is 40ºC, the fluid viscosity at this temperature is $1.143 \cdot 10^{-3}$ (Ns/m^2). It has been assumed that the electrolytic fluid produces no deposition within the cell as well as it does not produce any gas phase. This hypothesis would be completely true if the redox reaction was 100 % efficient. In reality, other competing reactions can occur with little gas production; these are disregarded as hypothesis [14]. Another assumed hypothesis is the one concerning the fluid density. Density is considered constant (1172 g/m^3) for all kind of flow.

The cell structure is surrounded by bipolar plates composed by structural support and electrical conductor. The electrodes, located on the side of each bipolar plate, are not involved in the electrochemical reactions. Nevertheless, they are important as they provide a surface facilitating the electron path. The membrane is located between both sides of the reactor. The membrane separates the two electrolytes, in order to preserve the electro-neutrality. The so considered volume 'A' (Fig. 1) is occupied by electrolyte. In this paper, the interest is focused on the uniformity of the electrolyte flow along this 'A' volume. Only the flow in the positive side of the cell is analyzed, as a symmetrical geometry is presented for both sides of the cell (positive and negative).

The uniformity of flow has a significant influence on the most important parameters of performance in the cell: the effective area of the electrode; the strength and efficiency; the useful life of the battery and electrochemical polarization (particularly under high current density variation [15].

The consulted references propose that the flow of electrolyte through the active layer has a high inference performance thereof [16]. In 1998, Moyabayashi et al. [17] concluded that the increase in energy efficiency is essentially determined by a uniform distribution of electrolyte. However, although the flow is homogeneous, there could be significant local variations in the surface of the electrodes, among others, causing strong changes of ph. Furthermore, the interest between different geometries and flow conditions in different redox cells have been considered in the literature, focused on understanding and improving the functioning of the whole reactor [18], [19], [20], [21], and the membrane position and configuration within the whole geometry [22].

Due to the fully compact battery system, the use of completely opaque key materials and the strong acidity of the electrolyte, the fluid distribution within the battery is often difficult to be determined, measured and quantified. However, the consulted references agree that research is vital to determine the optimal functioning of the battery pack [23], [24].

Thus, the strategies for redox cell design should pay the most interest in the analysis of the velocities at all points of the trajectories of the fluid. It is especially interesting in the inlet part of the cell [25]. Nevertheless, an exhaustive treatment of these flow fields, especially in the design phase, requires two important numerical tools: on the one hand, computational fluid dynamics (CFD) and on the other hand, statistical techniques. The use of CFD will help designers to simulate the velocity and pressure fields in the modeled geometry. This technique will suggest indicators of good performance of the design, allowing designers to compare different alternatives. Apart from this, statistical techniques will allow modelers to analyze the large number of individual generated velocities. The use of hypothesis test on these CFD data will help designers to analyze various aspects on the velocity fields. This will

lead modelers to determine that some designs are better than others. Following the methodology here described, several statistical tests are proposed for the design of the distribution channels within a cell.

The purpose of this paper is therefore to propose and describe a methodology for analyzing the electrolyte flow rate of a Redox cell (Fig. 1). This methodology will reveal the uniformity in the velocity near the membrane, the most sensitive point for ionic interchange. With the use of the proposed performance indicators, the modeler will have tools for optimizing the design of the cell. Finally, an optimized geometry is proposed to be implemented in a real prototype.

2. THE PROPOSED METHODOLOGY

The proposed methodology for designing redox cells considering flow uniformity is scheduled in Fig. 2. As it can be seen, this type of methodology has a well-defined and clear methodological approach.

The first step in this methodology is the definition of the initial geometry design. Afterwards, three parameters are proposed to develop the cell geometry. They will be analyzed with the CFD and statistical tools (Fig. 2). Each parameter is focused on different parts of the geometry, as this methodology is a sequential analysis. The parameters are proposed to improve the cell geometry in order to ensure the flow uniformity near the membrane: symmetry coefficient, uniformity coefficient and variability range coefficient. These values will be further defined.

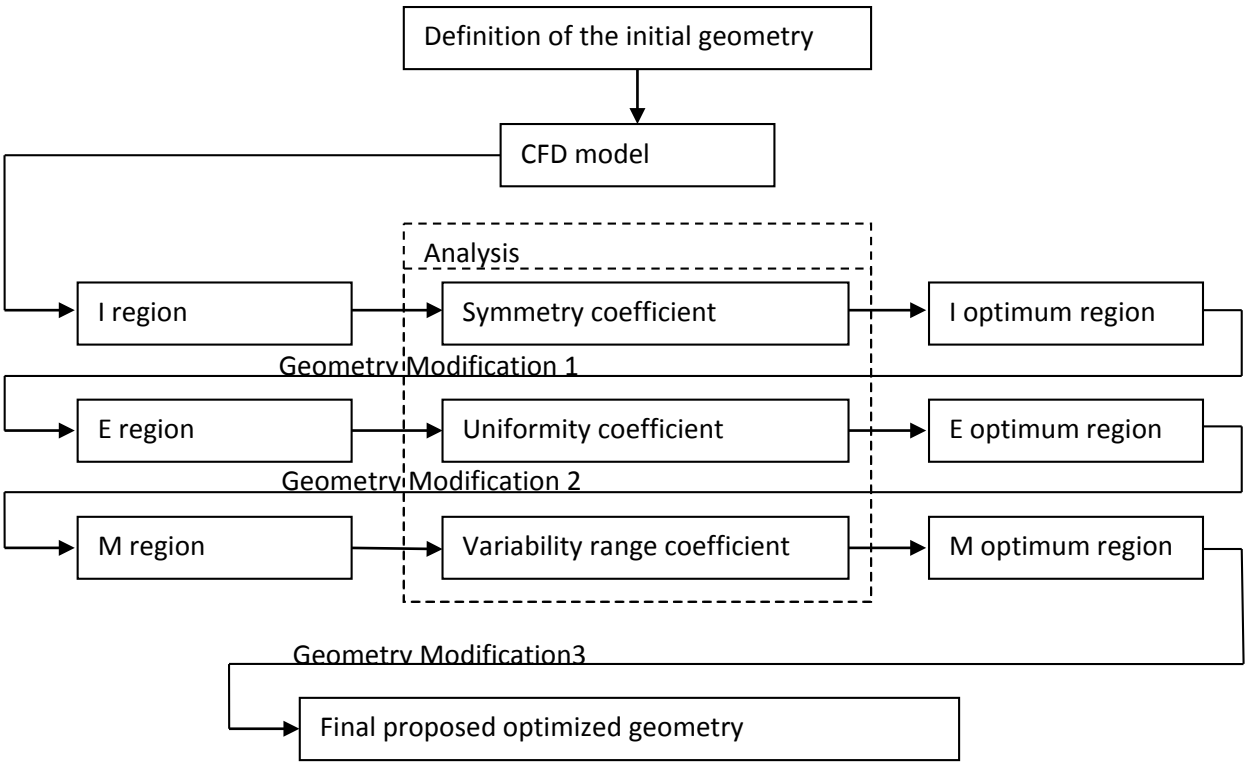

Fig. 2. Diagram of proposed methodology.

Some general initial boundary conditions used for this proposal methodology are:

- The range of flow rates for optimum operation is unknown. However, in this sort of cells, it is estimated that the value of the minimum flow is about 35 l/h (stoichiometric) and the maximum flow is around 150 l/h. The maximum flow is the most critical parameter that affects the design.
- The cell proposed is made up of 1 electron in the positive fluid and 2 electrons in the negative fluid.

Different efficient cell operation is caused by the velocity dispersion, for this reason it is important to analyze the velocity inside the cell, therefore the parameters to optimize and homogenize the inlet velocity and the inlet membrane velocity are proposed. The membrane is the most expensive part of this type of cell; it is around the 40% of the material cost [26]. The adequate behavior of the membrane depends on a correct interchange with the ionic flow. Furthermore, modeling the behavior of the flow in the cell is of paramount importance to ensure velocity uniformity [27] and then final performance in the cell.

The three parameters to be studied refer to different regions in the cell, described in Fig. 3, these parameters are: the symmetry coefficient (evaluated in I region); the uniformity coefficient (assessed in the E region); and variability range coefficient (considered in the M region).

- I region: This part refers to the entrance of the cell. In this region the symmetric flow is analyzed. The symmetry coefficient (C_U) will be defined to quantify the performance in this region.
- E region: This zone refers to the exit at the end of the channels. The parameter used to analyze this region is the uniformity coefficient (C_H) and it defines the average velocity per channels.
- M region: This one refers to the region located after the channels at the same distance of the membrane location. The variability range coefficient of velocity front (R_I) and maximum and minimum value of velocity is defined with the purpose of selecting the best position of the membrane.

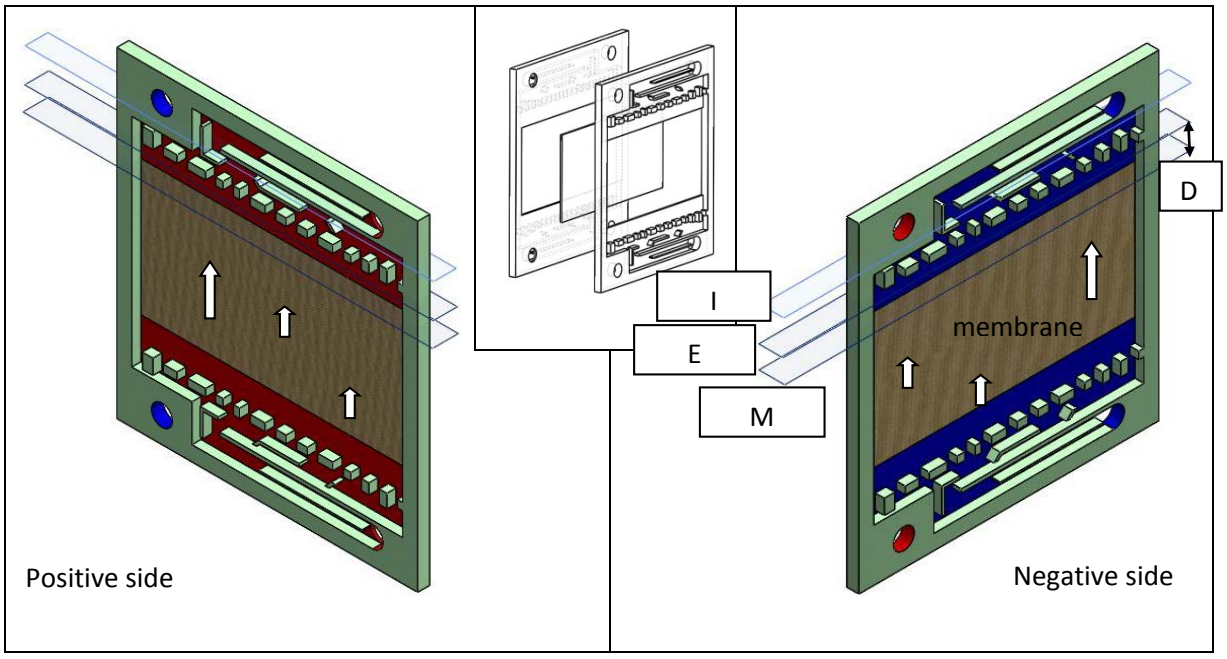

Fig. 3. Commercial cell geometry.

As it has been mentioned, the numerical tools used for this methodology are the Computational Fluid Dynamic and the hypothesis test, which will be simply described.

2.1 CFD analyses of the velocity field

A general purpose computational fluid dynamic software package has been employed to run the simulations: Star CCM+. The computational model solves numerically the governing laws of Fluid Dynamics. These equations, taking into account turbulent phenomena, are solved in a geometrical domain, given a number of suitable boundary conditions. In a CFD the relevant magnitudes (velocity) are calculated in a discrete manner at the nodes of a certain mesh or grid and they are represented along the mesh. The use of these computational tools to gain insight into the velocity field of the modeled flows currently constitutes a powerful tool for designers in devices involving fluid motion.

The advantage of using these models is that they can simulate real problems of Fluid Mechanics to any degree of complexity. Furthermore, they can help modelers to visualize hydrodynamic aspects otherwise impossible to be measured or represented in a real case (i.e. stream lines) that have great importance in the comprehension of the studied phenomena. The conservation equations solved by the code are those of mass and momentum. The continuity or mass conservation equation solved is the expression (1).

$$\frac{\partial \rho}{\partial t} + \nabla \rho \vec{v} = S_m \tag{1}$$

Where ρ is the fluid density, $\vec{V}$ is velocity and S_m represents the mass source contained in the control volume. For other geometries, suitable coordinates, namely spherical or cylindrical, should be used. Also, the momentum equation is considered by the equation (2).

$$\frac{\partial (\rho \vec{v})}{\partial t} + \nabla \rho (\vec{v}\vec{v}) = -\nabla p + \nabla \tau + \rho g + F \tag{2}$$

Where p is the static pressure; the gravitational and outer forces defined on the control volume respectively, and $\bar{\tau}$ the stress tensor, expression (3), where μ is the eddy viscosity. I is the unit tensor and the third term accounts for the effect of the expansion of volume.

$$\tau = \mu \left[\left(\nabla \vec{v} + \nabla \vec{v}^T \right) - \frac{2}{3} \nabla \vec{v} I \right] \tag{3}$$

All conditions and properties are defined via STAR-CCM+ and solved using the coupled solver. The results are displayed via post-processing tools available. The volume mesh in a simulation is the

mathematical description of the space (or geometry) of the problem being solved. The geometry model is designed to work on three-dimensional meshes.

Before introducing the geometry in the calculation software, the geometry must be properly prepared. To do this, the geometry of the experiment has been modeled using commercial CAD software. Once the geometry of the reactor is represented, it is imported to the calculation software and the meshing process is performed on the fluid domain.

The trimmed mesh has been chosen due to the flow movement by using the trimmer wake refinement and the volume shape tools in areas where a fine mesh is needed. Optimized mesh main parameters are described in Table 1.

Base size (mm)	3	Surface curvature (pts. /circle)	72
Relative minimum size (mm)	1.5	Maximum cell size (mm)	6
Relative target size (mm)	3	Remeshed surface (faces)	491,314
Volume mesh (final proposed optimized geometry)	655,913		

Table 1. Optimized mesh features.

The here proposed methodology is aimed to compare different geometrical alternatives for the cell under the same initial flow conditions. In this sense all the quantifications are based on CFD techniques. The particular numerical model implemented does not consider deformable meshes for calculations. However, in the real world, redox-flow battery stacks are not completely rigid, therefore, the distribution in the porous electrodes is subject to change once the membrane or the bipolar plates are deformed by flow/pressure distribution. These changes in the mesh have not been considered in this model. This is a potential limitation for the validity of the numerical model.

An input speed and an output pressure of the model have been designed. The other boundaries are represented by a wall condition; the one used by the computational code is similar to the one called ‘smooth tube roughness’ [28] that is well suited to the material properties of the cell.

The selective membrane does not affect the hydrodynamic movement of the fluid, as there is no pass of fluid across the membrane; only electronic transfer occurs in this process. As this does not affect velocity, pressure or turbulence, the boundary condition implemented for the membrane is wall.

Once the boundary conditions have been well defined and a suitable mesh in the full model is implemented, the computer code solves the equations of movement (conservation of mass or continuity (4), and conservation of movement quantity or Navier-Stokes (5)).

$$\nabla \overline{U} = 0 \tag{4}$$

$$\frac{\partial \overline{U}}{\partial t} + \nabla\left(\overline{UU}\right) - \nabla\left(\nu \nabla \overline{U}\right) = -\nabla \overline{p} + \overline{U'U'} \quad (5)$$

Where U represents the velocity vector, U 'indicates fluctuations around the value of the mean velocity, p is the dynamic pressure, ν is the kinematic viscosity and $\overline{U'U'}$ represents the so-called Reynolds stresses. In laminar flow conditions, the average velocities coincide with the snapshots and the Reynolds term vanishes, leading to a closed system of equations, which requires no turbulent solutions. In turbulent flow, as Reynolds stresses are not canceled, close solutions are needed which provide the sufficient equations to know the instantaneous velocities throughout the domain. At low Reynolds numbers, the most indicated solutions are k-Epsilon [29], [30], [31]. The Bibliography is profuse in the use of these techniques in similar engineering problems [32], [33] even in modeling environments close to the here described technique [34], [35].

In this modeling, three-dimensional simulations were performed using the STAR-CCM+ software [36]. This is based on the finite volume method (FVM) to solve the conservation of mass equation and the Navier-Stokes averaged equations in a curvilinear mesh, not taking into account the effects of temperature. Second order upwind scheme is used in this case for discretization. The advantage of this scheme over the first-order upwind scheme is that it is nominally second-order accurate. In order to meet the mass conservation condition a correction algorithm standard pressure (SIMPLE) is used. Thus, the code solves algebraic and iteratively equations considering gravity at all times until the residue numbers values are sufficiently low (less than 10^{-3}) considering that the resolution has converged.

2.2 Hypothesis testing applied on the CFD data

The goal in hypothesis testing [37], [38] is to analyze a sample of data in an attempt to distinguish between population characteristics that are likely to occur and population characteristics that are unlikely to occur.

There are two main keys in hypothesis testing such as null hypothesis and alternative hypothesis. On one hand, null hypothesis is a statement about the value of a population parameter (in our case *mean channel speed MCS*), represented by H_0 and always stated, in statistical terms, as an equality (=). On the other hand, alternative hypothesis is a statement about the value of a population parameter that must be true if the null hypothesis is false and is represented by H_1 and stated as an inequality (<,>,≠). Then formulated both, null and alternative hypothesis, in terms of the model parameter *MCS*.

H_0: MCS are the same in two different channels → $\mu_i = \mu_j \; \forall \; i \neq j$ (6)

H_1: MCS are NOT the same in two different channels → $\mu_i \neq \mu_j \forall i \neq j$ (7)

Our model has a total of 84 channels to be analyzed.

Any variation detected with a p-value ≤ 0.05 (this value is the level of significance of the test denoted using Greek letter α) is due to random phenomena intrinsic to the system, also called natural process variability.

Samples of all channels are obtained together for a particular run of Computational Fluid Dynamic scenario, since it is a stochastic process. The distribution of the average speed on all channels is known:

$$\bar{x}_{channel\_i} \approx N\left(\mu_i, \frac{\sigma_i}{\sqrt{n_i}}\right) \tag{8}$$

$$\bar{x}_{channel\_j} \approx N\left(\mu_j, \frac{\sigma_j}{\sqrt{n_j}}\right) \tag{9}$$

Every probability density function of speed is dependent from the point of view of the channels' distribution. The statistic used is the difference of sample means which is the non-centered moment of order {r ∈ N | r: 1} and since the difference of two normal distributions is a normal distribution yet, this gives:

$$\bar{x}_i - \bar{x}_j \approx N\left(\mu_i - \mu_j, \sqrt{\sigma_i^2 + \sigma_j^2 - 2Cov(x_i, x_j)}\right) \tag{10}$$

To use the normal distribution, values of simple data are first converted to standardized Z scores using the following transformation:

$$Z = \frac{\left(\bar{x}_i - \bar{x}_j\right) - \left(\mu_i - \mu_j\right)}{\sqrt{\sigma_i^2 + \sigma_j^2 - 2Cov(x_i, x_j)}} \approx N(0,1) \tag{11}$$

Z scores transforms data into the standard cumulative normal distribution whose mean is 0, and variance is 1. Z-scores provide a mapping from a distribution of some variable to a standardized scale. These mappings reflect the difference in terms of number of standard deviations away from the mean.

Because of the size of sample data is greater than 30, this is the reason we choose Z-scores as statistic parameter instead of t-Student.

Equation 12 and 13 summarize the main ideas in hypothesis testing:

Fail rejection region: $\{-z_{(\alpha/2)} \leq Z \leq z_{(\alpha/2)}\}$ (12)

Rejection region: {Z ∈ to any other region} (13)

Once exposed to perform hypothesis testing, this has to be applied. The mean speed at every channel is represented by a histogram; therefore, this plot represents the difference among channels, and with a simple glance detects which *MCS* are quite different among themselves.

By examining the results of hypothesis testing applied to the sample, the null hypothesis can be rejected or failed to be rejected. It will indicate which channels are significantly different from each other. In order to not introduce error analysis, the comparison made by hypothesis testing is performed 1-by 1 channel. The total numbers of comparisons are $\sum_{i=1}^{Total\_channels-1} i = 3486$. Doing 1-by-1 comparisons among the total number of channels, errors are avoided.

3. PROPOSED PARAMETERS ANALYSIS

The here depicted methodology is based on three different parameters to be considered: the symmetry coefficient, uniformity coefficient and variability range coefficient of velocity front.

3.1 Symmetry coefficient

The symmetry coefficient is the first parameter to be analyzed; it indicates the amount and the longitudinal distribution of flow that goes inside the cell. A poor distribution of the flow affects noticeably the correct distribution of the fluid.

To evaluate this coefficient it is necessary to know about the flow circulation along the cell. The coefficients (C_{S_A}, C_{S_B}) evaluate the percentage of flow on left and right side of the cell. This parameter is analyzed in I region.

$$C_{S\_A} = \frac{Q_i}{Q_T} = \frac{\sum_{i=0}^{n/2} v_i S_i}{\sum_{i=0}^{n} v_i S_i} \tag{14}$$

$$C_{S\_B} = \frac{Q_i}{Q_T} = \frac{\sum_{i=n/2}^{n} v_i S_i}{\sum_{i=0}^{n} v_i S_i} \tag{15}$$

Where:

v_i= i velocity channel.

S_i = i area channel.

The best design will be the one that shows coefficient (C_{S_A}) to be similar to coefficient (C_{S_B}); this design distributes the flow uniformity around the cell. To evaluate the optimum design the symmetry coefficient is proposed. The best design will be the one presenting a minimum coefficient. This symmetry coefficient is defined by (16):

$$C_u = \frac{c_{S\_A} + C_{S\_B}}{C_{S\_A}} \tag{16}$$

3.2 Uniformity coefficient

This coefficient evaluates the velocity for each channel, in this particular case, the goal is to maintain a constant velocity inside the cell and this can be analyzed with the uniformity statistic coefficient. This

means that a lower uniformity coefficient represents similar velocities of the channel output and this would be a good design.

The null hypothesis is true when the velocity of one channel is equal to the other channel and the alternative hypothesis occurs when the velocities are different. Therefore, the uniformity coefficient is defined, in this case, as the relation between the null and the alternative hypothesis.

$$C_H = \frac{\sum\left(-z_{\alpha/2} \le Z \le z_{\alpha/2}\right)}{\sum(Z)} \tag{17}$$

A good design is supposed when the uniformity coefficient is lower. Nevertheless, it is true that it could be represented by a punctual error because the design could have a very high coefficient through few channels. For this reason, it is very important to design a frequency graph to represent the accumulated errors in two dimensions. (E region, Fig. 3).

With the implementation of this parameter it is possible to only focus the cell design in the errors channels and improve it step by step.

3.3 Variability range coefficient of velocity front

The uniformity coefficient is obtained by the hypothesis test, if this coefficient is small; the velocity inside the channels presents more uniformity. Nevertheless, it does not solve all problems that are present in the design and for this reason it is necessary to define another parameter: the variability range coefficient of velocity front. It is evaluated in a range of D distances of the membrane (M region, Fig. 3).

This analysis allows modelers to determine the variability range of front velocity (maximum velocity and minimum velocity) and the interpolation curve. The position of the membrane will be determined by the correct processing of these data fields.

First of all, it is necessary to obtain the velocity data with the CFD tools. Then, these data are treated mathematically and cleaned if it is necessary. The obtained range is the difference between maximum and minimum velocity value. The aim of this point is to achieve the lowest range value.

Interpolation polynomial must be applied for the mathematical analysis, because it is a good tool to determinate the area that has a higher speed or slower than the medium velocity. The interpolator polynomial moves until the velocity average is situated in the coordinate's axis. Furthermore it is possible to calculate the above and underneath region by means of integration in the interpolator

polynomial. In this case, the area is positive when the velocity is higher than the medium velocity and the area is negative when the velocity is lower than the medium velocity.

$$U = | U_+ - U_- | \quad (18)$$

It is necessary to define two criteria to evaluate this coefficient; equations (19) and (20); the correct location of the membrane is determined for the range and the interpolated area, so, it is necessary to minimize the range and the interpolated area.

$$R_i = V_{max,f} - V_{min,f} \quad (19)$$

$$R_i < V_{m,t} \quad (20)$$

4. CASE STUDY: PARTICULAR DESIGN OF A REDOX CELL

In order to apply the methodology described here, a particular design is proposed. The objective is to obtain the geometry in which the flow is as much uniform as possible, considering the modification of several geometrical aspects.

4.1 Symmetry coefficient. Geometry modification 1

Symmetry coefficient is affected by the displacement of the cell inlet geometry radius. Therefore displacement (D_1) and (D_2) affects both radius positions (Fig. 4). As these radiuses directly concern the symmetry flow, the displacement of the radius was decided. If this parameter is amended, the asymmetry will be compensated because the inlet and the outlet are only in one side of the cell. Fig. 4 and Table 2 represent the considered changes in the D_1 and the D_2.

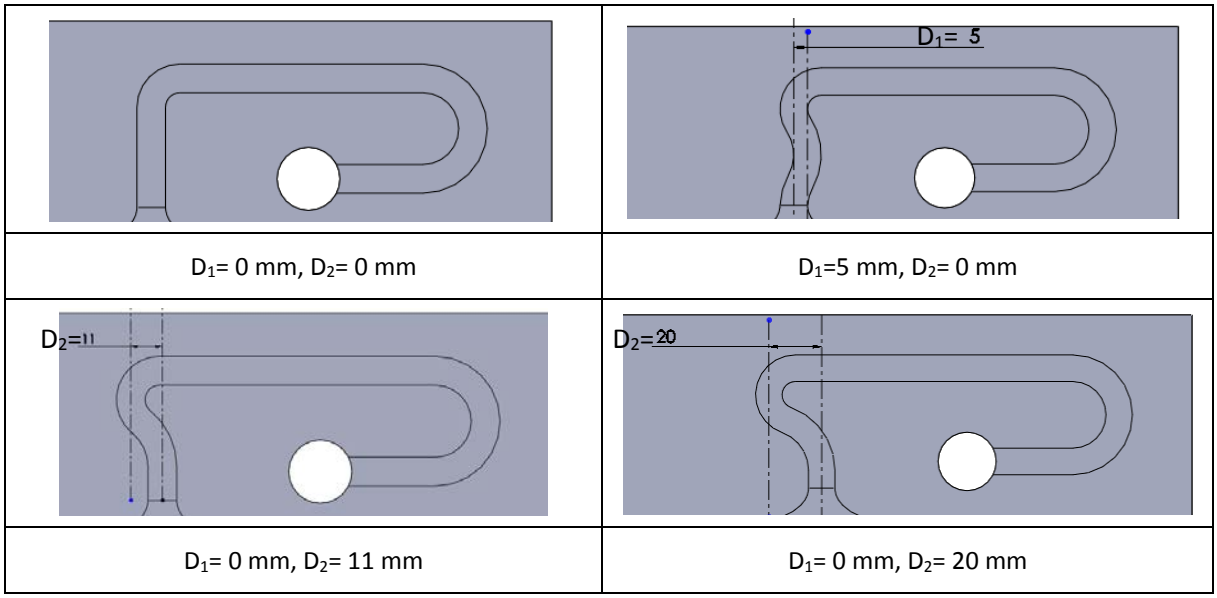

D_1= 0 mm, D_2= 0 mm	D_1=5 mm, D_2= 0 mm
D_1= 0 mm, D_2= 11 mm	D_1= 0 mm, D_2= 20 mm

Fig. 4. Symmetry alternatives of design.

	a) Alternative	b) Alternative	c) Alternative	d) Alternative
D_1(mm)	0	5	0	0
D_2(mm)	0	0	11	20

Table 2. Alternatives for radius of design.

In the bar diagram depicted in Fig. 5, the symmetry coefficient, C_U evaluated by expression (16), can be seen.

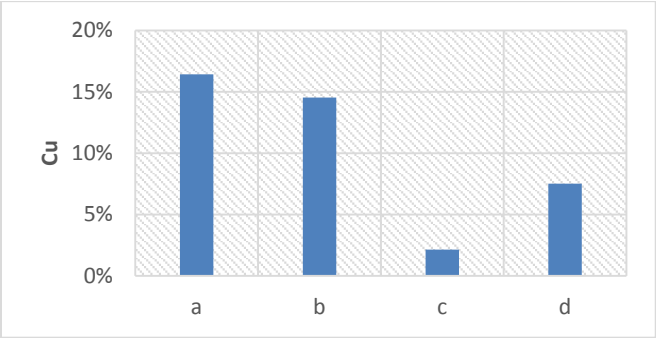

Fig. 5. Symmetry coefficient evaluated.

Fig. 4 and Table 2 depict the little changes proposed in the inlet region in order to improve the symmetry of the velocity fields in I region. It´s evaluated with the Symmetry coefficient, further quantified in Fig. 5. In order to provide more information about how these changes affect the velocity profiles, Fig. 6 is presented. In this Fig., the velocity magnitude for the nodes located along I region is represented in modulus, versus position for a) and c) alternatives. As it can be seen, the velocity profile resulting in c) alternative is more symmetrical. Left side velocity profile in a) alternative achieves considerably smaller values than right side velocity profiles. As the difference between these both velocities profiles affect the Symmetry coefficient, the c) alternative present's smaller coefficient and therefore better symmetry.

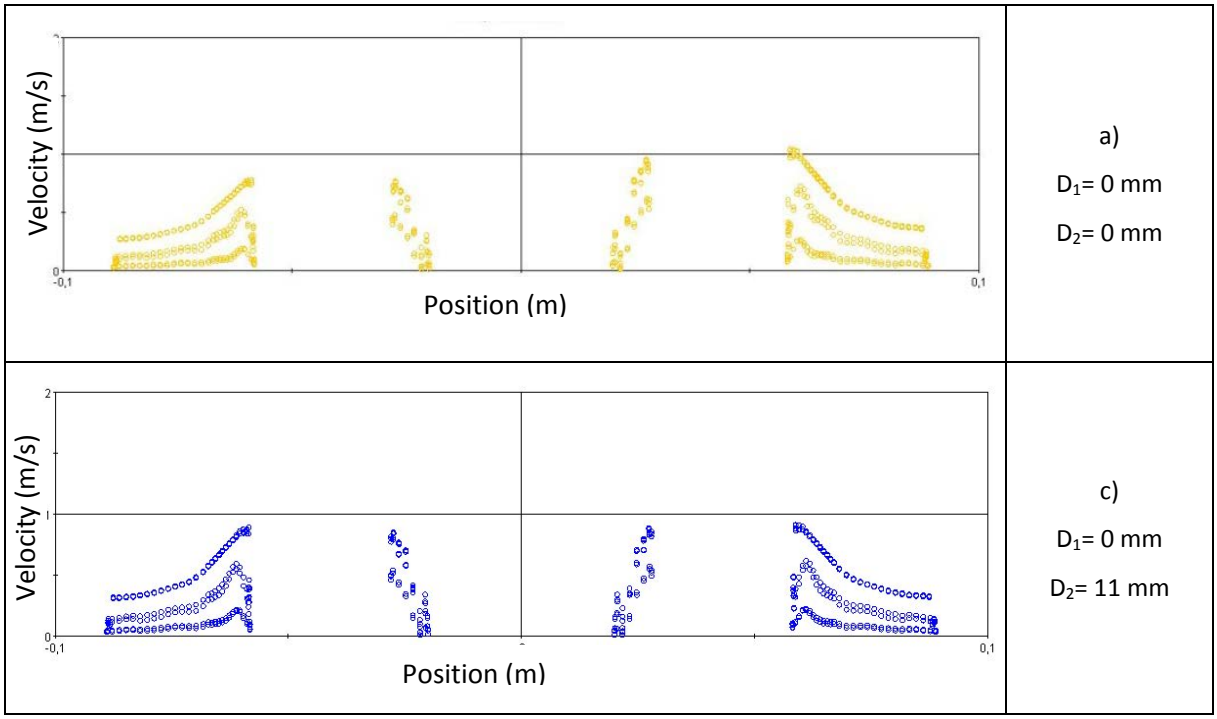

Fig. 6. Velocity profiles: a) and c) alternative.

The optimum velocity in I region is the c) alternative, where the value of the Symmetry coefficient is 2.39 %; this means that only a 2.39 % of the flow is asymmetric for a specific flow of 150 l/h.

The optimum region features are:

- D_1: 0 mm.
- D_2: 11 mm.

4.2 Uniformity coefficient. Geometry modification 2

The uniformity coefficient is obtained, considered in the E region (Fig. 3). The hypothesis test is used as it has been described in Section 2.3. If the velocity of channel 1 is statistically significant to the one in the other channel, the null hypothesis is true; in this case, it is evaluated $\sum_{i=1}^{83} i = 3486$ cases.

The uniformity coefficient is defined as the relation between the null hypothesis and all of these cases (equation 17). With this specific coefficient we can obtain a numerical comparison among different geometries.

The changes in the geometry affect inside the cell, in the E region. This area has been changed to obtain the lowest value of the uniformity coefficient. Fig. 7 shows the four different geometries analyzed with same flow. To do so, c) alternative of Fig. 4 is represented in these possibilities.

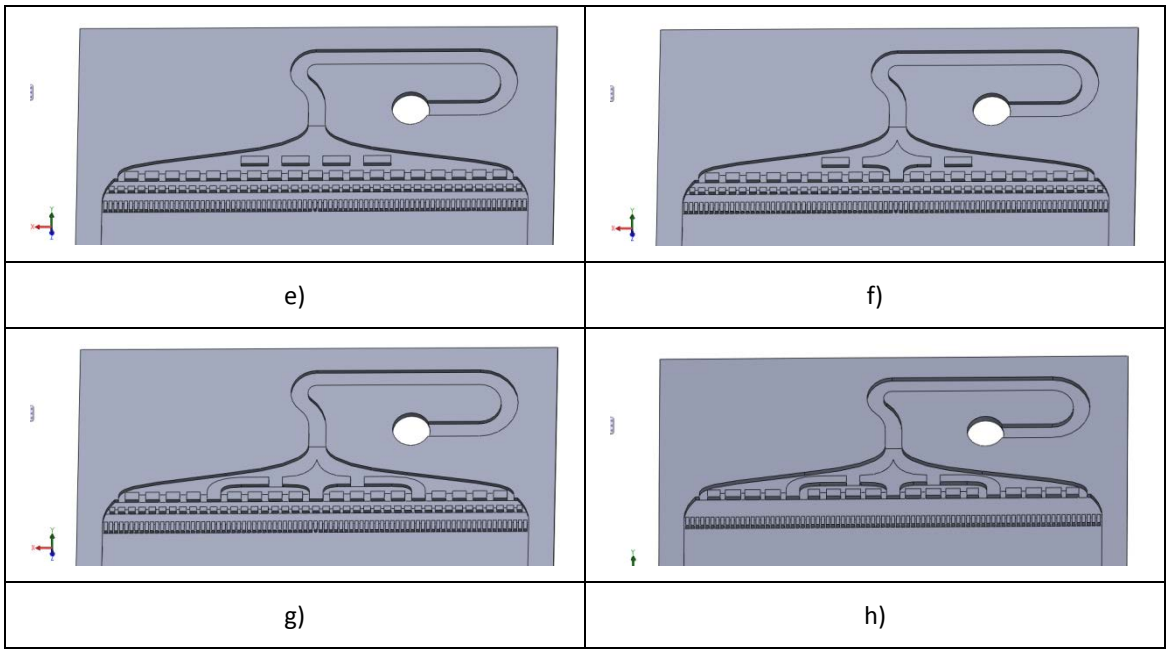

Fig. 7. Uniformity alternatives of design.

Once the geometry changes have occurred, the uniformity coefficient (C_H) for the e), f), g) and h) alternatives are represented in Fig. 8. In the bar diagram, the changes on the geometry influence can be seen. The lowest coefficient is the g) alternative, with a value of a 4.8 % of uniformity. It means that only 4.8 % of channels have a different value for mean velocity.

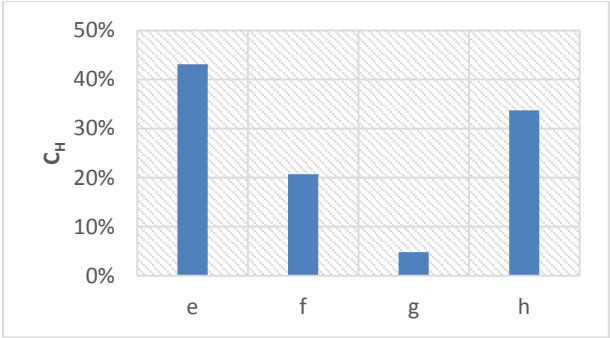

Fig. 8. Uniformity coefficient evaluated.

As it can be seen in Fig. 9, the modulus of velocities in the nodes located in E region show less variation in g) alternative than those in e) alternative. The velocities are, therefore, more uniform along E region and the range of variation is smaller in g) alternative.

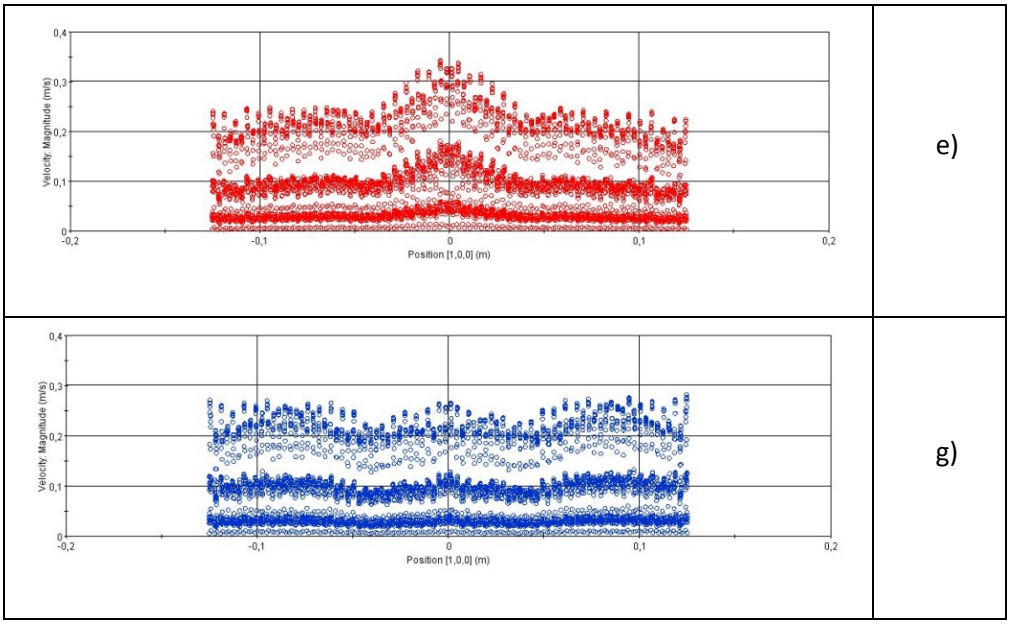

Fig. 9. Velocity profiles, e) and g) alternative.

A visual study is necessary to validate the symmetry and uniformity coefficient previously described. For this reason, a frequency graph (Fig. 10) is used to validate the technique mentioned and to represent the velocity differences in every channel. This diagram is a powerful tool to analyze velocities inside the cell because you can identify which channels are problematic.

The x-axis determines the number of channels (84) and the y-axis determines the channels rejecting the null hypothesis (83 possibilities). If the C_H coefficient is small, the average velocities of the channels are more equal and are represented by an empty bar diagram.

For the optimum geometry (g) alternative) design, channels with different velocities are represented in Fig. 10 Additionally, the symmetry coefficient can also be seen in the bar graph. A velocity symmetrical distribution is observed.

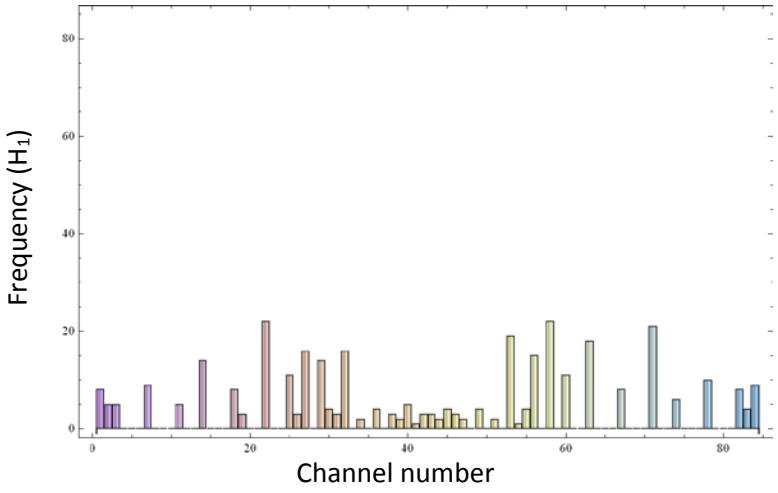

Fig. 10. Bar graph of g) alternative

4.3 Variability range coefficient of velocity front. Geometry modification 3

Finally, variability range coefficient is analyzed; this coefficient determines the position of the membrane. In order to experience a good functioning of the membrane, the velocity should be constant at the beginning of the membrane. The velocity at the position of the membrane is analyzed in this point. To do so, the 19 equation (distance D, Fig. 3) is proposed.

The variability coefficient of the range is represented in Fig. 11. This range decreases as the membrane distance (D) increases. Therefore, the evolution of the range coefficient of velocity front is decreasing in this case.

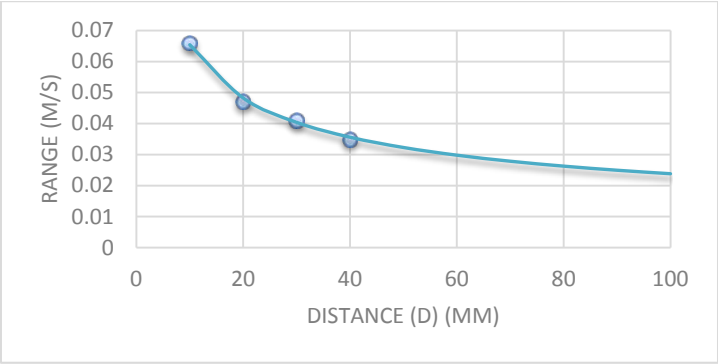

Fig. 11. Velocity range.

Furthermore, another aspect is also analyzed around the variability range. An Interpolator polynomial is used to model the curve of the velocity front with the intention of obtaining the area (equation 18) above or below the medium velocity. Fig. 12 shows the evolution of this area in four different points.

As represented in the figure, when increasing the distance (D) the net area above or below the medium velocity decreases; in addition, the membrane inlet velocity is more uniform.

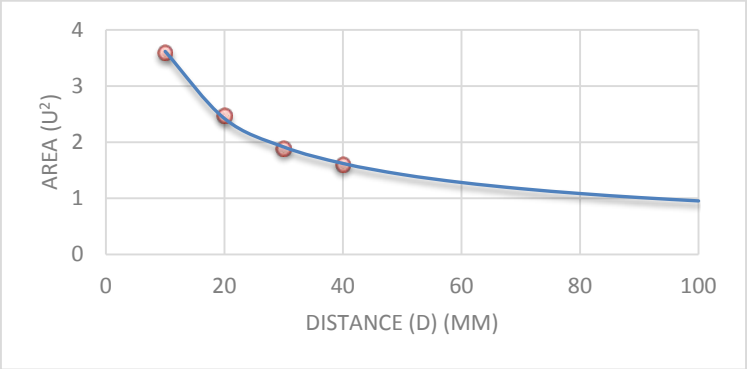

Fig. 12. Interpolator polynomial area.

The theoretical average velocity is 0.52 m/s. based on the analysis of Fig. 11 and Fig. 12, and the criterion set out in equation 20, the optimum distance is 30 mm. This is a design criterion and for other applications of this methodology, it could vary depending of the designer.

The Interpolator polynomial, maximum and minimum velocity for the distance suggested of 30 mm is represented in Fig. 13.

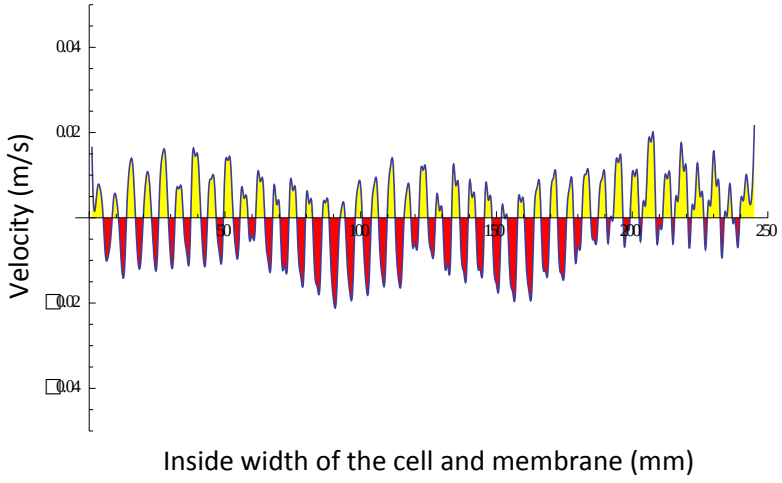

Fig. 13. Interpolation polynomial, D= 30 mm.

4.4 Final proposed model

From the analysis of all coefficient and geometry described in the preceding epigraphs, an optimum geometry of a full cell is proposed. In this improved geometry, the velocity is more symmetric and uniform than in the initial geometry; therefore the ionic exchange will be produced in all the membrane, as dead zones (regions will null velocity) will not appear.

Fig. 14 shows the final optimized geometry for the whole cell. The two rib lines are included in the design to achieve higher structural resistance. This is a step further to ensure the cell rigidity and to maintain the distance between the membrane and the electrode. These ribs will not affect the velocity field in the studied design regions.

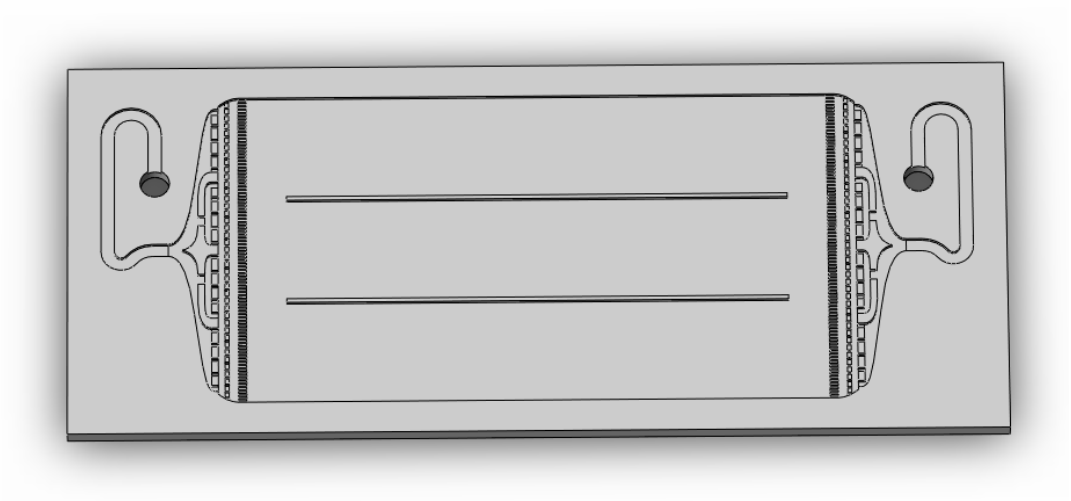

Fig. 14. Final optimized geometry.

In this case, some CFD representations of velocity vectors are provided in Fig. 15. The velocity vectors along the proposed geometry are shown (Fig. 15a). The initial flow distribution in both sides of the geometry is observed in I region, with a great symmetrical behavior (Fig. 15b). When the flow has passed across all the channels, the most uniform velocity vectors profile is observed in E region (Fig. 15 c). Finally, as expected, when the flow overcomes the membrane in M region the velocity is symmetrical, uniform and with a small variability, as expected (Fig. 15 d).

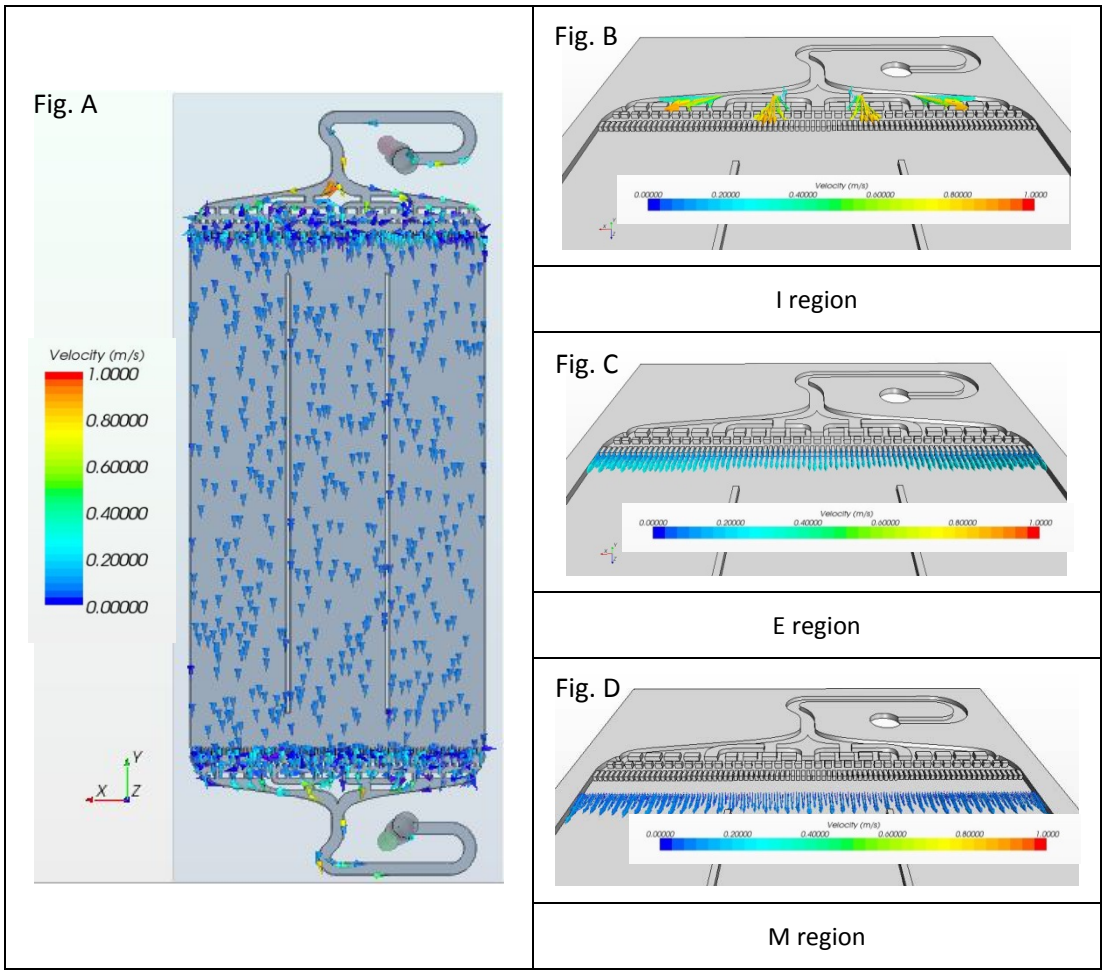

Fig. 15. Velocity vectors of the final geometry, I region, E region and M region.

In future researches, this geometry will be build and the velocity profile will be visualized to validate the here proposed methodology.

5. CONCLUSIONS

In this contribution, a methodology has been presented to help modelers to take decisions about the fluid-dynamic design in a redox cell. The methodology is based on the definition of three performance indicators: the symmetry coefficient, uniformity coefficient and variability range coefficient. These parameters will help to quantify the flow uniformity of the cell final design.

The symmetry coefficient indicates the amount and the longitudinal distribution of flow that goes inside the cell. In order to get these velocity profiles, a deep CFD analysis has been implemented.

The uniformity coefficient evaluates the velocity for each channel. In this particular case; the aim is to maintain a constant velocity inside the cell. In order to get this coefficient, a hypothesis test technique has been proposed, based on the CFD results, to check if the velocity profiles from different channels are equals or not.

Finally, a variability range coefficient is proposed. The velocity at a specific point of the membrane is analyzed to determine the velocity front variability. The objective is to find the more convenient position for the membrane with a constant velocity profile, as near as possible from the geometry channels.

The sequential consideration of these three parameters will let the modeler to determine the number of inlet channels, the distance among them and the configuration of the inlet geometry in order to make the velocity uniform when the fluid touches the membrane.

A case study is presented to illustrate the capability of the depicted methodology. An optimum geometry is generated for a 150 l/h cell. In this case, the proposed parameters have been used to determine the most convenient geometry among many different alternatives. A final design, in which only 4.8 % of the channels have a different value for mean velocity, has been proposed. This is a very uniform velocity for the flow arriving to the membrane.

In future research, this real cell geometry is going to be built in order to validate the velocity distribution provided by the CFD and the here proposed methodology. Further CFD models will have to consider the interaction between fluid and the solid boundaries. The influence of cell rigidity on the performance of the overall cell will be also analyzed in future studies.

6. REFERENCES

[1] M. Skyllas-Kazacos, M. Chakrabarti, S. Hajimolana, F. Mjalli y M. Saleem, «Progress in flow battery research and development,» *Journal of the Electrochemical Society,* vol. 158, pp. 55-79, 2011.

[2] M. Rychcik and M. Skyllas Kazacos, "Characterist of a new all-vanadium redox flow battery," *Journal of Power Sources,* vol. 22, pp. 59-67, 1987.

[3] R. Dell and D. Rand, "Energy storage-a key technology for global energy sustainability," *Journal of Power Sources,* vol. 100, pp. 2-17, 2001.

[4] Z. Yang, J. Zhang, M. Kintner Meyer, X. Lu, D. Choi, J. Lemmon y J. Liu, «Electrochemical Energy Storage for Green Grid,» vol. 111, pp. 716-732, 2011.

[5] L. Joerissen, J. Garche, C. Fabjan y G. Tomazix, «Possible use of vanadium redox-flow batteries for energy storage in small grids and stand-alone photovoltaic systems,» *Journal of Power Sources,* vol. 127, pp. 98-104, 2004.

[6] C. Ponce de Leon, A. Frias Ferrer, J. González García, D. Szanto y F. Walsh, «Redox flow cells for energy conversion,» *Journal of Power Sources,* vol. 160, p. 716–732, 2006.

[7] A. Weber, M. Mench, J. Meyers, P. Ross, J. Gostick y Liu, «Redox flow batteries: a review,» *Journal of Applied Electrochemistry,* vol. 41, p. 1137–1164, 2011.

[8] A. Frias-Ferrer, «Optimización de la hidrodinámica de reactores electroquímicos: empleo de métodos experimentales y numéricos,» *Thesis. Universidad de Alicante,* 2004.

[9] L. Thaller, «Electrically Rechargeable Redox Flow Cells,» de 9th Intersociety Energy Conversion Engineering Conference, Proceedings, 1974.

[10] A. Parasuramana, T. Lima, C. Menictas y M. Skyllas-Kazacos, « Review of material research and development for vanadium redox flow battery applications,» *Electrochimica Acta,* vol. 101, pp. 27-40, 2013.

[11] G. Codina, «Desarrollo de una planta de acumulación de energía eléctrica basada en el acumulador redox Fe/Cr,» *Thesis Universidad de Alicante,* 1992.

[12] «Vanadium Redox Flow Batteries: An In-Depth Analysis,» EPRI, Palo ALto, 2007.

[13] J. Mellentine, «Performance Characterization and Cost Assessment of an Iron Hybrid Flow Battery,» *Thesis. University of Iceland,* 2011.

[14] A. Bard y L. Faulkner, Electrochemical methods, Wiley, 2001.

[15] M. Chakrabarti, R. Dryfe y E. Roberts, «Evaluation of electrolytes for redox flow battery applications,» *Electrochimica Acta,* vol. 52, pp. 2189-2195, 2007.

[16] M. Li y T. Hikihara, «A Coupled Dynamical Model of Redox Flow Battery Based n Chemical Reaction, Fluid Flow, and Electrical Circuit,» *IEICE Transactions on Fundamentals of Electronics, Communications and Computer Science,* Vols. %1 de %2E91-A, nº 7, 2008.

[17] M. Moyabayashi, T. Tayama, Y. Kageyama y H. Oyama.Patente 5.851.694, 1998.

[18] C. Bengoa, A. Montillet, P. Legentilhomme y J. Legrand, «Flow visualization and modelling of a filter-press type electrochemical reactor,» vol. 27, pp. 1313-1322, 1997.

[19] A. Wragg y A. Leontaritis, «Local mass transfer and current distribution in baffled and unbaffled parallel plate electrochemical reactor,» vol. 66, pp. 1-10, 1997.

[20] J. Collins, X. Li, D. Pletcher, R. Tangirala, D. Stratton-Campbell, F. Walsh y C. Zhang, «A novel flow battery: A lead acid battery based on an electrolyte with soluble lead(II). Part IX: Electrode and electrolyte conditioning with hydrogen peroxide,» *Journal of Power Sources,* vol. 195, pp. 2975-2978, 2010.

[21] D. Aaron, Q. Liu, Z. Tang, G. Grim, A. Papandrew, A. Turhan, T. Zawodzinski y M. Mench, «Dramatic performance gains in vanadium redox flow batteries through modified cell architecture,» *Journal of Power Sources,* vol. 206, pp. 450-453, 2012.

[22] C. Jia, J. Liu y C. Yan, «A significantly improved membrane for vanadium redox flow battery,» *Journal of Power Source,* vol. 195, pp. 4380-4383, 2010.

[23] H. Chen, T. Ngoc-Cong, W. Yang, C. Tan, Y. Li y Y. Ding, «Progress in electrical energy storage system: A critical review,» *Progress in Natural Science,* vol. 19, nº 3, pp. 291-312, 2009.

[24] J. Cheng, B. Wang y L. Hong-Ling, «Numerical Simularion and Experiment on the Electrolyte Flow Distribution for All Vanadium Redox Flow Battery,» *Advanced Materials Research,* Vols. %1 de %2236-238, pp. 604-607, 2011.

[25] M. Lopez-Atalaya, G. Codina, J. Perez, J. Vazquez y A. Aldaz, «Optimization studies on a Fe/Cr redox flow battery,» *Journal of Power Sources,* vol. 36, pp. 147-154, 1992.

[26] B. Li, L. Li, W. Wang, Z. Nie, B. Chen, X. Wei, Q. Luo, Z. Yang y V. Sprenkle, «Fe/V redox flow battery electrolyte investigation and optimization,» *Journal of Power Sources,* vol. 229, pp. 1-5, 2013.

[27] D. Scamman, G. Reade y E. Roberts, «Numerical modelling of a bromide–polysulphide redox flow battery: Part 1: Modelling approach and validation for a pilot-scale system,» *Journal of Power Sources,* vol. 189, pp. 1220-1230, 2009.

[28] T. Cebeci y P. Bradshaw, Momentum Transfer in Boundary Layers, McGraw-Hill, 1977.

[29] L. Norris y W. Reynolds, Turbulent channel flow with a moving wavy boundary., Department of Mechanical Engineering, Stanford University, USA., 1975.

[30] M. Wolfstein, «The velocity and temperature distribution in one-dimensional flow with turbulence augmentation and pressure gradient.,» *International Journal Of Heat And Mass Transfer,* vol. 3, nº 12, p. 301, 1969.

[31] W. Xu, Q. Chen y F. Nieuwstadt, *International Journal of Heat and Mass Transfer,* vol. 41, pp. 3161-3176, 1998.

[32] M. Saqid Al-Bagdadi y H. Shahad Al-Janabi, «Effect of Design Parameters on the Hygro-Thermal Stresses in Proton Exchange Membranes of the Fuel Cells,» *Engineering Applications of Computational Fluid Mechanics,* vol. 2, nº 1, pp. 71-87, 2007.

[33] L. Yu, G. Ren, M. Qin y X. Jiang, «Performance Influencing Factors Simulation of Proton Exchange Membrane Fuel Cells with Different Flow Modes,» *Engineering Applications of Computational Fluid Mechanics,* vol. 2, nº 3, p. 344–353, 2008.

[34] J. Joshi y V. Ranade, «Computational Fluid Dynamics for Designing Process Equipment: Expectations, Current Status, and Path Forward,» *Industrial Engineer Chemical Research,* vol. 42, pp. 1115-1128, 2003.

[35] J. Santos, J. Geraldes , S. Velizarova y J. Crespo, «Characterization of fluid dynamics and mass-transfer in an electrochemical oxidation cell by experimental and CFD studies,» *Chemical Engineering Journal 157:379–392,* vol. 157, p. 379–392, 2010.

[36] STAR-CCM+, *User's Manual,* 2013.

[37] D. Moore, The Basic Practice of Statistics, Third ed., New York: W.H. Freeman and Company, 2003.

[38] W. Navidi, Estadística para ingenieros y científicos, First ed., New York: McGraw-Hill Companies Inc, 2006.

ANEXO IV: REDOX CELL HYDRODYNAMIC MODELLING: TOWARDS A REAL IMPROVED GEOMETRY BASED ON CFD ANALYSIS

ABSTRACT

A redox cell is an assembly consisting of electrodes surrounded by a volume of electrolyte (liquid). The redox cell device stores electrical energy, it is full of high acid flows and this acidity causes big difficulties for physical modeling. To overcome this problem, numerical and experimental analysis of those flows in a real redox cell have been developed and here described. A methodology to improve redox cells performance based on the analysis of the electrolyte flow is proposed. Improvements in the flow uniformity are achieved by means of the definition of some designed parameters based on CFD analysis.

The depicted methodology is applied to a specific redox cell geometry improving previous authors´ designs. This article quantifies parameters for this particular case and the proposed improvements. The considered CFD model is also validated with experimental data using a real scale cell built in transparent material. The convergence between experimental and numerical results is fairly good. Finally, the geometry designed based on this proposed methodology presents 0% dead zones or recirculations in the membrane area, which will definitely improve the overall interchange efficiency of the cell. This validated methodology is presented for a real future design strategy of these sorts of devices.

Keywords. Computational Fluid Mechanics, Hydraulic Experiment, Electrolyte Distribution, Electrolytic Reactor, Redox Iron Flow Cell.

1. INTRODUCTION

Flow batteries are a sort of devices used to storage electricity in which two chemical components dissolved in liquids are presented and separated by a membrane [1]. In these devices, ion exchange occurs through the membrane while both liquids circulate in their own respective space.

These sorts of devices are crucial for storing energy [2]. Storing is especially important in renewable energy uses that represents a significant percentage of the installed power capacity in the future. In this sense, Electric Energy Store Systems (EESS) are very important for future developments in energy grids [3] as they become a necessity in the renewable sources energy management due to the great variability of this sort of sources [4], [5].

Among all the EESS, electrochemical batteries are one of the most commonly used [6] as they are very adaptable and efficient. Besides, many types of technologies have been applied in batteries: lead-acid batteries [7], sodium/sulfur batteries [8], flow batteries [9], [10], [11], nickel-cadmium [12] and lithium ion [13]. Among all these types of technologies, in this article, an iron flow battery (redox cell) [14] will be analyzed in order to determine a real optimized geometry. This optimization is based on the achievement of a uniform velocity of the liquid electrolyte flow dissolving the present chemical species in the redox cell.

Uniformity of the electrolyte flow is crucial for ensuring the performance of the redox cell. If the flow is reversed or the velocity is negligible in any part of the redox cell, the efficiency of the whole redox cell will decrease [15], [16]. Furthermore, a deep analysis on the electrolyte flow velocity field is determinant for the design of the geometry inside the redox cell. In this sense, the work presented in this article is the following part of what was described in 2013 [17]. In the previous paper, the authors applied a CFD model in order to analyze the electrolyte velocity field inside the redox cell. In that particular case, a prototype of a redox cell in a scaled model was analyzed by means of a computational and an experimental analysis. As a conclusion of that research, the most turbulent zones were identified near the input-output; and a quantification of the reverse flow in the design was provided indicating the direction in which future improvements could be done. These proposed improvements are implemented in the present geometry and validated with measurements in the laboratory.

Following this research, in the present case, a real design of a redox cell has been developed. The designed geometry is deeply analyzed based on a methodological strategy supported on

CFD analysis. Some design parameters are proposed based on the uniformity and symmetry of the electrolyte flow velocity profile in some determinant sections of the geometry. When these parameters achieve the optimum value, a final geometry is proposed for all the studied regions of the redox cell.

In the previous paper [17], the model of a redox cell prototype in a smaller scale than in the present research was proposed. In this case, a complete different size and geometry for the cell have been developed. Apart from this, in the previous case [17] the magnitudes represented were streamlines, pressure in different points along the geometry, and velocity (x, y) in these points. In contrast of this, in this particular case different magnitudes are used to represent pressure and velocity: On the one hand, the pressure drop between inlet and outlet is considered; on the other hand, the velocity is here analyzed with the residence time, a magnitude that has not been previously represented in these sort of devices. Also, the range of the represented flow across the cells is very different in both researches.

Finally, the parameters presented in this paper to analyze flow uniformity are implemented in a real geometry for the first time. In previous works [17] only the volume of recirculation was analyzed.

In further research of the authors, a theoretical methodology for designing redox cells was developed [18], but it was not validated with experimental devices. As a final and paramount step of the complete research done, the improved designed geometry for the cell is built in a transparent material and some experiences to validate the model are proposed. To do so, pipe piezometer and dye liquid have been used. On the one side, measurements on the flow and pressure in different parts of the device are done in order to validate the CFD based analysis. On the other side, the visualization of the flow is performed by filming the pass of colored fluid across the built device to go further in the velocity validation.

2. DESIGN PARAMETERS

In previous researches of the authors [17], [18] a basic design was discussed and considered as a prototype. As a result of these researches and based on the literature, the importance of the velocity field of the fluid electrolyte for the performance of the redox cell was pointed out. Anyway, some areas with reverse flow and dead zones were present in initial designs. In addition, the initial designed must be commercially developable. The previously mentioned points invite researchers to move on improving the geometry to optimize the flow.

Here, a new geometry based on some proposed design parameters [18] is presented. The methodology for the design is based on a CFD analysis applied to slightly different geometries by improving some determining parameters. The estimation of these parameters on different geometries (with significant modifications on the prototype developed in 2013) led modellers to develop the present geometry. This geometry can also be industrially developed.

2.1. Design parameters definition

The dispersion of electrolyte flow is decisive for the efficient redox cell operation, specially in the membrane. In this part the ionic interchange occurs. Thus, in this research the determinant parameters to optimize and homogenize the velocities when the electrolyte flow arrives to the membrane are proposed.

The membrane is the most expensive part of this type of redox cell; it is around the 30% of the material cost [19]. The adequate behavior of the membrane depends on a correct interchange with the ionic flow. Furthermore, modeling the behavior of the flow in the redox cell is of paramount importance to ensure velocity uniformity [20] and then, final performance in the redox cell.

In Fig. 1 the most important parts of the redox cell can be observed. The design parameters proposed in this article will be evaluated by means of CFD analysis in the different regions in the redox cell. These parameters are: symmetry coefficient (evaluated in I region); uniformity coefficient (assessed in the E region); variability range coefficient (considered in the M region); and Volume of current main direction evaluated on the whole cell.

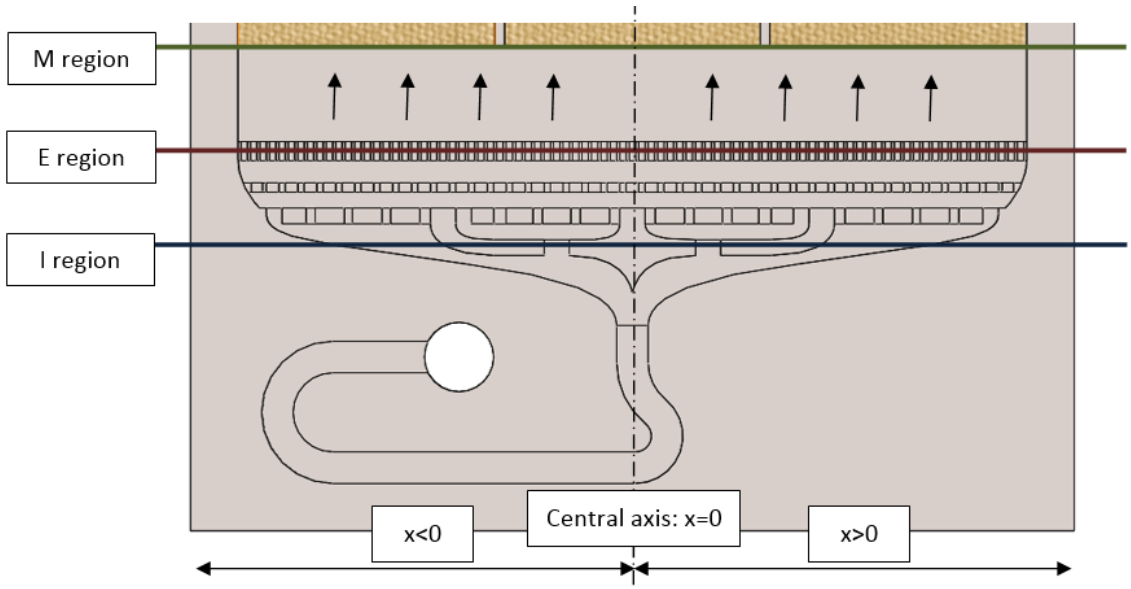

Fig. 1 Regions of the proposed parameters.

2.1.1. Symmetry coefficient

Although the design of the channels is largely symmetrical, the inlet and outlet of the liquid is located at one side of the redox cell, this can cause a non-equal division of the flow. To avoid this problem, the redesigning of the main channel (inlet and outlet) is needed, thus will compensate the fluid inertia. The geometric solution proposed is to add a curve in the main channel to avoid this asymmetry. The symmetry coefficient considers the difference in the percentage part of the flow circulating along both sides of the device. The flow will be completely symmetric when this coefficient is the minimum.

This symmetry coefficient evaluated in I region is defined by (1):

$$C_{Simmetry}(\%) = \frac{|Q_{x>0}| - |Q_{x<0}|}{|Q_{x>0}| + |Q_{x<0}|} \cdot 100 \quad (1)$$

Where:

$Q_{x>0}$: flow rate in right side (Fig. 1)

$Q_{x<0}$: flow rate in left side (Fig. 1)

The best design will be the one that shows the closest symmetry coefficient to zero; this design distributes the flow uniformity around the cell.

2.1.2. Uniformity coefficient

This coefficient is evaluated at the exit of the distribution channels of the geometry in the E region. This coefficient analyzes different average velocities for each channel. A hypothesis test is performed to assess whether the average velocities of each channel is meaningful and different or not. In this particular case, the goal is to maintain a constant velocity inside the redox cell. The lower the coefficient, the better the design.

Hypothesis testing [21], [22] has the objective of analyzing a sample of data in an attempt to distinguish between population characteristics that are likely to occur and population characteristics that are unlikely to occur.

Two main keys are to be considered in hypothesis testing: null hypothesis and alternative hypothesis. On the one side, null hypothesis is a statement about the value of a population parameter (*mean channel* velocity), it is always stated in statistical terms as an equality (=). On the other side, alternative hypothesis is a statement about the value of a population parameter that must be true if the null hypothesis is false and it is stated as an inequality (<,>, ≠). Then, in this particular case, null and alternative hypothesis refer to the channel velocity.

The level of significance of the test (α) is 0.05. Any variation detected with p-value ≤ 0.05 is property to random phenomena intrinsic to the system.

The null hypothesis (2) is true when the velocity of one channel is equal to the other channel and the alternative hypothesis (3) occurs when the velocities are different. Equation 2 and 3 summarize the main ideas in this particular hypothesis testing:

Fail rejection region: $\{-z_{(\alpha/2)} \leq Z \leq z_{(\alpha/2)}\}$ (2)

Rejection region: $\{Z \in$ *to any other region*$\}$ (3)

Therefore, the uniformity coefficient is defined, in this case, as the relation between the null and the alternative hypothesis using the value of velocities in E region.

$$C_{uniformity}(\%) = \frac{\sum\left(-z_{\alpha/2} \leq Z \leq z_{\alpha/2}\right)}{\sum(Z)} \cdot 100 \quad (4)$$

A good design is achieved when the uniformity coefficient is minimum. With the implementation of this parameter it is possible to focus only on the channels cell design with different flow from other channels and to improve the design step by step [18].

2.1.3. Variability range coefficient

This parameter is used for determining the velocity of the liquid in contact with the membrane. This part is the most important part of the redox cell. Uniform velocity near the membrane will cause the homogeneously ion exchange throughout the membrane. In this case, this parameter is defined as the difference between the maximum and minimum velocities in M region (Fig. 1)

$$R_i\ (\mathrm{m/s}) = V_{\max} - V_{\min} \tag{5}$$

For the correct working process of the redox cell battery a low variability range coefficient reduction is needed.

2.1.4. Rate of fluid circulating in the main direction (upwards)

This parameter evaluates the amount in percentage of the volume of fluid flowing in the main direction. This percentage can be seen also as an indicator of the uniform distribution of electrolyte considered an essential element for the proper functioning of the whole cell. The higher percentage, the better the internal operation of the redox cell and, therefore, less likely to appear dead zones or regions of recirculation (eddies). The definition of this parameter is indicated in equation 6.

$$V_{upwards}(\%) = \frac{V_{v+}}{V_{TOTAL}} \cdot 100 \tag{6}$$

In contrary, the percentage of volume flowing in the opposite direction or with null velocity (dead zone):

$$V_{downwards}(\%) = \frac{V_{v-} + V_{dead\_zones}}{V_{TOTAL}} \cdot 100 \tag{7}$$

where:

V_{v+}: Volume with velocity upwards.

V_{v-}: Volume with velocity downwards.

V_{dead_zones}: Volume with null velocities.

2.2. Geometry

Geometry designed and used for both the real cell and the computational model is necessary. This new geometry has been developed through an iterative computational process based on the depicted methodology. The previously parameters described have been determinant in the final geometrical design.

The most significant characteristics that describe this geometry are:

- Active membrane area: 0.0925 m^2.
- Number of channels: 84.
- Maximum channels spacing: 8 mm.
- Minimum channel spacing 1 mm.

The Fig. 2 shows the proposed geometry. In Fig. 2.a) the whole studied redox cell is observed, the central part of the redox cell (with ribs) supports the membrane. The inlet fluid is located at the bottom of the redox cell while the output is at the top:

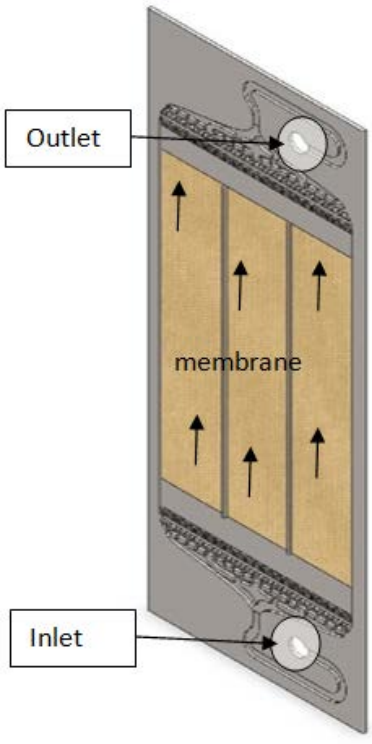

a) Whole redox cell geometry

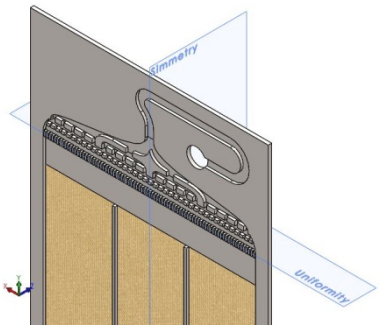

b) Outlet of the redox cell geometry

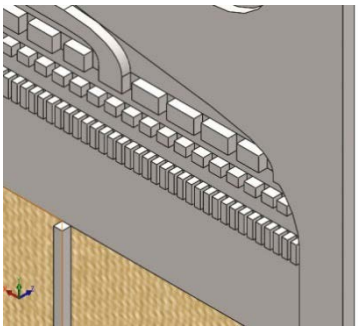

c) Channels of the redox cell geometry

Fig. 2 Redox cell geometry.

According to Fig. 2, inlet boundary condition is in the bottom part of the described cell. The flow comes into the cell and it is distributed into different channels in I region. Channels are differently distributed along the vertical distance in four steps until E region. Afterwards, the electrolyte flow uniformly goes to M region and reaches the membrane. Finally, the flow goes out of the cell passing across a symmetrical distribution of channels as it went into the cell.

As a part of the design process in this redox cell, the more convenient proposal for channel distribution in I region is shown in Fig. 2. The distance among channels is decreasing in four steps, respectively 8, 4, 2 and 1 mm of channels separation. With this, the symmetry and uniformity coefficients of the final design were optimum.

2.3. CFD analysis

This part describes the computational model which is used for the determination of the electrochemical flow velocity that has been previously presented. In this computational model, a few series of hypotheses are needed to be applied as they will make easier the resolution of mathematical equations.

The cathode is made of graphite of carbon felt. The anode is also made of graphite or carbon felt with a selective membrane as separator. The membranes are made up of cross-linked linear polymer chains, which form a three-dimensional network. Without the cross-linking, the membrane would be dissolved in water forming a polyelectrolyte solution. Ion exchange membranes have fixed ion functional groups and oppositely charged counter ions, present in sufficient numbers to render the whole exchanger electrically neutral. The reactions achieved in the cell (considered as an all-iron redox cell) are:

- $2Fe^{2+} \rightarrow 2Fe^{3+} + 2Fe$ *, during the charge*
- $2Fe^{3+} + 2Fe \rightarrow 2Fe^{2+}$ *, during the discharge*

The electrolyte composition for this purpose is 2m FeCl2 + 0.5m NH4Cl in deionized water, as based on [1]. It has been assumed that the electrolytic fluid produces no deposition within the cell as well as it does not produce any gas phase. This hypothesis would be completely true if the redox reaction was 100 % efficient. In reality, other competing reactions can occur with little gas production; these are disregarded as hypothesis [23]. So, only equations of an only fluid (liquid) are solved. This means that the electrolyte does not produce any gaseous or solid deposition inside the redox cell geometry

The constant density model makes the assumption that density is invariant throughout the continuum. The values of dynamic viscosity ($8.8871 \cdot 10^4$ Pa·s) and density (997.561 kg/m^3) of the electrolyte fluid is considered constant at the whole model. It has been verified that, the water at 20 ºC (used for the validation) has the same features as the electrolyte at 40ºC [24], [25].

Models based on temperature equations have been discarded because a constant temperature is considered. The analysis of the velocity and pressure are steady-state. The segregated model resolves the equations for each component of the velocity and for each component of the pressure. The complete formulation is described as the use of an array of variables juxtaposed and mesh performance resolved in the interpolation Rhie-Chow [26]. In order to meet with conservation of mass condition a standard pressure correction algorithm (SIMPLE) is used. The model solves algebraic and iteratively equations taking gravity always into account until numerical residuals are enough low (less than 10^{-3}) to consider that resolution has converged. This convergence is determined in this case, also by monitoring the principal variables of the study (velocities, pressures, turbulence parameters, etc.). When the value of these parameters is constant, there is no need to switch back to checking residuals. Furthermore, the convergence can be considered as an achievement.

Numerical simulations of flow in the above geometry were obtained with STAR-CCM+™ [27] which is a commercial CFD code. This code solves the basic conservation laws of Fluid Mechanics, i.e., the laws of conservation of mass, momentum and energy. The continuity or mass conservation equation used is:

$$\frac{\partial \rho}{\partial t} + \nabla \rho \vec{v} = S_m \tag{8}$$

where ρ is the fluid density, $\vec{v}$ is its velocity and S_m is the mass source in the control volume. Cartesian coordinates were used in this case.

The momentum equation is:

$$\frac{\partial (\rho \vec{v})}{\partial t} + \nabla \rho (\vec{v}\vec{v}) = - \quad p + \nabla \bar{\tau} + \rho \vec{g} + \vec{F} \tag{9}$$

where *p* is the static pressure; *ρ* and the gravitational and outer forces are defined on the control volume, respectively, and the stress is tensor defined by:

$$\bar{\tau} = \mu_T \left[\left(\nabla \vec{v} + \nabla \vec{v}^T \right) - \frac{2}{3} \nabla \vec{v} I \right]$$

(10)

where μ_T is the eddy dynamic viscosity and *I* is the unit tensor [27] .

Steady-state conditions were used for all simulations. For the closure problem, the *k–Epsilon* model was applied. This is a semi-empirical model based on the transport equations for kinetic turbulent energy (*k*) and the dissipation rate (*ε*). The turbulence equations were separately solved from the mass and momentum equations at each time step.

The initial value of flow to initialize flow domain is 50 l/h. In M region with flow rate of 50 l/h the Reynolds number is around 123. Nevertheless, in the inlet geometry the Reynolds number is 2398, so that turbulence may appear in the inlet redox cell and I and E region [28], [29]. In this case, despite of the low Reynolds number in the membrane area, turbulence occurs in the inlet and outlet redox cell geometry so, the most convenient solution is the *k-Epsilon* turbulence model [17].

A successful model is the realizable *k–Epsilon* model that [30] developed. This model contains an additional transport equation for the turbulent dissipation rate. Also, a critical coefficient of the model, is expressed as a function of mean flow and turbulence properties, rather than assumed to be constant as in the standard model. This procedure lets the model satisfy certain mathematical constraints on the normal stresses consistent with the physics of turbulence (realizability). The concept of a variable is also consistent with experimental observations in boundary layers.

In this particular case, other models such as the standard and realizable *k–Epsilon*, *k-Omega* and *Spalart-Allmaras* models have been applied [27]. The realizable *k–Epsilon* model is substantially better than the other models. In this case the comparison in pressure drop along the cell gives better results for realizable *k-Epsilon* model. The realizable model has been implemented in STAR-CCM+ with a two-layer approach. The Table 1 describes the accuracy when comparing the modeled and measured pressure drop of the 4 turbulent models performed.

Realizable k-Epsilon	3%
k-Omega	9%
Spalart Allmaras	11%
Standard k-Epsilon	27%

Table 1 Comparison of different turbulent models pressure VS experimental model pressure (%).

Boundary conditions need to be defined. Three kinds of boundary conditions were used: the velocity inlet, the pressure outlet and the wall. Flow rate (50 l/h) is settled as an inlet boundary condition. This flow rate is near of the stoichiometric flow. At the outlet geometry cell the model has the boundary condition of pressure outlet: atmospheric. For the others boundary's wall roughness "smooth tube roughness" is considered [31]. This is well suited to the material properties of the cell.

The boundary condition considered for the membrane is wall. The selective membrane does not affect the hydrodynamic movement of the fluid as no fluid pass across the membrane; only electronic transfer occurs in this process.

Trimmed cell meshers are used for the volumetric surface. These elements have a good performance of mesh when all fluid velocity goes in the same direction. In order to improve the overall quality of an existing surface and optimize it for the volume mesh models, the surface remesher can be used to triangulate the surface. To capture the layer boundary mesh in this geometry efficiently, prismatic layers surfaces have been implemented in inlets and outlets channels area. The prism layer mesh model is used with a core volume mesh to generate orthogonal prismatic cells next to wall surfaces or boundaries. This layer of cells is necessary to improve the accuracy of the flow solution. A prism layer is defined in terms of:

- Its thickness.
- The number of cell layers within it.
- The size distribution of the layers.

The following table 2 describes the basic features of the used mesh:

Base size (mm)	3	Curvature of the surface (pts. /circle)	72
Minimum size (mm)	1.50	Prism layer thickness (mm)	0.15
Target size (mm)	3	Number of Prism Layer	2

Maximum size (mm)	4.80	Prism Layer Stretching	1.50

Table 2 Characteristics of the general mesh.

The Table 3 describes the characteristics of the mesh used in the channels, inlet area and outlet area (the mesh refinement):

	Max	Min		Max	Min
Minimum size (mm)	0.375		Prism layer thickness (mm)	0.15	0.30
Target size (mm)	0.750	1.5	Number of Prism Layer	2	

Table 3 Characteristics of the refined mesh.

In the Fig. 3 the mesh used in this redox cell geometry can be seen. Fig. 3 a) shows in Plane Z all volumetric mesh generated in the redox cell geometry. Fig. 3 b) and 3 c) show in detail the surface mesh (adaptive refinement) and volumetric mesh respectively and, finally, in Fig. 3 d) the prismatic layer used for the capture of turbulence between channels is observed.

a) The geometric volumetric mesh

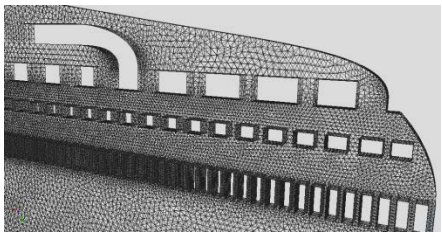

b) Surface mesh (detail 1)

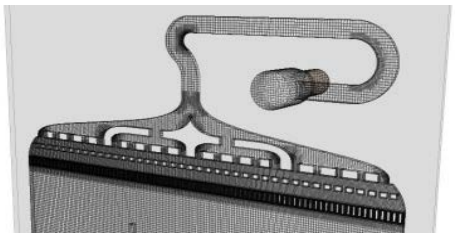

c) Volumetric mesh (detail 2)

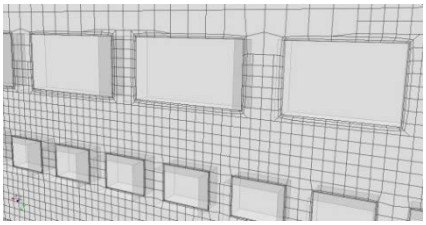

d) Prism layer mesh (detail 3)

Fig. 3 Geometry and mesh detail.

To verify the independence of the proposed feature mesh, different mesh simulations have been developed. In these simulations, the number and size of cells has been changed. It has been considered that mesh has not influence in final results when the difference between inlet and outlet pressure of one mesh is less than 1% regarding the following mesh. This comparison of pressure drop predicted by three different mesh is described in Table 4. The so called "Mesh 2" has been selected, as the difference in drop pressure prediction when compared with "Mesh 3" is less than 1%.

Pressure difference (%)	mesh 1 329,091	mesh 2 450,335	mesh 3 656,649
mesh 1	--	1	2
mesh 2	1	---	0
mesh 3	2	0	---

Table 4 Comparison of pressures drop predicted by different meshes (%).

Surface mesh		Volumetric mesh	
Faces	362,062	Mesh cells	450,335
Vertices	31,363	Interiors mesh cells	1,265,107

Table 5 Describes the final mesh features.

The turbulent viscosity ratio coefficient has determinate where the turbulence appears. The turbulent viscosity ratio, μ_t/μ, is directly proportional to the turbulent Reynolds number ($\mathrm{Re}_t \equiv k^2/(\varepsilon\nu)$). Re_t is large (on the order of 100 to 1000) in high-Reynolds-number boundary layers, shear layers, and fully-developed duct flows. However, at the free-stream boundaries of most external flows, μ_t/μ is fairly small. Typically, the turbulence parameters are set so that $1 \le \mu_t/\mu \le 10$. If this coefficient is higher than 10 the flow is turbulent.

In the Fig. 4 the turbulent viscosity ratio can be seen. This coefficient is higher than 10 in the channels and inlet area. For this reason, the prism layer mesh for capturing the turbulence appears in this area.

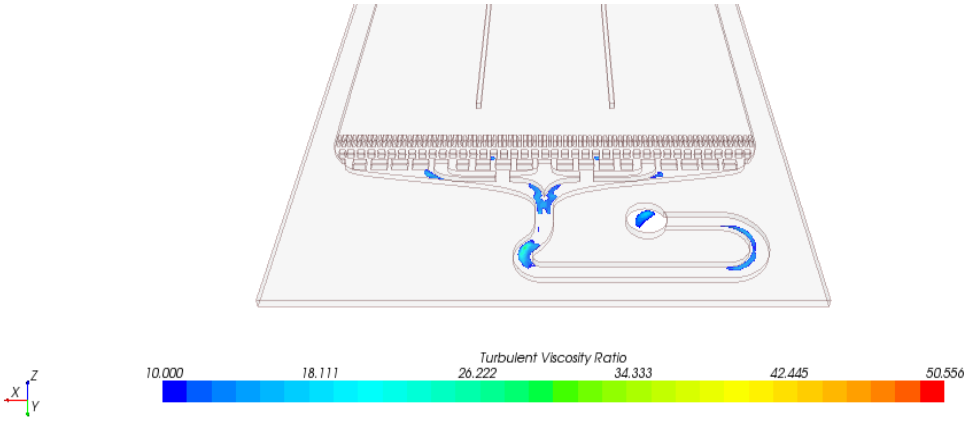

Fig. 4 Turbulence viscosity ratio volume higher than 10.

2.4. Results: Estimation of parameters in the proposed geometry

Once the computational model has been presented, the results of the four parameters estimated in the geometry based on CFD analysis are described.

2.4.1. Symmetry coefficient

The Flow mass (kg/s) is estimated in I region for x>0 y x<0. A flow mass is obtained for position x>0 the $7.07 \cdot 10^{-3}$ kg/s (right side) and for x<0 the $6.81 \cdot 10^{-3}$ kg/s (left side). The velocity field in I region can be observed in Fig. 5.

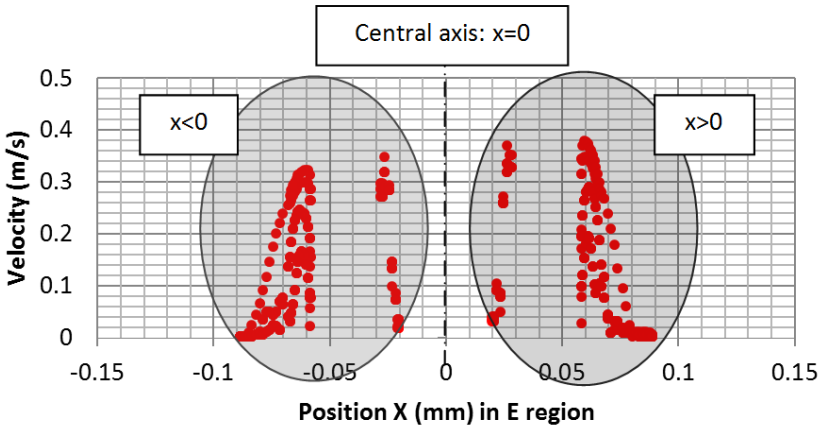

Fig. 5 Velocity VS position in I region.

Then, the symmetry coefficient value is:

$$C_{Simmetry}(\%) = \frac{7.07 \cdot 10^{-3}(kg/s) - 6.81 \cdot 10^{-3}(kg/s)}{7.07 \cdot 10^{-3}(kg/s) + 6.81 \cdot 10^{-3}(kg/s)} \cdot 100 = 2\%$$

The difference between the current flows on the left side compared to the right part is 2%.

2.4.2. Uniformity coefficient

Then, the velocity of flow passing each of the 84 channels is obtained in E region. The described hypothesis test is applied to compare one by one each channel. In Fig. 6 the average velocity for each channel is displayed.

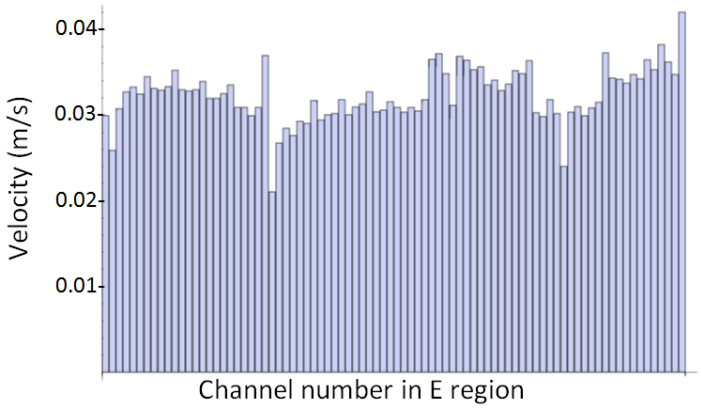

Fig. 6 Average velocity for each channel in E region.

Applying the hypothesis test, the uniformity coefficient is:

$$C_{uniformity}(\%) = \frac{\sum\left(-z_{\alpha/2} \le Z \le z_{\alpha/2}\right)}{\sum(Z)} \cdot 100 = \frac{315}{3570} \cdot 100 = 8.8\%$$

2.4.3. Variability range coefficient

This parameter is considered in M region, 30 mm away from the channels. In this position, the speed range is studied in the first contact between the fluid and the membrane. Fig. 7 shows the velocities in this M region.

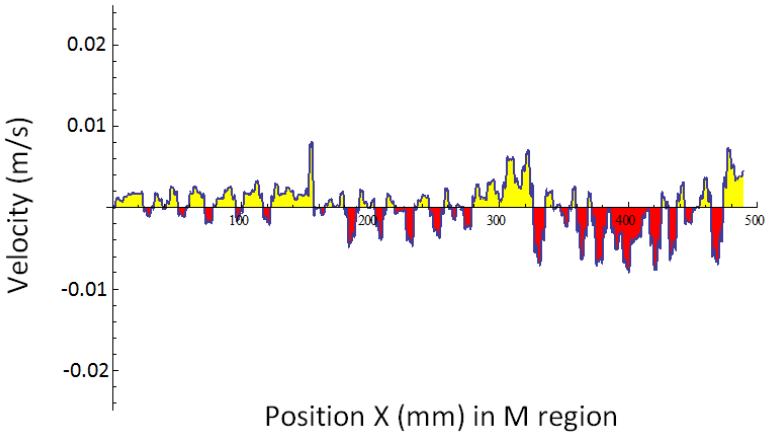

Fig. 7 Velocity profile in M region.

The maximum and minimum velocities are:

- Maximum velocity=-0.033 m/s.
- Minimum velocity= -0.018 m/s.

And the value for variability range coefficient is:

$$R_i = V_{\max} - V_{\min} = 0.015 \quad m/s$$

2.4.4. Rate of flow in the main direction (upwards)

To estimate this parameter, the cell volume of the velocities along the cell is obtained. Fig. 8 depicts the flow velocity in the main flow direction (upwards).

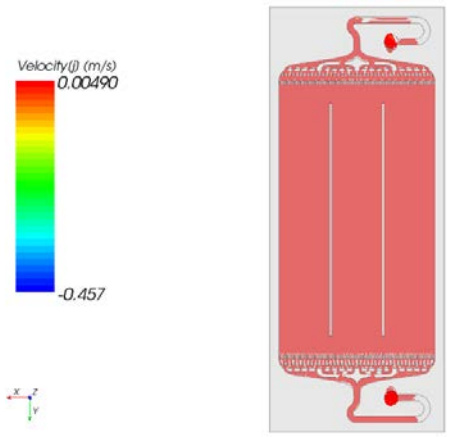

Fig. 8 Volume of the flow velocity moving upwards.

The non-colored parts are the reverse flow volumes. As it can be seen the only cells where velocities appear opposite the main fluid and dead zones are located at the input and output of the steering geometry.

	$V_{upwards}$	$V_{downwards}$
All volume	91.77(%)	8.83 (%)
Membrane region	100 (%)	0 (%)

Table 6 Volume of flow in main and opposite directions (upwards and downwards).

The percentage of mesh cells in the upwards direction the velocity is 91.17% in all of the geometry and particularly 100% in the area of the membrane. Cells with dead zones and downwards direction the velocity in all the geometry is 8.83% and 0% in the membrane area, as depicted in Table 5. Comparing with previous designs [17] this represents an improvement higher than 15%.

3. COMPUTATIONAL MODEL VALIDATION

With the described geometry based on the numerical model and design parameters, a real cell has been built in real scale with transparent material. Pressure and velocities have been recorded in the Laboratory of Fluid Mechanics of Universitat Politècnica de València, Spain.

CFD analysis for the design must be then validated with real flow. This real device is then used to validate the CFD for this improved design. The comparison between experimental model (velocity and pressure) with those obtained from the numerical model are used to give validity to the results of the CFD. Results will be analyzed for any aspect considered in validation.

3.1. Pressure validation

The first measured magnitude is pressure. It is measured by means of piezometric tubes in the inlet and outlet regions of the cell. The difference of pressure between both points has been recorded for a fixed flow. At the same time, pressure can be modeled by the CFD for the whole geometry as described in Fig. 9.

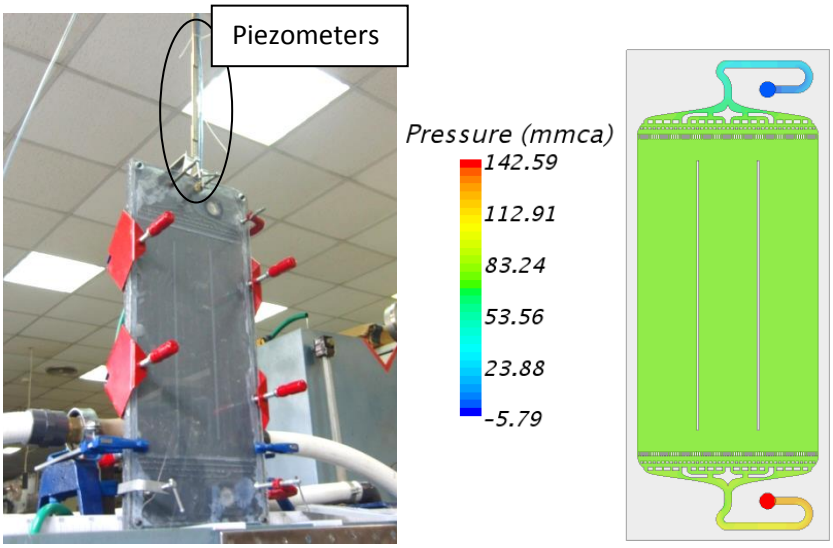

Fig. 9 Left: Experimental prototype setup. Right: Pressure along the whole cell geometry.

In this case, 15 measurements with different flows have been performed. Therefore, the experimental curve representing the head losses versus flow can be obtained:

$$P(mmwc) = 0.2584 \cdot Q^{1.6066} \qquad (11)$$

This differential pressure is 138.80 mmwc for a flow of 50 l/h. In the computational model and the flow rate of 50 l/h pressure drop between the inlet and outlet has been obtained, this

value is 142.49 mmwc. The error shown when comparing experimental and computational model for this particular flow of 50 l/h is 3%. Fig. 10 shows the experimental measurements performed in front of the model obtained from the computational model.

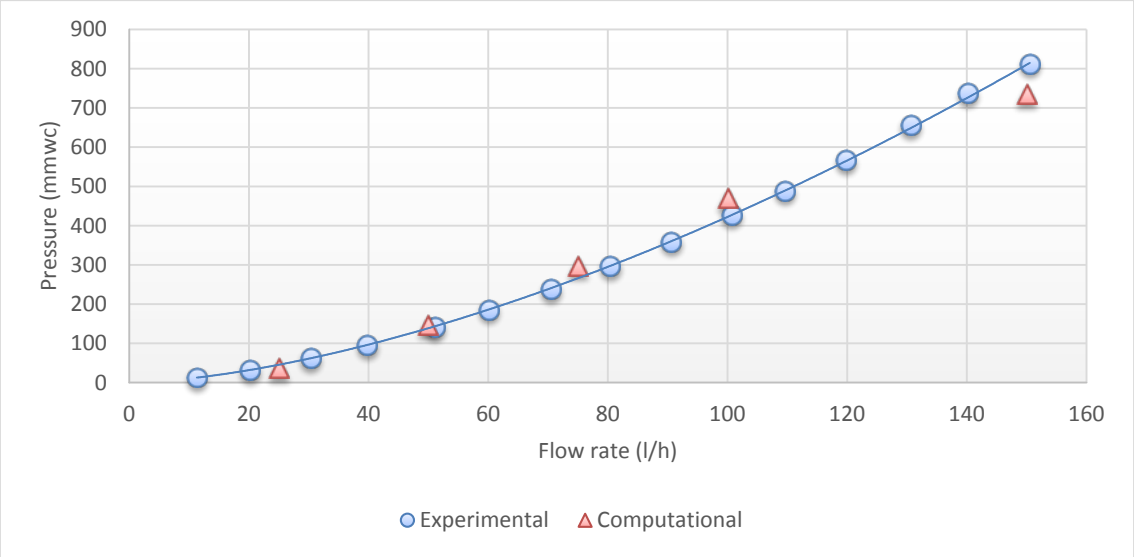

Fig. 10 Head losses inside the cell VS flow.

3.2. Velocity and time residence

The analysis for the validation of the velocity field is carried out in two ways. The first one consists on comparing the total time that the dye remains in the cell. The second one consists on qualitatively comparing the experimental model with the numerical model in 4 steps. The function used for this comparison is called Residence Time [32].

The Residence Time is a function of the passive scalar model. The passive scalar model solves one or more transport equations for user-defined variables that can be represented by arbitrary scalar values. The function used for this comparison is called Residence Time based on transport equation for the dye present in the flow. The transport equation for the passive scalar component ϕ is (12):

$$\frac{\partial}{\partial t}\int_V \alpha_i \rho \chi \phi_j dV + \oint_V \alpha_i \rho \chi \phi_j (v - v_g)\cdot da = \oint_A \left[\alpha_i \chi \left(\frac{\mu}{\sigma} + \frac{\mu_t}{\sigma_t} \right) \nabla \sigma_j \right] \cdot da + \int_V S_{\phi_j} dV \quad (12)$$

where:

- j is the component index

- σ is Schmidt number, assumed to have a value of 0.9.
- χ is the void fraction
- α_i is the volume fraction of phase i (set to 1 for single phase flows)
- S_{ϕ_j} is a source term for passive scalar component j. The source term is not multiplied internally by the volume fraction. ϕ_j, is assumed to be positive-definite.

The initial numerical value can be held in the scalar field and the value can be specified at boundaries. For wall boundaries, a zero flux is set. A passive scalar source term and its derivative at the region level can be also defined. An inherent assumption of this model is that the scalar values do not contribute to the bulk physical properties of the fluid.

Passive scalar model can be used to simulate residence time (the mean age of fluid) for a single phase. A passive scalar is defined on the fluid, increasing steadily over time in value. In effect, defining the passive scalar attaches a clock to each volume element of moving fluid. These virtual clocks can be used to measure the residence time of the fluid in different parts of the chamber. The model follows these clocks, under an Eulerian consideration to measure the time that the fluid is within the control volume.

Therefore, in the experimental model the time from the first dyed particle passing through cell is 21 seconds. Considering this as the residence time for the steady state is comparable to the residence time obtained from the computational model. It can be seen in the Fig. 11 that the residence time for the first particle is 26 seconds.

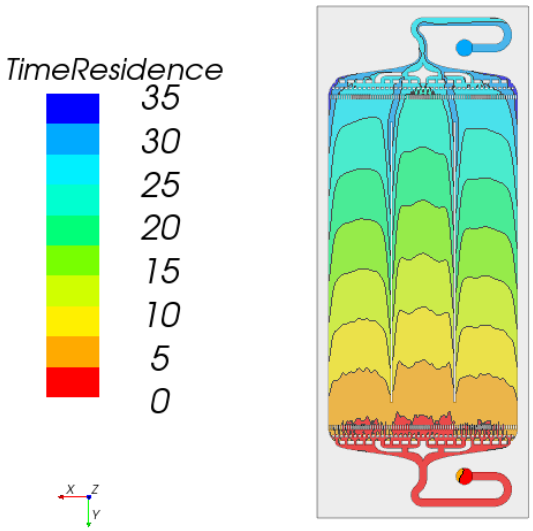

Fig. 11 Residence time in the computational model.

Comparing these two values a difference of 19.23% is obtained between the experimental time and time calculated by numerical analysis for this first dyed particle. This comparison should be considered in a qualitative manner as the experimental value is achieved by visualization techniques and the numerical value is approximated by a formula within the CFD code. Therefore, it can be considered that this error of assessment is acceptable for validating this new parameter.

The next step in validation is based on the comparison of velocities in the dyed flow with the numerical profiles of calculated velocities as depicted in Fig. 12. Velocity profiles for different advancing steps of dye positions are represented by both experimental and numerical modeling.

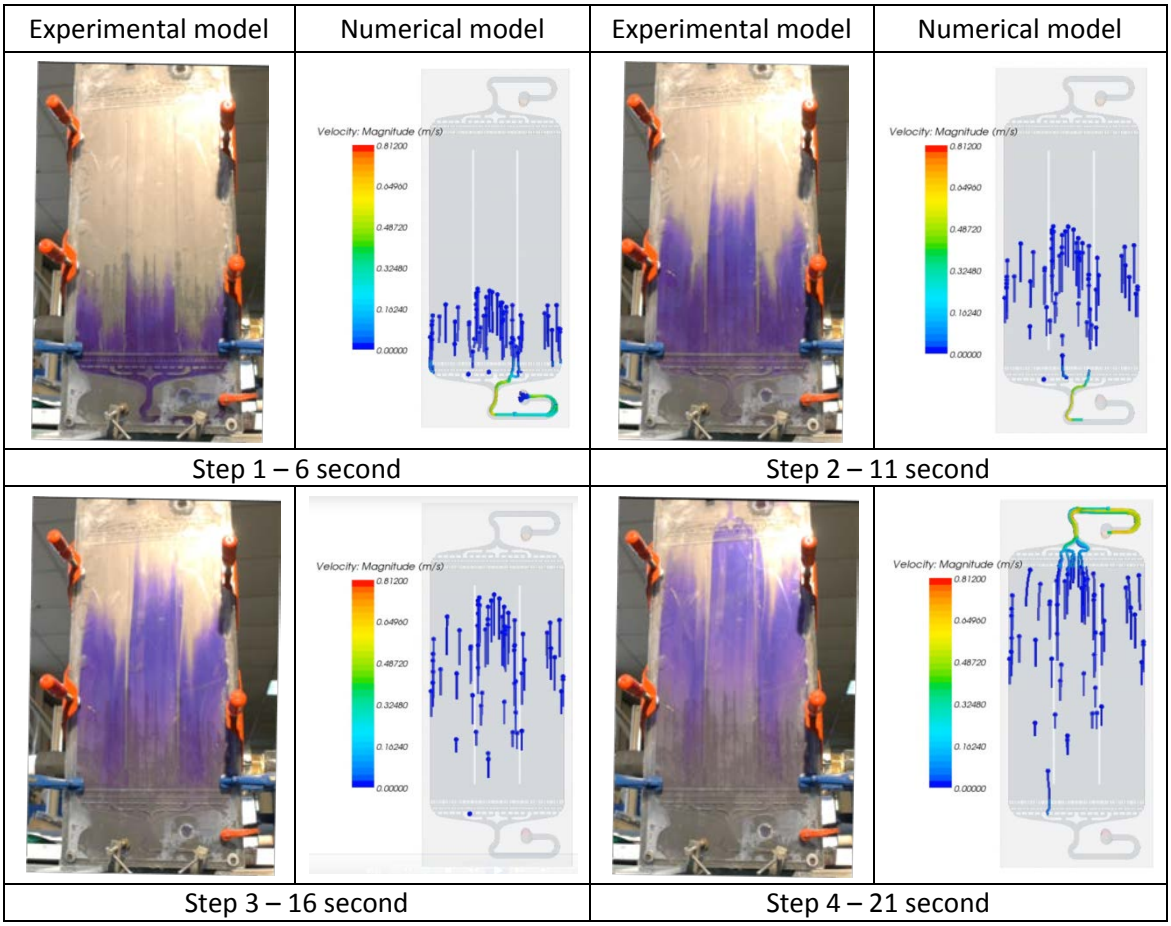

Fig. 12 Experimental VS numerical velocity profiles.

It can be seen in this Fig. 12 that the velocity profile obtained from the experiment is quite similar to the computational velocity profiles in the four steps. The dyed flow appears before in the central region than in all there other regions because the distance to the inlet is shorter.

Qualitatively, it can be said that the experimental velocity profiles approach reasonably well the computational velocity profiles.

4. CONCLUSIONS

This article describes a developed and improved redox cell geometry previously designed by the authors. To make improvements in this real redox cell, the methodology is based on a CFD analysis of the whole represented structure. This CFD proposals have been validated with experimental data.

The parameters quantified in this geometry were: symmetry coefficient, uniformity coefficient, variability range coefficient and rate of fluid in the main direction. This design has been built in transparent material and uses a colored flow to be observed in the Laboratory of Fluid Mechanics of Universitat Politècnica de València, Spain.

Comparing the experimental model to the computational one for a flow of 50 l/h, a methodology for validation is proposed. Differential pressure and velocity fields are compared in both models with an acceptable convergence between them. This leads to two conclusions: the proposed design is suitable for improvements, and the considered geometry parameters are a powerful tool for similar cell designs as they can be used for comparison.

The proposed parameters refer to the uniformity of velocity in different regions of the cell. In this particular case, the symmetry coefficient shows a flow difference of 4% between both sides of the geometry. The uniformity coefficient provokes that an 8% of the channels are statistically different on the basis of the velocity value. The variability range coefficient is 0.015 m/s; this ensures a uniform flow in all the membrane. In the membrane turbulence or dead zones will not occur. The three parameters previously described guarantee significant improvements and flow uniformity all over the membrane surface.

The validated model let designers to analyze velocities inside the whole geometry of the cell so; dead zones and recirculation in the membrane area can be estimated. In this particular case, in the membrane region, this recirculation volume minimizes to 0%, considerably improving previous designs in which this value arised up to 17%. This means that the proposed design in this article substantially improves the membrane useful surface benefiting the ionic interchange homogenously. Thus, both; a methodology based on the use of CFD to design redox cells and an improved model have been presented. They have been validated as a real application that substantially improves the nowadays existing technology.

5. REFERENCES

[1] J. Mellentine, «Performance Characterization and Cost Assessment of an Iron Hybrid Flow Battery,» *Thesis. University of Iceland,* 2011.

[2] J. Cheng, B. Wang y J. Yang, «Adsorption and Diffusion of VO2+ and VO2 + across Cation Membrane for All-Vanadium Redox Flow Battery,» *Solvent Extraction and Ion Exchange,* vol. 27, pp. 312-327, 2009.

[3] Eyer, M. James, Corey, P. Garth, Iannucci y J. Joseph, «Sponsoring Organization: USDOE 2004,» 2004.

[4] J. Kondoh, I. Ishii, H. Yamaguchi, A. Murata y K. Otani, «Electrical energy storage systems for energy networks,» *Energy Conversion and Management,* vol. 41, pp. 1863-1874, 2010.

[5] L. Jörissen, «Energy Storage,» *Encyclopedia of Electrochemical Power Sources,* pp. 215-231, 2009.

[6] D. Linden y T. Reddy, Handbook of Batteries, Third ed., McGraw-Hill Professional.

[7] S. Vazquez, S. Lukic, E. Galvan, L. Franquelo y J. Carrasco, «Energy storage systems for transport and grid applications,» *IEEE Trans Ind Electron,* vol. 57, pp. 3881-3895, 2010.

[8] R. Walawalkar y J. Apt, «Market Analysis of Emerging Electric Energy Storage System,» DOE/NETL-2008/1330, 2008.

[9] J. Leadbetter y L. Swan, «Selection of battery technology to support grid-integrated renewable electricity,» *Journal of Power Sources,* vol. 296, pp. 376-386, 2012.

[10] C. Parker, «Energy Storage Systems: Batteries,» *Encyclopedia of Electrochemical Power Sources,* pp. 53-64, 2009.

[11] J. Escudero-González y P. López-Jimenez, «Iron redox battery as electrical energy storage system in the Spanish,» *International Journal of Electrical Power & Energy Systems,* vol. 61, pp. 421-428, 2014.

[12] A. Shukla, S. Venugopalan y B. Hariprakash, «Nickel-based rechargeable batteries,» *Jounal*

Power Sources, vol. 100, pp. 122-148, 2001.

[13] F. Rahman, S. Rehman y M. Abdul-Majeed, «Overview of energy storage systems for storing electricity from renewable energy sources in Saudi Arabia,» *Renewable and Sustainable Energy Reviews,* vol. 16, pp. 274-283, 2012.

[14] C. Ponce de Leon, A. Frias Ferrer, J. González García, D. Szanto y F. Walsh, «Redox flow cells for energy conversion,» *Journal of Power Sources,* vol. 160, p. 716–732, 2006.

[15] C. Bengoa, A. Montillet, P. Legentilhomme y J. Legrand, «Flow visualization and modelling of a filter-press type electrochemical reactor,» vol. 27, pp. 1313-1322, 1997.

[16] A. Wragg y A. Leontaritis, «Local mass transfer and current distribution in baffled and unbaffled parallel plate electrochemical reactor,» *Chemical Engineering Journal,* vol. 66, pp. 1-10, 1997.

[17] J. Escudero-González, A. Alberola y P. López-Jiménez, «Redox Cell Hydrodynamic Modelling. Simulation And Experimental Validation,» *Engineering Applications of Computational Fluid Mechanics,* vol. 7, nº 2, pp. 168-181, 2013.

[18] J. Escudero-González y P. López-Jiménez, «Methodology to optimize fluid-dynamic design in a redox cell,» *Journal of Power Sources,* vol. 251, pp. 243-253, 2014.

[19] B. Li, L. Li, W. Wang, Z. Nie, B. Chen, X. Wei, Q. Luo, Z. Yang y V. Sprenkle, «Fe/V redox flow battery electrolyte investigation and optimization,» *Journal of Power Sources,* vol. 229, pp. 1-5, 2013.

[20] D. Scamman, G. Reade y E. Roberts, «Numerical modelling of a bromide–polysulphide redox flow battery: Part 1: Modelling approach and validation for a pilot-scale system,» *Journal of Power Sources,* vol. 189, pp. 1220-1230, 2009.

[21] D. Moore, The Basic Practice of Statistics, Third ed., New York: W.H. Freeman and Company, 2003.

[22] W. Navidi, Estadística para ingenieros y científicos, First ed., New York: McGraw-Hill Companies Inc, 2006.

[23] A. Bard y L. Faulkner, Electrochemical methods, Wiley, 2001.

[24] A. Frias-Ferrer, «Optimización de la hidrodinámica de reactores electroquímicos: empleo de métodos experimentales y numéricos,» *Thesis. Universidad de Alicante,* 2004.

[25] G. Codina, «Desarrollo de una planta de acumulación de energía eléctrica basada en el acumulador redox Fe/Cr,» *Thesis Universidad de Alicante,* 1992.

[26] I. Demirdzic y S. Muzaferija, «Numerical method for coupled Fluid Flow, heat transfer and stress analysis using unstructured moving meshes with cells of arbitrary topology,» *Computer Methods in Applied Mechanics and Engineering,* vol. 125, pp. 232-255, 1995.

[27] STAR-CCM+, *User's Manual,* 2013.

[28] C. Brown, A. Montillet , P. Legentilhomme y J. Legrand, «Studies of space-averaged mass transport in FM01-LC laboratory electrolyser,» *Journal of Applied Electrochemistry,* vol. 23, pp. 38-43, 1993.

[29] A. Bannari, C. Cirtiu, F. Kerdouss, P. Proulx y H. Menard , «Turbulence intensity in an electrochemical cell: Effect on reactor performance,» *Chemical Engineering and Processing: Process Intensification,* vol. 45, pp. 471-480, 2006.

[30] T. Shih , W. Liou, A. Shabbir, Z. Yang y J. Zhu, «A new k-E eddy viscosity model for hight Reynolds number turbulent flows - Model developmente and validation,» *NASA TM 106721,* 1994.

[31] T. Cebeci y P. Bradshaw, Momentum Transfer in Boundary Layers, McGraw-Hill, 1977.

[32] C. Castelain, A. Mokrani, P. Legentilhomme y Peerhossa, «Residence time distribution in twisted pipe flows: helically coiled system and chaotic system,» *Experiments in Fluids,* vol. 22, nº 5, pp. 359-368, 1997.